UNIVERSITY OF NAIROBI

DEPARTMENT OF PHYSICS

OPTICAL AND ELECTRICAL CHARACTERIZATION OF Cu_2ZnSnS_4 DEPOSITED BY *SILAR* TECHNIQUE.

A research thesis for Master of Science degree in Physics

By

Jacinta Akoth Okwako

I56/69295/2013

A thesis submitted in partial fulfillment of the requirements of the award of Master of Science degree (Physics) of the University of Nairobi

December, 2018.

DECLARATION

This thesis is my own original work and has not been submitted for the award of a degree at any other University. Where other people's work has been used, this has been properly acknowledged and referenced in accordance to the University's requirements.

Jacinta Akoth Okwako
I56/69295/2013
University of Nairobi

Signature: ……Date: …….

This thesis has been submitted for examination with our approval as University supervisors,

Dr. Alex A. Ogacho
Department of Physics
University of Nairobi

Signature: ……Date: …….

Dr. Robinson J. Musembi
Department of Physics
University of Nairobi

Signature: ……Date: …….

Prof. Francis W. Nyongesa
Department of Physics
University of Nairobi

Signature: ……Date: …….

ABSTRACT

Currently, Copper Indium Gallium Sulphide (CIGS) is the most efficient thin film material used as an absorber layer in photovoltaic solar cells. Unfortunately, the material poses a challenge in the future sustainability because some of its constituent elements are toxic and scarce on the earth crust (Indium and Gallium). Therefore, there is dire need to replace Indium and Gallium with Zinc and Tin which are abundant on the earth crust and environmentally benign in order to form Copper Zinc Tin Sulphide (CZTS) as an alternative absorber layer for thin film based photovoltaic device. CZTS also has an ideal direct band gap of 1.5 eV as an absorber layer, high absorption coefficient, and suitable optical and electrical properties for thin films solar cells.

In this study, a two-stage combinatorial process that involve deposition of the Cu-Zn-Sn-S thin film using SILAR technique followed by a sulphurisation process in sulfur rich tube furnace is presented. The Copper Zinc Tin Sulphide (CZTS) thin film was deposited onto a Transparent Conducting Oxide (TCO) glass substrate using Successive Ion Layer Adsorption Reaction (SILAR) coating machine with stirrer at room temperature of $27\pm1^{o}C$ and the number of cycles was varied between 20 and 70 cycles at an interval of 20, 40, 60 and 70 cycles. The samples were then annealed in a tube furnace at a temperature of $450^{o}C$ and $550^{o}C$ for 30 minutes each.

The effects of annealing temperature and film thicknesses on the optical, electrical and structural properties of the film samples before and after annealing were investigated. The electrical properties of the CZTS thin film samples were measured using four-point probe, while optical properties UV-VIS- IR spectrophotometer. It was observed that, the resistivity of the film samples decreases with an increase in annealing temperature and also with an increase in the thin films' thickness. Samples annealed at $550^{o}C$ had the lowest resistivity with optical band gap ranging from1.49eV to1.54eV. The calculated absorption coefficient of all the samples, both as-deposited and after annealing, was $\geq 10^{4}$ cm^{-1}. The phase purity of the film sample was determined using Raman spectroscopy which confirmed the formation of quality CZTS film after annealing at $550^{O}C$. Elemental composition of the film sample was carried out using X-ray Fluorescence (XRF) instrument which confirmed that the formed CZTS film was nearly stoichiometric.

TABLE OF CONTENTS

DECLARATION ..... **ii**
ACKNOWLEDGEMENT ..... **iii**
DEDICATION ..... **xvi**
LIST OF SYMBOLS ..... **vii**
LIST OF ABBREVIATIONS ..... **ix**
LIST CHEMICAL COMPOUNDS AND FORMULAE ..... **xi**
LIST OF FIGURES ..... **xiii**
LIST OF TABLES ..... **xv**
ABSTRACT ..... **iii**
CHAPTER ONE: INTRODUCTION **1**
1.1 Introduction **1**
1.2 Need for Solar Energy **2**
1.3 Photovoltaic Thin Film **3**
1.3 Current trends in PV technology **4**
1.4 CZTS Compounds as an Alternative to CIGS Alloys **5**
1.5 Problem of statement **6**
1.6 Objectives **6**
1.6.1 General Objective 6
1.6.2 Specific objectives 6
1.7 Justification and Significance of the Study **7**
CHAPTER TWO: LITERATURE REVIEW **8**
2.1 CZTS(Se) CRYSTAL STRUCTURE **8**
2.2 Electrical and Optical Properties of CZTS **9**
(b) Optical Properties **10**
2.3 CZTS Thin Film Deposition Technique **10**
2.3.1 Vacuum-Based Techniques 11
2.3.2 Solution-Based Techniques 17
2.4: Fabrication of films using successive ionic layer adsorption and reaction process **24**
2.4.1 Advantage of SILAR comparing other methods: 24
CHAPTER THREE: THEORETICAL BACKGROUND **26**
3.1: Solar spectrum **26**

3.2: Raman Spectroscopy **27**
3.3: X-Ray Fluorescence Theory **29**
3.4: Spectrophotometry **31**
3.5: Optical and Electrical Characterization **32**
CHAPTER FOUR: MATERIALS AND METHODS **37**
4.0 Overview **37**
4.1 Sample Preparation and Thin Film Deposition Process 37
4.1.1 Cleaning of glass substrate *37*
4.1.2 Preparation of precursor *37*
4.2 Fabrication of CZTS using SILAR technique 38
4.2.1 Annealing of CZTS thin film *40*
4.3 Sample Characterization **41**
4.3.1 Film Thickness Measurement 41
4.3.2 Electrical Characterization 42
4.3.3 Optical Characterization 43
4.3.3.1 Transmittance and Reflectance Measurement *43*
4.3.4 Raman Characterization of CZTS thin films 44
4.3.5: Compositional Analysis using XRF 44
CHAPTER FIVE: RESULTS AND DISCUSSION **45**
5.1 Optical Properties of CZTS films **45**
5.1.1 Effect of Dipping cycles on film Thickness 45
5.1.2 Effect of Dipping Cycles on Transmittance and Reflectance 46
5.1.2.1 As-Deposited *46*
5.1.2.2 Annealed at $450^{O}C$ *48*
5.1.2.3 Annealed at $550^{O}C$ *50*
5.1.3 Effect of Annealing on Film Thickness 53
5.1.4 Effect of Dipping cycles on Transmittance and reflectance for annealed samples . 53
5.1.5 Optical Absorption Coefficient 55
5.1.6 Optical Band Gaps as a function of Post-Deposition Treatment 58
5.2 Elemental and Structural Characterisation **62**
5.2.1 X-Ray Flouresence Analysis (XRF) 62
5.2.2: Raman Spectra Analysis 63
5.3 Electrical Properties of CZTS **66**
CHAPTER SIX: CONCLUSIONS AND RECOMMENDATIONS **71**

6.1 Conclusion **71**
6.2 Recommendations **72**
REFERENCES **73**

LIST OF SYMBOLS

A	Cross sectional area
α	Absorption coefficient
ε_∞	High frequency optical dielectric constant
ε_0	Static dielectric constant
σ	Electrical conductivity
E	Illumination intensity
E_g	Band gap energy
eV	Electron volts
g	Gram
I	Current
I_{mp}	Maximum Power Current
I_{sc}	Short circuit current
J	The ideal current density
J_{sc}	Short circuit current density
M	Molarity
n	Refractive index
ρ	Electrical resistivity
P_{in}	Power in
P_{out}	Power output
P_m	Maximum power
P_{mp}	Maximum Power Point
R_s	Series Resistance
R_{sh}	Shunt Resistance
S	Seconds
t	Thickness
V_H	Hall voltage
V_{mp}	Maximum Power Voltage
V_{oc}	Open Circuit Voltage
w	width
λ	Wavelength
η	Solar to electricity conversion efficiency
Ω	Ohm

^{O}	Degree
^{O}C	Degrees centigrade
%	Percentage

LIST OF ABBREVIATIONS

a-Si	Amorphous Silicon
atm.	Atmosphere
CBD	Chemical Bath Deposition
CCG	Constant Current Generator
CuInGaS(Se)	
CIGS	Copper Indium Gallium Diselenide
CdTe	Cadmium telluride
cm	Centimetre
c-Si	Crystalline Silicon
CVD	Chemical Vapor Deposition
CZTSSe	Copper zinc tin sulphur selenium
CZTS	Copper zinc tin sulphur
EDX	Energy dispersive x-ray
EMPA	Eidgenössische Materialprüfungs- und ForschungsAnstalt (Swiss Federal Laboratories for Materials Testing and Research)
ETA	Extremely thin absorber
eV	Electron Volt
FF	Fill Factor
GW	Gigawatt
IBM	International Business Machines
IEA	International Energy Agency
IEEE	Institute of Electrical Electronic Engineering
KrF laser	Krypton fluoride laser
KCN	Potassium cyanide etchant
$mAcm^{-2}$	Milliamperes per Square Centimetre
min	Minute
mm	Millimetre
Mo	Molybodenum
M.Sc.	Master of Science
mV	Millivolts
MW	Megawatt
NCs	Nanocrystals
nm	Nanometre

n-type	Negative type
O-Kα	Oxygen K_{alpha}
PLD	Pulsed Laser Deposition
PMT	Photomultiplier
p-type	Positive type
PV	Photovoltaic
PVD	Physical Vapor deposition
RFMS	Frequency Magnetron Sputtering
Rpm	Revolutions per minute
SCCM	Standard Cubic Centimetre per Minute
SILAR	Successive Ion Layer Adsorption Reaction
SLG	soda- lime glass
SEM	Scanning electron microscopy
TAC	Technology and Application Center
TCO	Transparent Conducting Oxide
TFPV	Thin Film Photovoltaic
TiO_2	Titanium Oxide
TW	Terawatt
USA	United States of America
XRD	X-ray diffraction
ZWS	Zeitschrift für Wirtschafts- und Sozialwissenschaften (Centre for Solar Energy and Hydrogen Research)
μm	Micrometre

LIST CHEMICAL COMPOUNDS AND FORMULAE

Al	Alluminium
Ar	Argon gas
Cd	Cadmium
CdI_2	Cadmium Iodide
CdS	Cadmium Sulphide
$CdSO_4$	Cadmium Sulphate
CdTe	Cadmium Telluride
Cu	Copper
CuCl	Copper chloride
$CuSO_4$	Copper (II) Sulphate
Cu_3S	Copper (III) Sulphide
Cu_6Sn_5	Copper-Tin Alloy
Cu_2SnS_3	Copper tin sulphide
Cu_2ZnSnS_4	Copper Zinc Tin Sulphide
CuZn	Copper-Zinc Alloy
Ga	Gallium
H_2O	Water
H_2S	Hydrogen sulphide
In	Indium
MoS_2	Molybodenum Sulphide
N_2	Nitrogen gas
Na	Sodium
NaOH	Sodium Hydroxide
Na_2S	Sodium Sulphide
$Na_2S_2O_3$	Sodium Thiosulphate
S	Sulphur
Sn	Tin
SnS	Tin sulphide
$SnSO_4$	Tin (II) Sulphate
SnSe	Ti Selenium
Te	Tellurium
Zn	Zinc
ZnO	Zinc Oxide

ZnS	Zinc Sulphide
$ZnSO_4$	Zinc (II) Sulphate

LIST OF FIGURES

Figure 1.1: Examples of solar cells applications: (a) building integration, (b) Car, (c) Space cell (d) solar cooker. 3
Figure 1.2: Abundance on earth's crust and cost of constituent elements for CIGS, CdTe, and CZTS(Se) absorber materials for thin film solar cells (Das et al., 2016) 6
Figure 2.1: Schematic representation of kesterite and stannite structures [(a) and (b) Minlin and Xingzhong, 2013; (c) adapted from Hall et al., 1978. 8
Figure 2.2: Schematic diagram of thermal evaporation. 13
Figure 2.3: Schematic diagram of a Sputtering unit. 15
Figure 2.4: Schematic diagram of the high-pressure pulsed-laser deposition system 16
Figure 2.5: Schematic diagram of a typical tube-furnace chemical vapor deposition system. 17
Figure 2.6: Schematic diagram of a typical spray pyrolysis deposition system 19
Figure 2.7: Schematic diagram of a typical electrochemical deposition system 20
Figure 2.8: Schematic diagram of SILAR technique 24
Figure 3.1: Solar irradiance spectrum above atmosphere and at Earth surface (Iqbal, 2012) .. 27
Figure 3.2: Different solar radiation spectrum labeled AM0 in space, AM1 at the earth's surface for normal incidence and AM1.5 at earth's surface, where $\theta = 48.2^{o}$ 27
Figure 3.3: An illustration of energy transfer model of Rayleigh scattering, Stokes Raman and anti-Stokes Raman scattering. 29
Figure 3.4: Bohr model of an atom. 30
Figure 3.5: A schematic diagram of x-ray fluorescence process 30
Figure 3.6: The direct (a) and indirect (b) band gap transitions in semiconductors 33
Figure 3.7: Regular 3-D conductor 34
Figure 3.8: Schematic of 4- point probe configuration 35
Figure 4.1. Schematic representation of successive ionic layer adsorption and reaction (SILAR) method. 38
Figure 4.2: SILAR coating equipment 39
Figure 4.3: Labtech tube furnace 41
Figure 4.4: KLA tencor alphastep surface profilometer 41
Figure 4.5: Jandel sheet resistance equipment 42
Figure 4.6: Shimadzu UV-VIS-NIR double beam 3700 DUV spectrophotometer 44
Figure 5.1: variation in film thickness with number of dipping cycles for as deposited CZTS thin film samples 45
Figure 5.2: variation of Transmittance and reflectance spectra for as-deposited CZTS thin film samples with dipping cycles (a) Transmittance and (b) Reflectance 47
Figure 5.3: Variation of Transmittance and reflectance spectra with different film thickness at 650nm and 826nm for as deposited CZTS thin film samples (a) Transmittance and (b) Reflectance 48
Figure 5.4: Transmittance and reflectance spectra showing the different number of cycles of CZTS thin film samples annealed in sulfur rich atmosphere at 450^{o}C (a) Transmittance and (b) Reflectance. 49

Figure 5.5: Variation of Transmittance and reflectance spectra with different film thickness at 650nm and 826nm for CZTS thin film samples annealed at 450^{o}C (a) Transmittance and (b) Reflectance 50
Figure 5.6: Spectral transmittance showing the different number of cycles of CZTS thin film samples annealed in sulfur rich atmosphere at 550^{o}C (a) Transmittance and (b) Reflectance. 51
Figure 5.7: Variation of Transmittance and reflectance spectra with different film thickness at 650nm and 826nm for CZTS thin film samples annealed at 550^{o}C (a) Transmittance and (b) Reflectance 52
Figure 5.8: Thickness variation with the number of cycles for CZTS thin film samples As-deposited, annealed in sulfur atmosphere at 450^{o}C and at 550^{o}C 53
Figure 5.9: Change in transmittance for CZTS thin film samples As-deposited, annealed in sulfur atmosphere at 450^{o}C and at 550^{o}C (a) deposited with 20 cycles and (b) deposited with 70 cycles. 54
Figure 5.10: Change in reflectance for CZTS thin film samples as-deposited, annealed in sulfur atmosphere at 450^{o}C and at 550^{o}C (a) deposited with 20 cycles and (b) deposited with 70 cycles. 55
Figure 5.11: Absorption coefficient of the as-deposited CZTS thin film samples 56
Figure 5.12: Absorption coefficient of the CZTS thin film samples annealed in sulfur atmosphere at (a) 450^{o}C and (b) 550^{o}C 57
Figure 5.13: Variation of absorption coefficient with the number of cycles at 826nm for CZTS thin film samples of As-deposited, annealed in sulfur atmosphere at 450^{o}C and at 550^{o}C 58
Figure 5.14: Optical band gap for as deposited CZTS thin film samples with different number of dipping cycles 59
Figure 5.15: Optical band gap for CZTS thin film samples annealed in sulfur rich atmosphere at 450^{o}C 60
Figure 5.16: Optical band gap for CZTS thin film samples annealed in sulfur rich atmosphere at 550^{o}C 61
Figure 5.17: Raman spectra of CZTS thin film sample As-deposited 65
Figure 5.18: Raman spectra of CZTS thin film sample annealed in a sulfur rich atmosphere at 450^{o}C 66
Figure 5.19: Raman spectra of CZTS thin film sample annealed in a sulphur rich atmosphere at 550^{o}C 66

LIST OF TABLES

Table 4.1: SILAR coating parameters used 39
Table 5.1: Band gaps of CZTS thin film samples at different temperatures 62
Table 5.2: Elemental composition of Cu_2ZnSnS_4 film sample with 70 cycles as-deposited, annealed at 450^OC and annealed at 550^OC 63
Table 5.3: Sheet resistance and resistivity of film samples annealed at 450^oC 67
Table 5.4: Sheet resistance and resistivity of film samples annealed at 550^oC 68
Table 5.5: Refractive index (n) and dielectric constant (ε_∞) values of the as deposited CZTS thin films 69
Table 5.6: Refractive index (n) and dielectric constant (ε_∞) values of the CZTS thin films annealed at 450^oC 69
Table 5.7: Refractive index (n) and dielectric constant (ε_∞) values of the CZTS thin films annealed at 550^oC 70

DEDICATION

I dedicate this piece of work to my beloved parents, George and Rosemary who sacrificed a lot of their scarce resources to lay down the foundation of my education and their constant prayers and encouragement that brought me this far. To Rosemary Ida Atieno and Shirlene Stacy Anyango who have been the source of my inspiration.

ACKNOWLEDGEMENT

First and fore most I would wish to give praise to the Almighty God for the good health both in mind and body and for having brought me this far. Words can never be enough in expressing how thankful I am to those incredible people in my life who made this thesis possible. I would like to thank them for making my time during my research in the University of Nairobi, a period I will treasure.

I wish to pass my heartfelt gratitude to my research supervisors; Dr. Alex A. Ogacho, Dr Robinson J Musembi and Dr. Francis W. Nyongesa who were always there to extend moral support at that hour of need. Thanks for supporting my research ideas, for giving me the leeway to do independent work and for teaching me.

The skillful technical assistance of Mr. Boniface Muthoka and Ms Evelyne Odera of Condensed Matter Research Group, University of Nairobi is highly appreciated. I don't forget to thank those who ensured my well-being while I was working on this thesis. In a special way I would wish to thank Emily, Sr. Mary, Patrick, Newton, Isaac, Hellen and Simon for their friendship and stress releasing stories. I am very grateful to my colleague Josephat Mogusu for his enthusiastic support and pleasant co-operation. Special thanks to my life partner Godwin Asiimwe for encouraging me and constantly being there for me during my frustrating moments.

I would like to thank my parents for always encouraging me to pursue my education and for always providing wisdom, love, support and guidance throughout my life. I thank my siblings for encouraging and supporting me throughout my life and career and for being a constant presence during my many times of stress, excitement, frustration and celebration. Last but not least, I would like to thank University of Nairobi for the scholarship and International Science Program (ISP) Uppsala, Sweden for financial support.

CHAPTER ONE: INTRODUCTION

1.1 Background of the Study

Energy is very vital component in the life cycle of humankind and it is being used in many ways to improve the living standards of human being. The increasingly growing population has seen the world energy consumption being on the rise. The modern world has encountered a lot of challenges with the traditional energy sources such as fossil fuels because of their limited resources and they are non-renewable. From the environmental point of view, burning of fossil fuels results in production of carbon dioxide and sulphur dioxide which are responsible for global warming and acidic rain hence causing air and water contamination. The emergence of renewable energy such as solar energy, wind energy, bio gas, hydropower, tidal waves were as a result of these problems with conventional fossil fuels (Asif and Muneer, 2007).

The utilization of solar energy and wind energy are the current trend of the world energy in the area of non-renewable energy sources. This is because these categories of renewable energy are widely available and easier to use. Wind energy has not been extensively utilized compared to solar energy due to the geographical limitation. Solar cell is a type of device that directly converts the solar energy to the electrical energy and is also known as photovoltaic (PV) device. Today's market is dominated by crystalline silicon based PV technology (Deligianni *et al*., 2011). This is mostly due to a well- established knowledge on silicon material science and engineering, available abundant supply of silicon raw material and the advantages of low ecological impact but high efficiencies (Goetzberger *et al*., 2003). However, the low optical absorption ($\sim 10^2$ cm^{-1}) and a complicated manufacturing process has led to a high installation cost for silicon-based PV technology (Miles *et al.*, 2005; Sagadevan, 2013).

Currently, in addition to crystalline silicon, there are other several materials available in the market which have potentials to generate appreciable electrical energy from the solar energy. These materials are amorphous silicon (a-Si), cadmium telluride (CdTe), copper indium (gallium) diselenide (CI(G)S), TiO_2 based dye-sensitized, copper zinc tin selenide (CZTS) etc.(Sagadevan, 2013)

1.2 Need for Solar Energy

According to the current trending energy sources, solar energy is seen as one of the options which will be of great importance in future production of energy (Ananthan and Mahalaksmi, 2014). This source has the capability to meet all the energy needs in the universe in the foreseeable future (Solangi *et al.*, 2011). From the previous reports (Solangi *et al.*, 2011), the sun deposits ~ 120,000 TW of electromagnetic radiation on the surface of the Earth annually and this exceeds human needs by far even in the most aggressive energy demanding situations. Harvesting of 20 TW of this solar power would be realized if only 0.16% of land on Earth is covered with a solar system device with a power efficiency of 10%. This is equivalent to almost twice the current rate at which fossil energy is being consumed globally (Eisenberg and Nocera, 2006). From the comparison, the illustration clearly indicating that solar energy as a source has a great potential to provide energy of greater magnitude than any current human technology can achieve.

Energy from solar is clean, self-contained, reliable, quiet, long-term, needs little maintenance where necessary, year-round continuous and unlimited operation at moderate costs (Saxena *et al*., 2011; Farahbod *et al*., 2014). Unfortunately, nearly 57 years after its invention, solar photovoltaics still contributes merely 1 % of the world's on-grid electricity despite all the above mentioned benefits. This can be attributed to high initial cost of purchase of solar cells which makes them unaffordable to most of the needy consumers. According to a statistical review of world energy resources in 2016,results showed that 40 % of the electrical energy is generated from coal, 22 % comes from natural gas, 16.4 % is fueled by water generators, 11% is generated from nuclear reactors and only 1 % of electricity is generated from solar cells (Conti *et al*., 2016).

Currently, countries like the United States, Germany, Brazil, Italy and Spain are turning to solar energy for the production of electricity. This is because the mineral based energy is associated with high capital investments, radiation and greenhouse gas emissions. Photovoltaic being a renewable energy, it is one of the best alternatives to the "conventional" energy such as nuclear, hydro, and coal. 15% of the world production of electricity is by nuclear (IAEA, 2007). Countries like France, Japan, and USA depend on nuclear power plants which contributing an equivalent of 75%, 30%, and 19% respectively in their whole energy resources

(Altomonte, 2012). Many countries including Germany and Japan, are gradually switching to renewable energy such as photovoltaic in order to reduce risk factor of nuclear energy.

Total energy capacity of the world in 2010 was 4742 GW in which the share of the solar energy was 37 GW, an equivalence of 0.78% (Altomonte, 2012). In 2009, the new installation of solar energy was 7.1 GW and it increased to more than double in 2010 (17.5 GW). The top 10 companies which share the almost total market are as follows: Q- cells, Sharp, Suntech, Kyocera, First Solar, Motech, Solar World, Jasolar, Yingli, and Sanyo. PV power plants of several hundred MW can be designed for different applications. Some examples are shown in Figure 1.1 below.

Figure 1.1: Examples of solar cells applications: (a) building integration, (b) Car, (c) Space cell (d) solar cooker.

1.3 Photovoltaic Thin Film

Photovoltaic (PV) solar cells are emerging as some of the most promising technology in providing alternative sources of energy. These types of solar cells are classified broadly into the following types of technologies: thin film solar cells, multifunction solar cells, quantum dot solar cells, extremely thin absorber (ETA) solar cells, and organic/polymer type of solar cells

(Wu *et al*.,2015). Thin film is a promising technology for mass production of low cost photovoltaic (PV) solar cell. This is because thin film technology translates to minimal material usage in the fabrication requirement; photo-generated carriers also traverse short paths thus minimizing bulk recombination losses. Additionally, thin film technology may also lessen the stringent material quality (purity) requirements. Thin film technology therefore offers a promising technology that can deliver electric energy that is comparable to those from fossil fuels (Pawar *et al*., 2010).

Present thin film PV technologies include amorphous silicon, CuInGaS(Se) (CIGS), CdTe, dye sensitized solar cell technologies among others (Wu *et al*., 2015). A US company known as SunPower have recently developed a silicon module claiming a world efficiency of 24.1% (SunPower, 2016). A Swiss Federal Laboratories for Materials Science and Technology (EMPA), have developed CIGS thin film solar cells on flexible polymer foils with a new record efficiency 20.4% (EMPA, 2013). A team working in the Japan's Solar Frontier in a partnership with the Japan's New Energy and Industrial Technology Development Organization have recently attained the CIGS new record efficiency of 22.3% (Solar Frontier, 2015) while a team working in the Centre for Solar Energy and Hydrogen Research (ZSW) have claimed the present CIGS highest efficiency world record of 22.6% (ZWS, 2016). CdTe recorded efficiency stands at 21.5% achieved by First Solar certified at the Newport Corporation's Technology and Applications Center (TAC) PV Lab (First Solar, 2015). Despite their success and potential, these technologies require an indispensable constituent In, Ga and Te all of which are rare earth metals. Additionally, Cd used in CdTe solar cell is highly toxic and hence not environmentally friendly (Pawar *et al*., 2014).

1.3 Current trends in PV technology

Thin film photovoltaics (TFPV) technology is faced with several major challenges since its emergence: competing with silicon based PV in terms of power conversion efficiency manufacturing costs and the need to contain only earth-abundant and non-toxic materials without severe degradation in the long term (Bremaud, 2009). Moreover, TFPV solar cells will remain in the small minority as long as crystalline silicon (c-Si) solar PV manufacturing costs decreases. In recent years, TFPV technology has experienced rapid growth and achieved significant technological advances hence consolidating its place in the solar market. From a physical aspect, TF solar cells are more advantageous on the grounds that they have a direct

band gap, a high absorption coefficient which enables the absorption of most of the solar spectrum using only few microns of materials as well as reduction in sensitivity to recombination at grain boundaries (Bremaud,2009). Technologically, TF solar cells' cost of fabrication can be reduced by exploiting manufacturing actions like roll-to-roll or allow the usage of flexible substrates and monolithic interconnections (Bremaud, 2009).

1.4 CZTS Compounds as an Alternative to CIGS Alloys

There is a growing demand for alternative materials to the well-established CdTe, CIGS and Si-variants despite thin film solar cell (TFSC) technology's current encouraging advantage. It is estimated that the abundance of Indium, Cadmium and Tellurium in the earth crust to be 0.16 ppm, 0.15 ppm and 0.001 ppm respectively (Das *et al*., 2016). This is significantly lower compared to the abundance values of copper, zinc, tin and sulphur which is estimated to be 68, 79, 2.2 and 420 ppm respectively. Furthermore, Zinc and Tin are much more available compared to Indium (Das *et al*., 2016). It is estimated that the availability of Zinc and Tin is about 500 and 14 times higher and also the annual global production of these elements is 20 and 340 times more compared to the scarce and expensive Indium (Das *et al*., 2016). On the other hand, cadmium metal is well known for its toxicity issues and in some countries it has experienced legislative action forcing industries to restrict or completely refrain from its use (Tickner *et al*., 1999). It goes without question that there is a great need for the identification of a new thin film material compounds which comprise more sustainable and non-toxic elements coupled with excellent device performance. Device performance is very vital in reinforcing the development and commercial viability of thin film technology. Extensive research has been ongoing seeking alternative thin film materials to potentially substitute current materials in order to address and meet the growing urge for the above issues. It emerges that CZTS is the best alternative choice for thin film solar cell absorber material because of its direct band gap of 1.4-1.6 eV with a large optical absorption coefficient ($\geq 10^4$ cm^{-1}) and p-type conductivity. The constituent elements of CZTS thin film material are earth abundant, cheap and environmentally friendly compared to its counterpart elements like Indium, Cadmium, tellurium and Sellenium. Figure 1.2 shows the abundance and cost of constituent elements for CIGS, CdTe and CZTS(Se). It is evident from the figure below that the price of Indium, Tellurium, Gallium and Sellenium are high compared to Copper, Zinc, Tin and Sulphur. Sulphur is the most abundant on the earth crust and least costly.

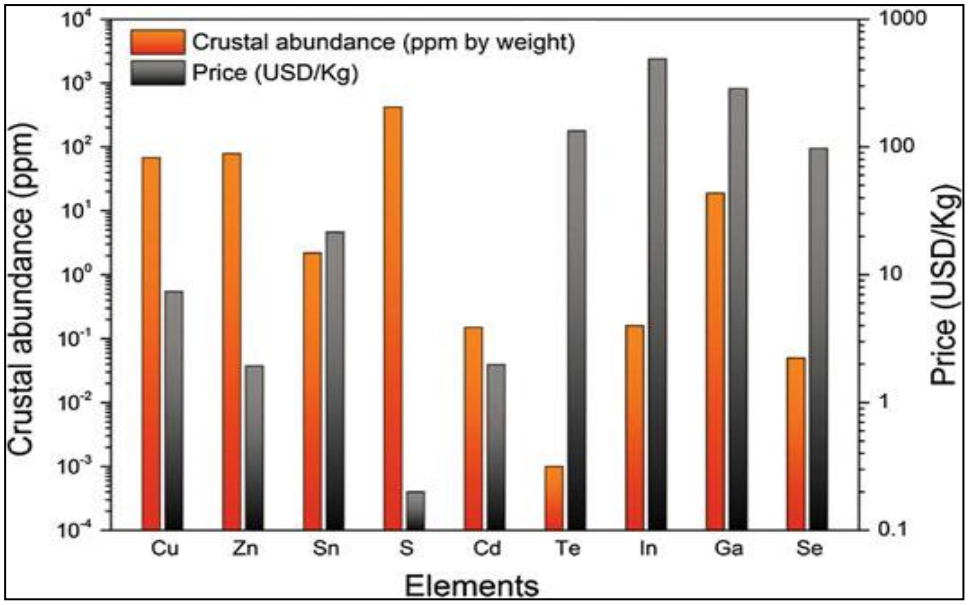

Figure 1.2: Abundance on earth's crust and cost of constituent elements for CIGS, CdTe, and CZTS(Se) absorber materials for thin film solar cells (Das *et al.*, 2016)

1.5 Statement of problem

Enormous research studies have been carried out on CZTS solar cells using different techniques in the world and the reports attests to CZTS remains a promising, as abundant and non-toxic alternative to high performing CIGS based technology. However, key issues related to carrier transport, absorber quality and interface recombination or interface buffer layers need additional attention to be optimized for this technology to remain competitive compared to CIGS.

1.6 Objectives

1.6.1 General Objective

The overall objective of the study is to optimize the deposition parameters and investigate the optical and electrical characteristics of CZTS thin films deposited using the *SILAR* technique.

1.6.2 Specific objectives

The specific objectives of this study were:

a) To optimize the deposition parameters of CZTS using low cost *SILAR* technique
b) To evaluate the optical and electrical properties of CZTS thin films deposited by *SILAR* method

c) To determine the effect of annealing temperatures and thin film thicknesses on the optical and electrical properties of CZTS thin films.

1.7 Justification and Significance of the Study

Human development and survival highly depends in the availability of clean energy which is key for healthier living and necessary for mitigation of the negative climatic change. The world is struggling to maintain constant supply of energy and according to the current reports, energy from fossil fuels such as coal oil and gas is being used to power more than 80% of the world's economy. These fuels are proving to be no longer sustainable due to their daily escalating prices and they also emit greenhouse gases upon combustion. On the other hand, solar energy is clean, available in large quantity and is capable of providing a significant amount of the world's energy demand that can be used to solve the energy crisis that is foreseen in the decades to come. The mostly used solar panels that has reached a high efficiency are made from high purity crystalline silicon which are costly for a common consumer to own. On the other hand, the thin films such as CIGS and CdTe which have also achieved remarkable efficiencies are facing a problem of either containing toxic elements such as Cadmium or the elements are rare such as Tellurium or Indium. CZTSs' potentially inexpensive manufacturing technology promise cheaper solar energy as well as a promising alternative to CIGS. CZTS contains abundant earth metals which are non-toxic and hence environmentally friendlier. Additionally, if this technology is fabricated using an easier and cheaper technique such a *SILAR* technique, it gives CZTS solar cell an exceptional chance to taking up a large fraction of the world's solar PV market.

CHAPTER TWO: LITERATURE REVIEW

2.1 CZTS(Se) CRYSTAL STRUCTURE

CZTS or CZTSSe can form in two distinct crystal structures namely kesterite and stannite structures (Hall *et al.*, 1978). Compounds whose crystal structures form in a similar manner like kesterite minerals are also referred to as kesterites. In a similar way those whose crystal structures take the form of stannites are referred to also as stannites. For

CZTS, the only notable distinction between kesterite and stannite crystals lies in the distinctive ordering of the cation sub-lattice as shown in Figure 2.1 (Jiang and Yan, 2013)

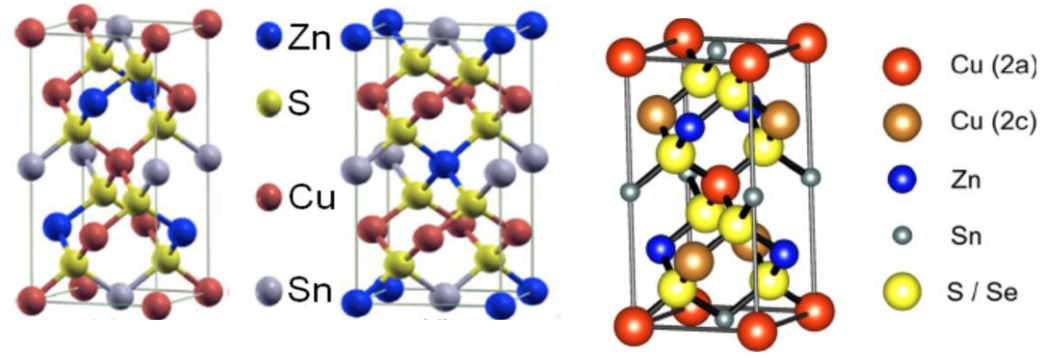

(a) Kesterite (b) Stannite CZTS (c) Kesterite CZTS/Se

Figure 2.1: Schematic representation of kesterite and stannite structures [(a) and (b) Jiang and Yan, 2013; (c) adapted from Hall *et al.* 1978**.**

Kesterite solar cells technologies use sulfur rich, Cu_2ZnSnS_4 *(CZTS*); selenium rich $Cu_2ZnSnSe_4$ (*CZTSe*) and their alloys $Cu_2ZnSn(S,Se)_4$ (*CZTSSe*). Sulfur selenium alloy based technology $Cu_2ZnSn(S_xSe_{1-x})$ (*CZTSSe*) has the best record conversion efficiency of 12.6% (Wang *et al*., 2013). In addition, selenium rich compounds, until now the Zn-rich and Cu-poor kesterite solar cells have shown better conversion efficiencies. Zn– rich structures are more tolerant to stoichiometric deviations, while Cu – rich structures are prone to formation of copper rich regions in the grain boundaries thus increasing recombination losses and adversely affecting open circuit voltage (V_{OC}) (Bag *et al.*, 2012). The V_{OC} deficit, defined as difference

between E_g (in eV) and V_{OC} (in V) can be decreased by diminishing the bang gap together with tight control of the formation of Cu_2X possibly by its removal by KCN etching.

Structurally closer to kesterites is another naturally occurring mineral called stannite. Kesterite and stannite crystal structures are so close that x-ray diffraction (XRD) spectroscopy cannot resolve them. To distinguish between these two structures neutron spectroscopy is required (Tsukasa *et al.*, 2011). X-ray diffraction cannot distinguish between Cu and Zn due to similarity of their cross-sections; hence a synchrotron light or neutron source is required for that purpose of distinction as well as for differentiation of their secondary phases (Nozaki *et al.*, 2012).

2.2 Electrical and Optical Properties of CZTS

(a) Electrical Properties

Internal defects usually occur as a results of doping CZTS materials. Chen *et al.*, (2010) came up with the first principle of theoretical calculations for the energy formation and the transition energy levels for a series of intrinsic point defects and defect complexes in CZTS. They were able to show that p-type conductivity can be formed when the 'Cu' atoms sits on the place of 'Zn' atoms (Cu_{Zn} antisite) which has a lower formation energy and relatively deeper acceptor level compared to the 'Cu' vacancy. They also state that all donor defects possess higher formation energy hence this is agreement with the experimental findings of p-type conductivity. Occurrence of n-type doping is difficult in CZTS when the formation energy of acceptor defects is low.

Several resistivity values of CZTS thin films which have been reported before seem to be varying mainly between ~10^{-3} Ω.cm and 10^{1} Ω.cm (Jiang and Yan, 2013). Also, resistivity values as high as 10^{4} Ω.cm have been reported (Katagiri *et al.*, 1997). Different authors in their different studies have reported about the hole concentration to be varying from 10^{16} cm^{-3} to 10^{21} cm^{-3} (Chaudhari and Tiwari, 2012; Fernandes *et al.*, 2010; Rajeshmon *et al.*, 2011; Ito and Nakazawa, 1988). Observations made from the results of Hall effect measurement indicated that hole mobility of CZTS changed from lower than 0.1 to as high as 30 $cm^2 \cdot V^{-1} \cdot s^{-1}$. A number of reported values were in the range of 1 to 10 $cm^2 \cdot V^{-1} \cdot s^{-1}$ (Jiang and Yan, 2013). The reported low mobility clearly indicates that the maximum thickness of the CZTS absorber

layer is supposed to be smaller compared to the thickness of the absorber layer in CIGS thin film solar cells.

(b) Optical Properties

The optical band gap of kesterite based CZTS has been theoretically determined to be 1.50 eV and it has a high absorption coefficient of approximately 10^4 cm^{-1} which is able to ensure minimization of material used on the device (Singh *et al.*, 2015). Various reseachers have previously carried a study on CZTS thin films using different techniques and the obtained results showed that the band gap of these films varied from 1.4 eV to 1.6 eV (Jiang and Yan, 2013).

Raman spectrum is commonly seen to be a vital technique which can be used to characterise samples in order to reveal Raman peaks in CZTS films especially for the peaks associated with ternary phases namely Cu_xS, ZnS, Sn_xS, Cu_2SnS_3, and Cu_3SnS_4. According to a report by Fontane *et al.*, (2011), 338 cm^{-1} is the universally acknowledged peak of CZTS. In addition, other peaks which are being associated by CZTS are at 96 cm^{-1}, 166 cm^{-1}, 250 cm^{-1}, 251 cm^{-1}, 287 cm^{-1}, 288 cm^{-1}, 289 cm^{-1}, 337 cm^{-1}, 338 cm^{-1}, 352cm^{-1}, 370 cm^{-1} and 372 cm^{-1} (Fontane *et al.*, 2011).

Low temperature of about 5K photoluminescence spectra have been recorded from CZTS thin films during a study on the recombination mechanisms. Researchers have previously observed a broad peak which was centered around 1.24eV and it was associated with the typical donor-acceptor pair transition that involved creation of tail states by potential fluctuations. From the research, it was claimed that the presence of potential fluctuations indicated CZTS was strongly compensated. Moreover, time-resolved PL data indicated that lifetime of free carriers in CZTS thin film was lower than 1 ns (Jiang and Yan, 2013).

2.3 CZTS Thin Film Deposition Technique

Various techniques have been used in deposition of CZTS thin films such as sputtering, spray pyrolysis, evaporation, successive ion layer adsorption reaction (*SILAR*), spin coating from precursor solution etc. (Vanalakar *et al.*, 2014). The deposition techniques of the thin film can

be categorized broadly into two major groups, namely vacuum-based techniques and solution-based techniques. Vacuum-based technique comprises of evaporation, sputtering, pulsed laser deposition and chemical vapor deposition while solution-based techniques involve spray pyrolysis, nano-crystal ink based approaches, precursor- ink based approaches and electrochemical deposition.

2.3.1 Vacuum-Based Techniques

This technique widely involves deposition of thin film by sputtering and evaporation. CZTS thin films are made by high temperature metal sulfides, sufidation of stacks of metals or by combining the two (Wang, 2011). This technique calls for patience since the processes involved are slow and requires up to numerous hours of thin film deposition and annealing. The advantage of this technique is that the thin film obtained exhibit controlled stoichiometry and high uniform potential (Wang, 2011). Below is a brief description of each of the Vacuum based technique namely evaporation, sputtering, pulsed laser deposition

(a) Evaporation

Katagiri *et al.* (1996) were the first to give a report on CZTS thin films from evaporation by sulfirization of Cu/Sn/Zn stack in N_2+H_2S (5%) atmospher at 500°C and the solar cells were found to have a power conversion efficiency of 0.66%. An indepth stoichiometric analysis of the sulfurized film samples showed that volatile zinc re-evaporated when the samples were heated for long. In another research, Katagiri *et al* (2001a) were able to improve the device efficiency to 2.62% by substituting the Zn with ZnS and elevating the heating temperature to 550^{O}C. Katagiri *et al.*, (2001b) also reported on the significant improvement on the final film adherence to the Mo/SLG substrate when Zn was replaced by ZnS in the initial precursor stack**.**

Independently, Ito and Nakazawa, (1988) and Katagiri *et al*. (2003) reported further improvement on the devices when the annealing chamber was improved by using rotary pump with a steel chamber and turbo pump instead of the quartz glass tube furnace. They also used CdI_2 instead of $CdSO_4$ for the deposition of CdS, and introduced a Na_2S layer between the ZnS precursor layer and Mo in order to control Na-doping in the CZTS films. As a results of these improvements, they were able to fabricate a solar cell device with a conversion efficiency of 5.45% , an open circuit voltage (V_{OC}) of 582 mV and short circuit current density (J_{SC}) of 15.5 mA/cm^2 .In a different study carried out by Katagiri (2005), they tried to combine different

precursor stacks in order to come up with a solar cell device with a smoother CZTS layer since they were having a problem with the surface morphology of 5.45 % efficient device reported earlier. They observed that a smoother CZTS film could be realized with the use of multiple periods of $Cu/SnS_2/ZnS$ stacks. The film morphology improved as a result of better intermixing of the initial precursors as well as increment in the sulfur content of the precursor layer.

Using co-evaporation on heated substrates, Friedlmeier *et al*., (1997) from Stuttgart University were able to fabricate a CZTS device with a conversion efficiency of 2.3%. They varied the substrate temperature between 300 and 600 °C and also used Copper, Zinc Sulphide, Tin Sulphide or tin and Sulphur as the sources for the deposition of CZTS films. Significant amounts of Sn were found to be lost by re-evaporation when films were subjected to a higher substrate temperatures of more than 400°C. According to a report by Tanaka *et al*. (2006), CZTS films which are deposited using co-evaporation from Cu, Zn, Sn, and S precursors showed a preferential orientation along the [112] plane. There was an increment in the grain size as the substrate temperature increased from 400 – 600 °C.

Lately, there have been increased studies on fast co-evaporation of CZTS thin films with an aim of making the thin film deposition more viable for commercial manufacturing. Schubert *et al.* **(**2011**)** carried out a study to determine the possibility of fabricating a Cu-rich CZTS thin film using co-evaporation technique at a substrate temperature of $550^{O}C$. They observed that the as deposited film contained both CuS and CZTS phases but the CuS was later gotten rid of using KCN etching. The fabricated solar cell device using these films after etching had an efficiency of 4.1% coupled with a V_{OC} of 541mV, J_{SC} of $13.0mA/cm^2$ and fill factor (FF) of 59.8%. In another report, Wang *et al*. (2010) from IBM deposited CZTS thin films using co-evaporation method with low substrate temperature of 110°C then annealed the synthesized film in sulphur atmosphere at 540 °C for a few minutes. The device made using these films were found to be 6.8% efficient with a V_{OC} of 587mV, J_{SC} of $17.8mA/cm^2$ and FF of 65%. The obtained CZTS thin films were found to be 660nm thick.

Recently Bar and his team **(**Bar *et al*., 2011a**)** published a report on the effect of KCN etching on the surface properties of CZTS thin films. It was found that KCN etching resulted to a preferential etching of copper and to some extent tin too which led to an increased surface band gap from 1.53 eV to 1.91 eV. In another report by the same authors, they carried out an analysis on the effect of oxidation on the surface properties of CZTS films. They found that tin, zin and

sulphur were oxidized when the thin films were exposed to air. The surface of the films were observed to be Cu-deficient which was attributed to the presence of copper free surface species such as $ZnSnS_3$, or even a mixture of ZnS and SnS_2 (Bar *et al*., 2011b).

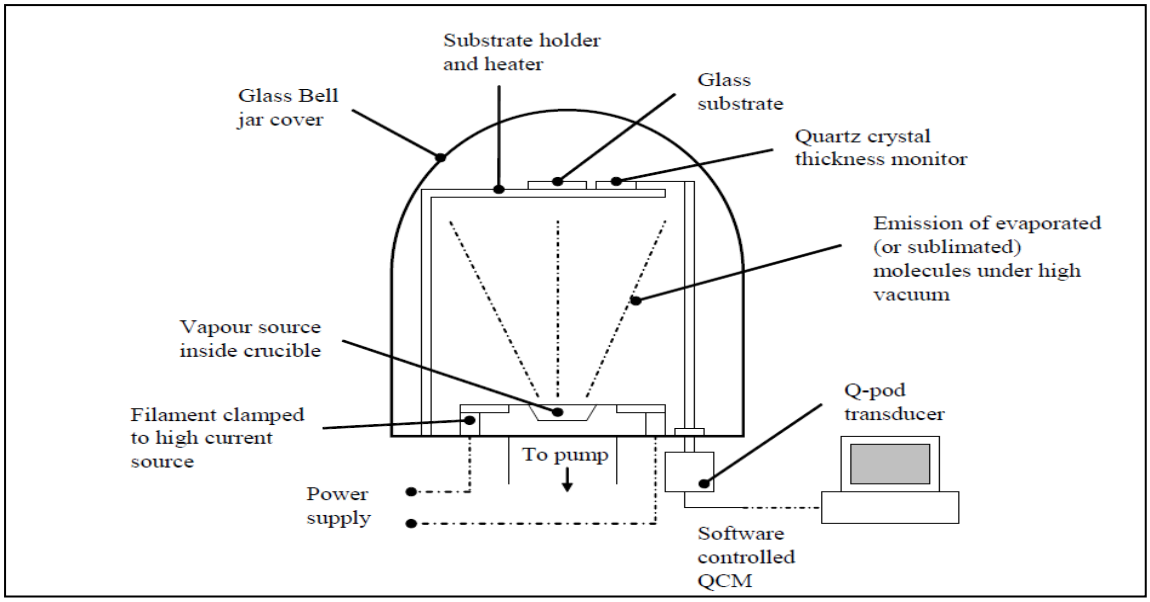

Figure 2.2: Schematic diagram of thermal evaporation.

(b) Sputtering

Beam sputtering technique has been used before in deposition of CZTS thin films from a pressed targets of CZTS **(**Ito and Nakazawa, 1988). They observed that CZTS band gap was 1.45 eV. Tanaka *et al*. (2005) synthesized CZTS thin films by annealing heated Cu/Zn/Sn (bottom) stacks in sulfur atmosphere. The films were found to peel off easily when they were sputtered at room temperature followed by annealing at high temperature. However, a well adhesive film was obtained when heated substrates were sputtered followed by S annealed at the same temperature. Stoichiometric CZTS films were obtained at a lower substrate temperatures of less than 400°C. Notably, a Zn-poor thin film was obtained at a temperature high than 450^{O}C due to Zn losses.

Katagiri *et al*. **(**2007) fabricated the best solar cells using sputtering technique. The group managed to fabricate a CZTS device with a conversion efficiency of 5.74% by employing a reactive co-sputtering of Cu, SnS, and ZnS in H_2S atmosphere (20%). In order to come up with a fine intermix and uniform precursors, the film samples underwent a rotation (20rpm) as the

precursors were being sputtered. It was found that the best devices were obtained when Cu/(Zn + Sn) = 0.87, Zn/Sn = 1.15, and S/(Cu + Zn + Sn) = 1. Later in a separate study, Katagiri *et al*., (2008) reported on a more improved efficient pure sulfide CZTS device whose efficiency was 6.77%. This improvement was achieved as a result of etching of metal oxide particles which are present on the CZTS layer by soaking the film samples in the distilled water before the deposition of CdS. Katagiri *et al*. **(**2009) varied the Cu:Zn:Sn ratio in an attempt to determine its effects on the performance of the CZTS device. They were able to obtain a more efficient CZTS solar device when the composition range is narrow around Zn/Sn≈1.25 and Cu/(Zn+Sn)≈0.9. In addition, it was found that there was little effect on the device properties when H_2S concentration was varied from 5% to 20%. The use of lower H_2S concentration for anneals was then suggested in order to minimize the wearing of the sulfidation chamber.

Edoff *et al*. (2012) carried out a study to determine the effect of replacing ZnS precursor with Zn on the properties of CZTS thin films. They observed that the films obtained by using ZnS were smooth, contained fewer voids, the grains were smaller in size and Sn loss reduction. This observation was associated with the early nucleation in the film samples which were sputtered using S containing precursors. Chalapathy *et al*. (2011) reported 4.59% efficient CZTS solar cells when they synthesized CZTS thin films by annealing a stack of Cu/ZnSn/Cu precursor in Sulphur atmosphere. They observed that the thin film morphology was sensitive to the annealing temperature. The films which were annealed at 560°C resulted to bi-layer morphology while the film annealed at 580°C did not.

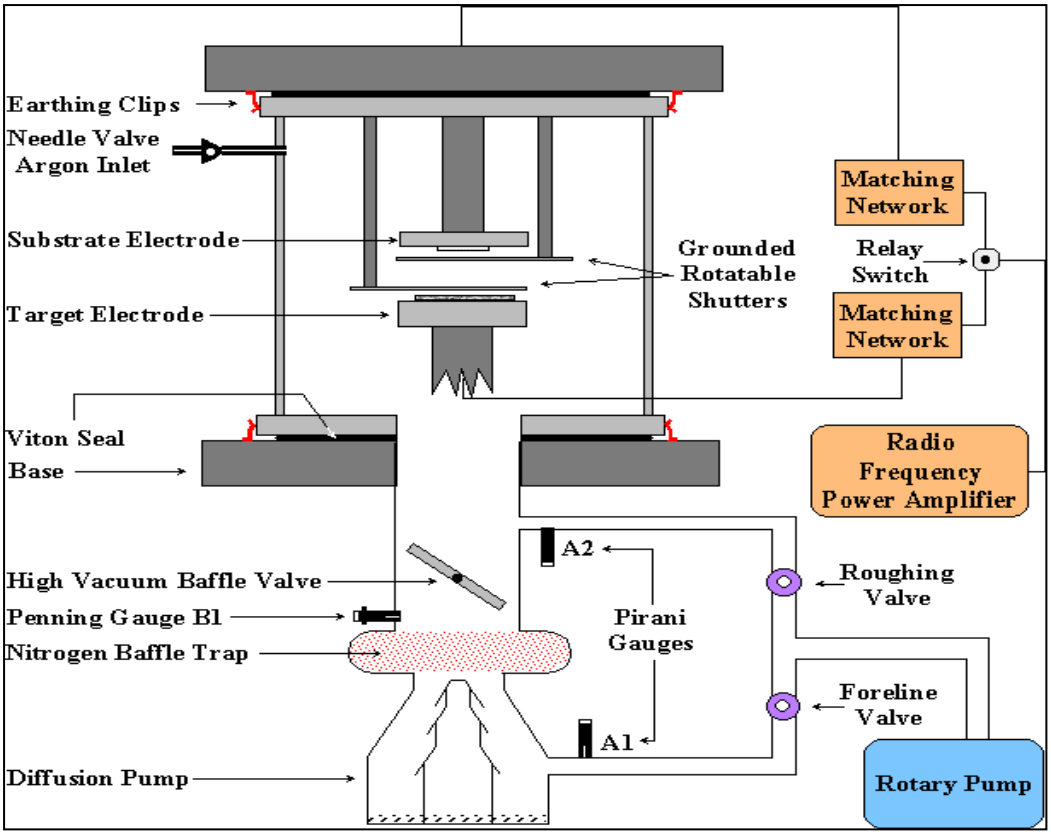

Figure 2.3: Schematic diagram of a Sputtering unit (Ali,1999).

(c) Pulsed Laser Deposition (PLD)

Moriya *et al*. (2007) fabricated the first CZTS solar cell using PLD of which they obtained films with an efficiency of 1.74% when annealed at 500^{O}C. In the study, the CZTS targets were ablated using KrF laser pulses. During thin film deposition, the substrate was held at room temperature. The authors carried out the grain growth by annealing the samples in N_2 atmosphere for an hour. The observed that the films showed no significant Sn loss and had formed Cu-Sn-S phase along with CZTS. In a different study, Moholkar *et al*. (2011) reported a CZTS device with an efficiency of 3.14%. CZTS were synthesized the same way to Moriya *et al*.,(2007) except annealing where they annealed their film samples in N_2 + H_2S (5%) atmosphere at 400°C.

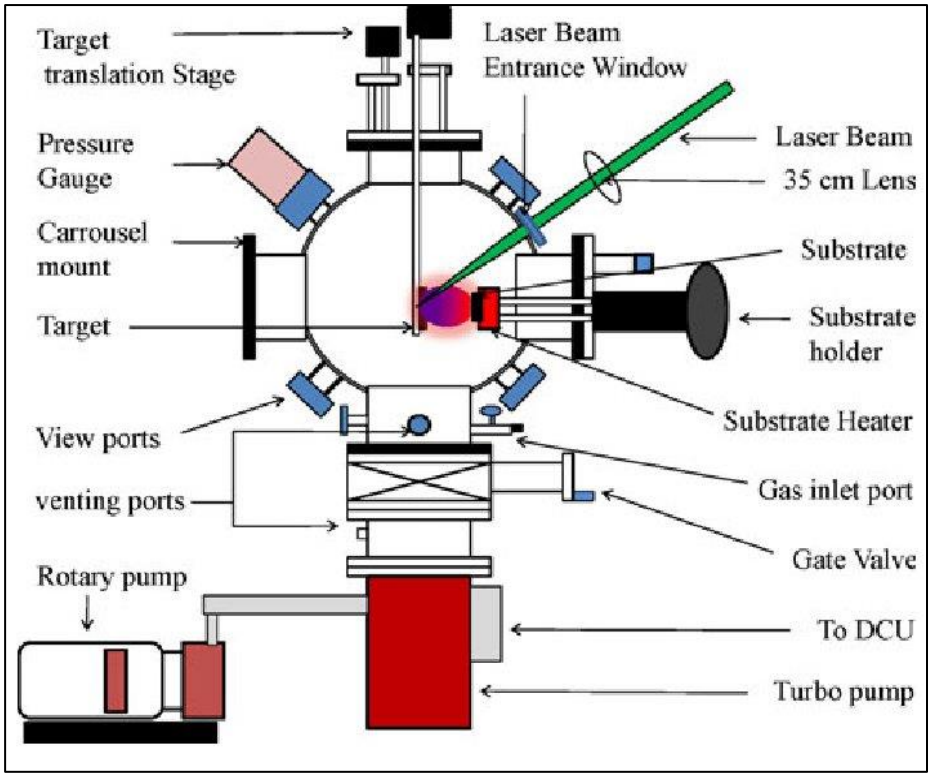

Figure 2.4: Schematic diagram of pulsed-laser deposition system (Mostako and Khare,2012).

(d) Chemical Vapor Deposition (CVD)

CZTS thin film using aerosol assisted CVD technique was first fabricated by Ramasamy *et al*. (2011). They used a toluene solution of the diethyldithiocarbamate complexes of Cu, Zn, and an alkyl derivative of Sn. It was observed that the three complexes decomposed in a narrow temperature range of 280-300°C and this enhanced the formation of a single phase of CZTS. The films that were prepared using different substrate temperatures showed varied stoichiometry which made stoichiometric control of the final film difficult. Washio *et al*. (2012) fabricated CZTS films by sulfidazing the oxide of the films which were prepared by open atmosphere CVD. The oxide films were then annealed at a temperature range of 520-560°C in an N_2+H_2S (5%) atmosphere for three hours. The fabricated solar devices which were obtained using these films were found to have a conversion efficiency of 6.03% even though all the results from EDX indicated that the films were having O-Kα peaks. The devices with a compositional ratios of Cu/(Zn + Sn) = 0.78 and Zn/Sn = 1.29 resulted in the most efficient devices.

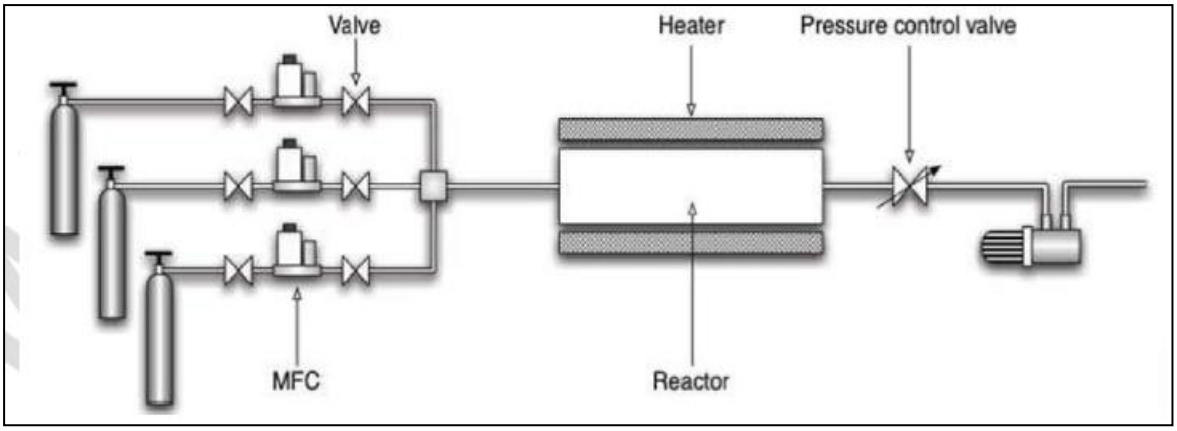

Figure 2.5: Schematic diagram of a typical tube-furnace chemical vapor deposition system (Miao *et al*. 2011)

2.3.2 Solution-Based Techniques

Solution-based techniques are low-cost and are being used as an alternatives to the expensive vacuum-based techniques. These techniques have shown tremendous potential for CZTS processing as detailed below.

(a) Nanocrystal Ink Based Approaches

The first reports on CZTS nanocrystal films were reported in 2009 in three different publications within. From the reports, the synthesized films had varied diameters ranging between 10-20 nm with a band gap of about 1.5 eV (Riha *et al.*, 2009; Guo *et al.*, 2009; Steinhagen *et al*., 2009). Large grained CZTSSe films were obtained by selenization of doctor bladed thin films from CZTS NCs dispersed in hexanethiol at 500°C for 20 min and this resulted in a device with an efficiency of 7.2%. The efficiency of these devices were found to be limited by the presence of a carbon-rich layer at the Mo/CZTSSe interface (Guo *et al*., 2010).

Shi *et al*. (2011) synthesized CZTS nanorods which had a diameter of about 200 nm by making use of template directed synthesis together with metal chlorides, ethylenediamine and sulfur/selenium precursors. For easy extraction of the nanowires, the templates were dissolved using NaOH solution. Lu *et al*. (2011) have synthesized wurtzite phase CZTS nanoprisms and nanoplates by using dodecanethiol instead of oleylamine as capping agent. They found that the

nanocrystals had a band gap of 1.4 eV. Dai *et al*., (2010) varied the stoichiometry of the CZTS nanocrystals which resulted in the variation of films' energy band gap between 1.23 eV and 3.48 eV. They also found that the NC had a diameter of about 3.5 nm and this was independent of stoichiometry.

(b) Spray Pyrolysis

Spray pyrolysis is widely used for fabrication of thin-films because the apparatus used are easy to handle and the fabrication process is simple (Wang and Bell, 2011). Nakayama and Ito (1996) synthesized the first CZTS thin films by spray pyrolysis. They synthesized CZTS thin films by spraying a solution of metal chlorides and thiourea (sulfur source) in deionized water onto soda- lime glass (SGL) substrates at a temperature of 280-360°C and then annealed in an atmosphere of Ar gas containing 5% H_2S at 550^{o}C. The results showed that the as-deposited films were sulphur deficient while the annealed films were stoichiometric. Cu-rich films contained traces of Cu_xS whereas Zn-poor films contained Cu_2SnS_3 impurity phase. Madarasz *et al*. (2011) carried out a study on the thermal behavior of CZTS thin films made by spray pyrolysis. They reported that the formation of precipitate CuCl (thiourea).0.5 H_2O can only be prevented by the use of excess thiourea. Kamoun *et al*.(2007) investigated the influence of substrate temperature on the property of the film by spray pyrolysis. They found that substrate temperature of 340^{o}C produced the best crystallinity of the film as well as improving its optical property. Kumar *et al*. (2009a) using a similar solution system, a single phase of CZTS was achieved by optimizing the process of deposition using a substrate temperature of 370°C and an optimized precursor concentration. They found that the films had a direct band gap of 1.43 eV which is consistent with CZTS and their results showed that a polycrystalline CZTS films with better crystallinity could be obtained in the temperature range of 643-683 K, which was slightly higher than Kamoun's results. In the separate studies, the authors further investigated the effect of starting-solution pH on the growth of Cu_2ZnSnS_4 thin films (Kumar *et al*., 2009b) and copper salt and thiourea concentrations on the formation of Cu_2ZnSnS_4 thin films (Kumar *et al*., 2009c) using the same technique. The interesting bit is that sulphides based secondary phases (Cu_xS or ZnS) were also found in the film. The application of the film in solar cell was not evaluated using the above CZTS films made by spray pyrolysis.

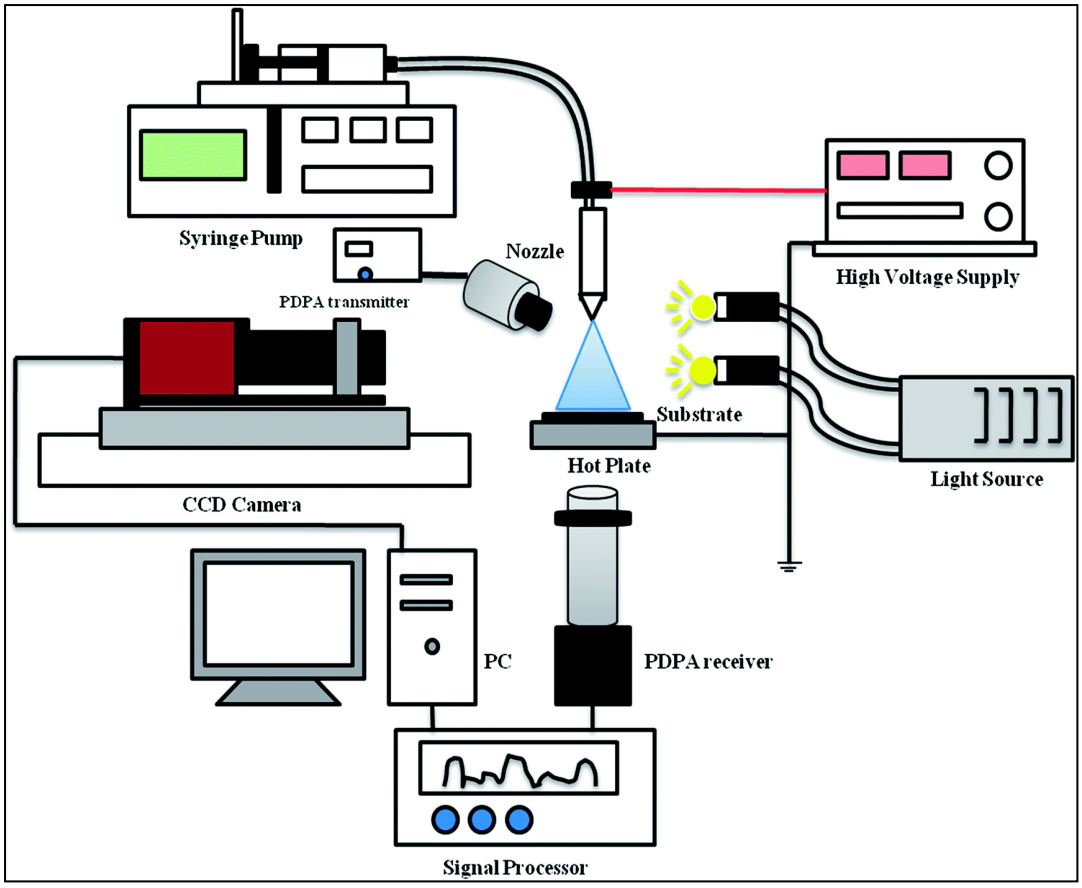

Figure 2.6: Schematic diagram of a typical spray pyrolysis deposition system.

(c) Electrochemical Deposition

Electrochemical deposition technique has been widely used both in research and industrial community to fabricate thin film absorber layer such as CdTe and CIGS cells. Electrochemical deposition will be a cost-effective technique for large-scale fabrication thin film if only all the elements in CZTS can be deposited on the substrate at the same potential. Scragg *et al*. (2008) synthesized the first CZTS films using electrochemical technique by covering the already deposited metal stack of Cu/Sn/Zn with a layer of sulfur then annealing in Ar gas for 2 hours at 550°C. They found that the fabricated solar cells had an efficiency of 0.8%. This efficiency was very low and was found to be due to both high shunt conductance and series resistance. They found that it was still impossible to obtain a pure CZTS film phase using this method despite changing the precursor stoichiometry. The best quality films were obtained when Zn/Sn=1. Annealing in N_2+H_2S (5%) was also found to give larger grains (Scragg *et al*., 2009). In a later study, Scragg *et al*. (2010) improved the process of deposition by using Cu/Sn/Cu/Zn stacks, used a rotating disc electrode for sample deposition and a KCN etch in order to get rid of the Cu_xS phase. This resulted to a solar cell device with an efficiency of 3.2%.

CZTS thin films have also been synthesized by annealing co-electrodeposited Cu-Zn- Sn films in S atmosphere for 2 hours (Araki *et al*., 2009). They found that the films which was slightly Zn-efficient films resulted to a 3.16% efficient solar cell. For the co-electrodeposition, the components were Copper (II) sulphatepentahydrate, zinc sulfate heptahydrate, tin (II) chloride dihydrate and tri-sodium citrate dihydrate. After annealing, there was no presence of phase separation by the co-electrodeposited films. Ennaoui *et al*. (2009) employed the same deposition process used by Araki et al., (2009) and came up a solar device whose efficiency was 3.4% efficient. The Cu-Zn-Sn films were annealed in Ar + H_2S (5%) with a total processing time of 8 hrs, which involved a 2 hr. anneal at 550°C. The device efficiency was limited by the presence of Zn-rich regions (probably ZnS), Zn-deficient regions (probably Cu_2SnS_3), and voids near the Mo/CZTS interface. When the authors studied XRD of the annealed thin films, they found out that there was formation of Cu_2SnS_3 and ZnS which can react to form a single phase CZTS film at a temperature of about 570°C. The formation reactions for Cu_2SnS_3 found to be different for both Cu- deficient and Cu-efficient films.

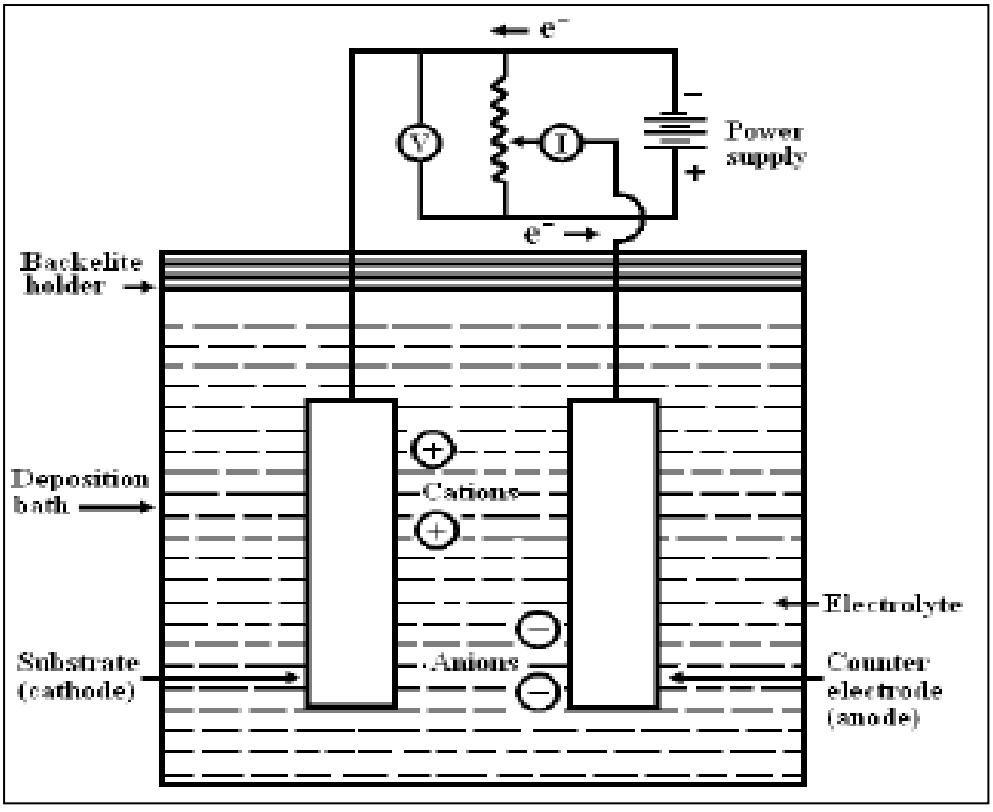

Figure 2.7: Schematic diagram of a typical electrochemical deposition system (Shelke *et al*. 2011).

(d) SILAR Technique

SILAR technique is one of the recent techniques and only a few studies have been reported on the deposition of CZTS thin films using this method. [a]Mali *et al*.,(2012) were the first to report on SILAR grown CZTS thin films. In their study, they used two different solutions to produce CZTS thin films on fluorine doped tin oxide glass substrates which were later on used to investigate the photo-electrochemical conversion (PEC) efficiency of light to electricity. They observed that their best solar cell sample showed V_{OC} of 390 mV, J_{SC} of 636.9μA/cm^2, a FF of 0.62 and a power efficiency of 0.396% under irradiation of 30Mw/cm^2. In another study, [b]Mali *et al*.,(2012) used a similar technique to synthesize novel kesterite Cu2ZnSnS4 nanoflakes. The results revealed that the film was Cu rich and S poor with a total conversion power of the CZTS cell being 1.85% under 30mW/cm^2 illumination.

Patel *et al*., (2014) reported the influence of deposition parameters and annealing on Cu_2ZnSnS_4 thin films grown on glass substrate using SILAR method. The deposition parameters which were varied were number of cycles and precursor concentrations and the samples were annealed at different ambient temperatures in Sulphur and tin sulphide atmosphere. For both sets of precursor concentrations, the CuS and CZTS phase formation were observed to begin simultaneously in the initial phase reaction and the CZTS phase became dominant as the number of cycles increased. A good grain growth was observed when the as deposited films were annealed in the presence of Sulphur and tin sulphide atmosphere. However, the grain size distribution was found to get better in the film annealed in the presence of Sulphur at 500^{o}C.

Kahraman *et al*., (2014) reported CZTS thin films grown on soda lime glass substrates using SILAR technique which was later on sulfurized. In the study, the influence of deposition cycles of layers on the morphological, compositional, structural and optical properties of the samples were investigated. It was observed that the optical absorption coefficient of the films was about 10^4cm^{-1} while the optical band gaps of the films were estimated to be between 1.36 and 1.50 eV. Henry *et al*., (2015) synthesized CZTS thin films using SILAR technique and used the films to investigate the electrical and optical properties of CZTS thin films. The fabricated CZTS films showed good optical absorption coefficient larger than 10^4 cm^{-1} in the visible region with a band gap of about 1.54 eV which is close to the optimum value for solar cell

application. The refractive index was found to be 2.85 while the electrical resistivity of the film samples were found to be in the order of $10^{-2}\Omega$cm at room temperature.

Su *et al*., (2012) fabricated CZTS films by sulfurizing two stacked precursor sulfide layers glass/ ZnS/Cu_2SnS_x via successive ionic layer adsorption and reaction (SILAR). The two stacked precursors were initially synthesized by SILAR technique then later on annealed at 500^{o}C for 30 minutes in sulfur atmosphere. The results revealed that the film thickness of the two samples increased from 340nm to 410nm and 350nm to 420nm after annealing due to an increase in grain size. The thin films also had a kesterite structured CZTS, optical band gap of 1.5eV and p-type conductivity with a carrier concentration in the order of 10^{18} cm^{-3}.

Sakthivel and Baskaran, (2013) carried out a research to fabricate CZTS thin film solar cells using SILAR and spray pyrolysis. They observed that the film samples deposited by SILAR technique achieved an optical absorption coefficient in the order of 10^4cm^{-1} with a band gap of 1.53 eV which is quite close to the theoretical optimal value for a single- junction solar cell. The conversion efficiency of SILAR deposited solar cell was found to be 1.22% with a short circuit current density of 9.28mA/cm^2, open circuit voltage of 0.32V and fill factor of 41% under AM 1.5 (100mW/cm^2). In another study using a similar technique, the same group reported on the influence of number cycles on structural, surface morphology, optical and electrical properties of CZTS thin film solar cells (Sakthaivel and Baskaran, 2013). Results revealed that the as deposited thin film had polycrystalline kesterite CZTS and an increased grain size after a completion of 120. The morphological study showed a compact film with some voids at some places. They also observed that the band gap decreases with an increase in the film thickness which was related to the change in the barrier height of the crystalline film. On the other hand, the film which was prepared at higher thickness exhibited lower conduction due to higher absorption behavior of the material (Sakthaivel and Baskaran, 2013).

Lokhande *et al*., (2011) reported on the photosensitivity of CZTS thin film grown at room temperature by novel chemical method. The as deposited CZTS thin film was annealed at 673K for 3 hours in order to study the effect of annealing treatment on the properties of the material. The film grown on an area of 21cm^2 achieved a film thickness of 2.4µm after 150 SILAR cycles after which the film thickness decreased with further increase in the deposition cycles. The deposition over 21cm^2 was a confirmation to the feasibility of SILAR method for large area deposition. The band gap was observed to decrease from 1.6 to 1.5 after annealing which

is close to the optimum band gap value for solar cell indicating that solar cell is promising for solar cell application.

[a]Suryawanshi *et al*., (2014) reported on the influence of different anionic bath immersion times on the photoelectrochemical performance of CZTS thin films prepared by a modified SILAR sequence. The thin films which were were deposited on the Mo coated glass substrate using SILAR method for 80 cycles were fabricated by sulfurization of the CZTS precursor films under H_2S (5%) + N_2 (95%) atmosphere at 580^oC for 1 hour. The anionic dipping time was varied from 5 to 15 seconds. It was observed that the best PEC of 2.33% with a maximum J_{sc} of 12.88Am cm^{-2}, V_{oc} of 0.42 and FF of 0.43 was achieved with lower value of anionic bath immersion time. Consequently, the best optical direct band gap of 1.52 was also obtained with the dipping time of 5s. In another study, [b]Suryawanshi *et al*., (2014) synthesized a photochemically active CZTS thin films by the sulfurization of stacked Cu_2SnS_3 and ZnS precursor layers at deposited by SILAR technique. The CZTS precursor films were sulfurized at different temperatures ranging from 500 to 575^OC at an interval of 25^OC. The results on the compositional analysis showed that the ratio of Cu/(Zn+Sn) decreases from 0.98 to 0.91 with an increase in the sulfurization temperature though still indicating that the nearly stoichiometric CZTS thin film can be easily achieved. The films sulfurized at 575^OC showed the highest short circuit current density of 8.27 $mAcm^{-2}$with a power conversion efficiency of 1.06%.

It is clear from the literature that kesterite solar cell is the best alternative to CIGS solar cell that stands a chance to compete with silicon solar cell. This is only possible once the optical and electrical characterization is optimized so that best conversion efficiency is achieved.

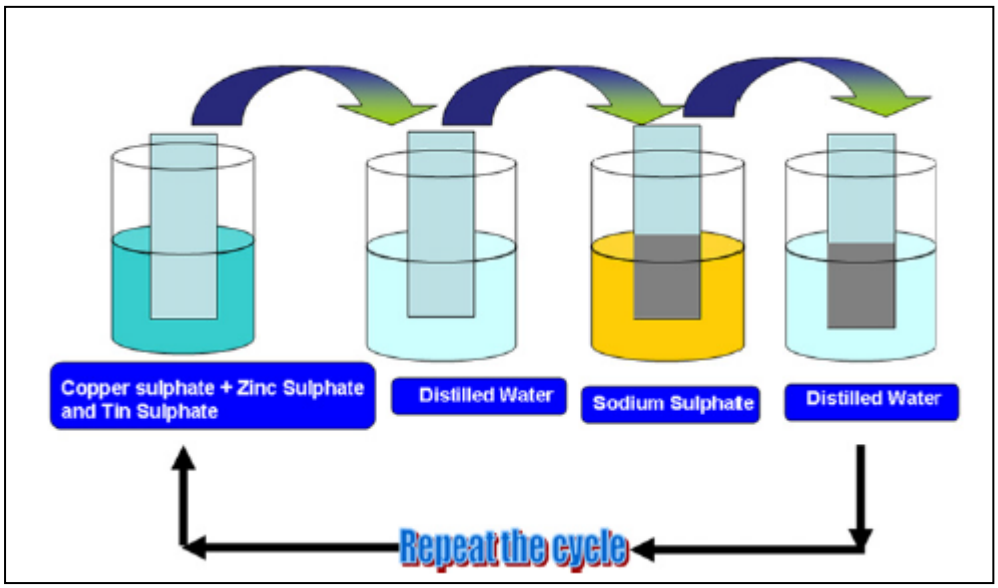

Figure 2.8: Schematic diagram of *SILAR* technique ([a]Mali *et al*. 2012).

2.4: Fabrication of films using successive ionic layer adsorption and reaction process

The Successive Ionic Layer Adsorption and Reaction (SILAR) method is one of the newest technique and is also known as an improved version of Chemical Bath Deposition process. It is a relatively newer and less experimented before. The procedure involves immersion of substrate in cationic and anionic precursor solution and rinsing in deionized water in between them to obtain the growth of desired film. The main difference between SILAR and CBD is growth mode. In CBD technique, all the precursors are present at the same time in the reaction beaker whereas in SILAR technique the substrate is separately rinsed in each precursor and this include immersion in deionized water in between them. As the rinsing isolates the individual steps, the growth of desired film takes place layer by layer. The number of the deposition cycles directly controls the thickness of the film to be produced.

2.4.1 Advantage of SILAR comparing other methods:

SILAR method is simple and it has lot of advantages over other processes. First and foremost, it is one of the easiest method when it comes to the process of doping films of any element by adding proportional amount of the required element in cationic precursor solution. SILAR technique does not require any high-quality target or substrates neither does it require high vacuum at any stage compared to the closed vapour deposition method. Importantly, it is easier to control the thickness of the required films as well as the deposition rate of the film by changing the the number of cycles and rinsing duration. Notably, this method does not result to any kind of local overheating that could be harmful to the deposited materials and there is no any kind of restrictions whatsoever in regards to the substrate material, dimensions or its surface structure.

In addition, the technique is less costly, simple and suitable for large area deposition. The deposition process can be done using locally available materials which are quite affordable. A large number of varied substrates can be deposited since it's a chemical method hence an insoluble surface which can be freely accessed by the solution would stand as a suitable substrate for the deposition to take place. There is minimal possibility for the oxidation or corrosion to take place since the deposition process takes place at room temperature and its easier to obtain stoichiometric films. Last but not least, it is easier to control the preparation

parameters in order to obtain better grain structures because the deposited layers are ions and not atoms.

Generally, this technique has not been extensively used in research as a method of deposition of CZTS thin films therefore there is still limited information regarding this technique. Moreover, most of the reported research on CZTS thin films using *SILAR* technique have carried out their investigation using the ordinary set up and so far no research has been carried out using SILAR Coating system with stirrer equipment. With the ordinary set up, it is easier to lose track of number of cycles and dipping time because of using stop clock as a result of fatigue. This explains why it is not a popular technique when it comes to investigation of CZTS thin films. This equipment makes it easier to optimize the deposition parameter such as adsorption and reaction time hence getting more viable results. With equipment in use, the possibility of optimizing the deposition parameter will make solar cells based on CZTS thin film technologically viable for an economic feasibility study. Optimization of deposition parameters using *SILAR* coating with stirrer equipment to investigate and characterize CZTS thin film as an absorber layer as reported in this work will contribute more to the successful usage of CZTS deposited by *SILAR* technique.

CHAPTER THREE: THEORETICAL BACKGROUND

3.1: Solar spectrum

Solar radiation can be assumed to be radiations from a black body with a temperature T≈ 5800 K (Nelson, 2003). As the sunlight passes through the atmosphere, it is attenuated as a result of scattering and absorption processes. Solar irradiance occurs within a wide range of wavelengths. The loss in spectrum resulting from the atmosphere is measured using a factor called Air Mass factor. Air Mass is the path length which light follows through the atmosphere. This element of spectra is very important in the quantification of reduction in the power of light due to absorption in the atmosphere. The Air Mass is defined using equation below:

$$AM = \frac{1}{Cos(\theta)} \tag{3.1}$$

where θ is the elevation angle of the sun.

The Air Mass is 1 when the sun is directly perpendicular to the Earth's surface. The standard illumination is known to be AM1.5G (the G stands for global) and it corresponds to an elevation angle of 48.2^{o} which has been normalized to give $1Kw/m^2$.

The standard illumination outside the Earth's atmosphere is known as AM0 because the light cannot overcome the atmosphere barrier. AM0 is used to predict the expected performance of solar cells in space while AM1.5G is used to measure the performance of the cells in the laboratories. The figure 3.1 shows a comparison between AM0 and AM1.5G spectra.

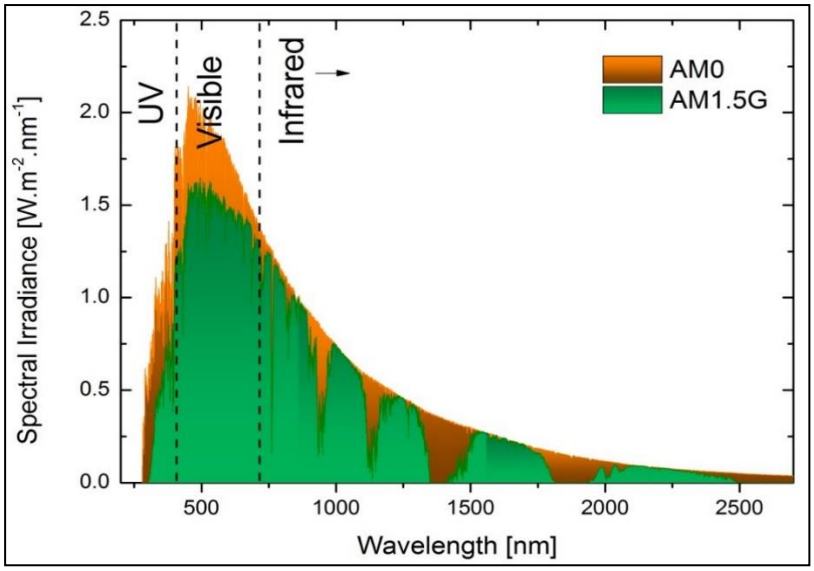

Figure 3.1: Solar irradiance spectrum above atmosphere and at Earth surface (Iqbal, 2012)

An illustration of different solar radiation spectrum is shown in figure 3.2.

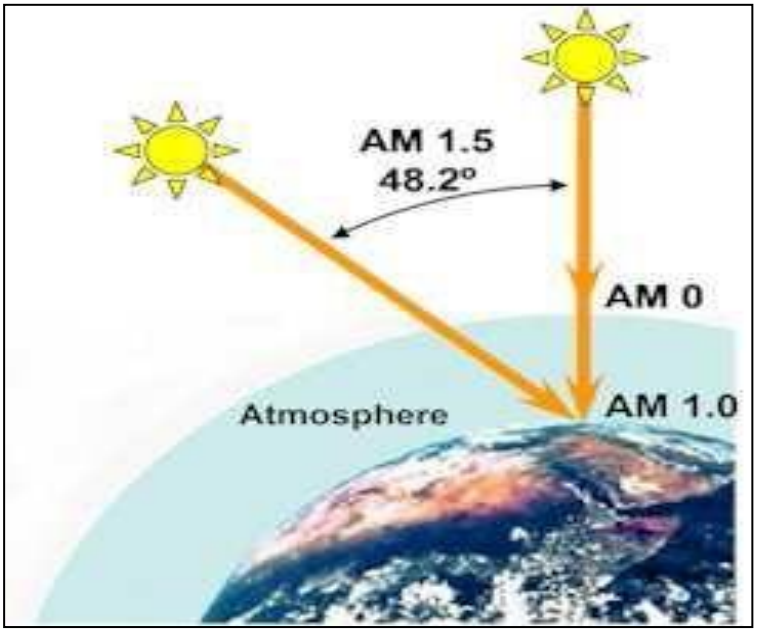

Figure 3.2: Different solar radiation spectrum labeled AM0 in space, AM1 at the earth's surface for normal incidence and AM1.5 at earth's surface, where $\theta = 48.2^{o}$

3.2: Raman Spectroscopy

(a) Raman Theory

Raman spectroscopy is one of the most popular approaches to study the vibrational structures of molecules combined with infrared spectrum**.** Once monochromatic radiation having a wavenumber $\tilde{v}_o$ is incident on a system, majority of it is transmitted without change, and some

of the radiation is scattered. If the frequency of the scattered radiation is analyzed, it will be observed that not only the wavenumber $\tilde{v}_o$ associated with the incident radiation is present, but also, in general, pairs of new wavenumbers of the type $\tilde{v}' = \tilde{v}_o + \tilde{v}_m$. In molecular systems, the wavenumbers $\tilde{v}_m$ are found to lie principally in the ranges associated with transitions between rotational, vibrational, and electronic levels.

The modified frequencies origin, found in Raman scattering is explained in terms of energy transfer between the incident radiation and the scattering system. When a system interacts with radiation of wavenumber $\tilde{v}_o$, it makes an upward transition from a lower energy level E_1 to an upper energy level E_2. It must then acquire the necessary energy, $\Delta E = E_2 - E_1$, from the incident radiation. The energy ΔE is expressed in terms of a wavenumber $\tilde{v}_m$ associated with the two levels involved, where

$$\Delta E = hc\tilde{v}_m \qquad (3.2)$$

This energy requirement is considered to be provided by the absorption of a photon of the incident radiation of energy $hc\tilde{v}_o$and the simultaneous emission of a photon of smaller energy$hc(\tilde{v}_o - \tilde{v}_m)$, so that scattering of radiation of lower wavenumber, $\tilde{v}_o - \tilde{v}_m$ occurs. Interaction of the radiation with the system may alternatively cause a downward transition from a higher energy level E_2 to a lower energy level $E1$, in which case it produces energy

$$E_2 - E_1 = hc\tilde{v}_m \qquad (3.3)$$

Again a photon of the incident radiation of energy $hc\tilde{v}_o$ and the simultaneous emission of a photon of higher energy$hc(\tilde{v}_o + \tilde{v}_m)$, so that scattering of radiation of higher wavenumber, $\tilde{v}_o + \tilde{v}_m$, occurs.

In Rayleigh scattering, even if there is no resultant change in the energy state of the system, the system still participates directly in the scattering act, causing one photon of incident radiation $hc\tilde{v}_o$ to be absorbed and emitted simultaneously in the same magnitude, so that scattering of radiation of unchanged wave number $\tilde{v}_o$, occurs.

In terms of wavenumber, a Raman band is to be characterized not by its absolute wavenumber, $\tilde{v}' = \tilde{v}_o \pm \tilde{v}_m$, but by the magnitude of its wavenumber shift $\tilde{v}_m$ from the incident wavenumber. These wavenumber shifts are known as Raman wavenumbers. It is necessary to

differentiate between Stokes and anti-Stokes Raman scattering, we can define Stokes scattering ($\Delta\tilde{\nu}$) to be positive and anti-Stokes scattering ($\Delta\tilde{\nu}$) to be negative, that is $\Delta\tilde{\nu} = \tilde{\nu}_o + \tilde{\nu}'$as shown in figure 3.3.

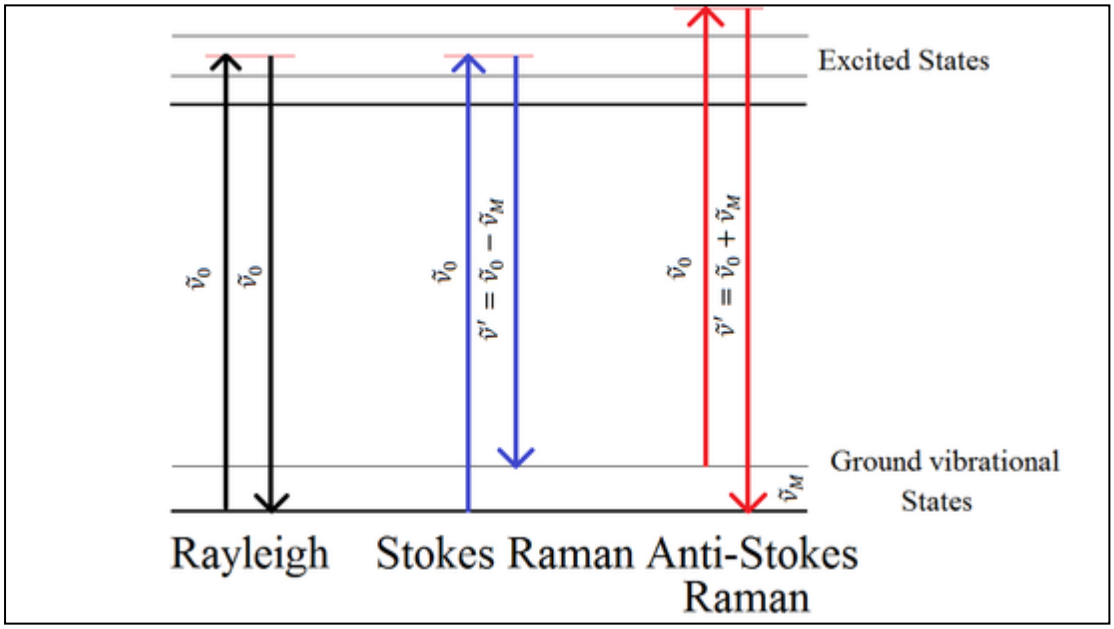

Figure 3.3: An illustration of energy transfer model of Rayleigh scattering, Stokes Raman and anti-Stokes Raman scattering.

The intensity of anti-Stokes relative to Stokes Raman scattering decrease quickly with wavenumber shift increase. This is because anti-Stokes Raman scattering involves transitions from a populated higher energy states to a lower energy state. Raman spectroscopy is employed widely to study the composition and crystal structure of solid and fluid (liquid and gases) samples. This will be used to guide us on the structural properties of CZTS thin films by giving us the different phases of CZTS.

3.3: X-Ray Fluorescence Theory

An electron can be expelled from its atomic orbital (Bohr model of an atom as shown in figure 3.4) by the absorption of a light wave (photon) of sufficient energy. The energy of the photon (*hv*) must be greater than the energy with which the electron is bound to the nucleus of the atom. When an inner orbital electron is ejected from an atom, an electron from a higher energy level orbital will be transferred to the lower energy level orbital.

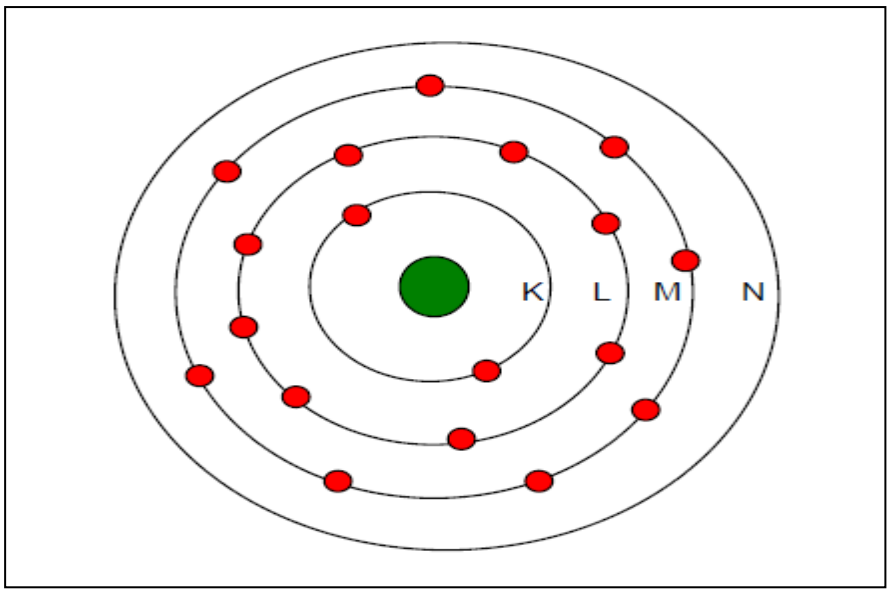

Figure 3.4: Bohr model of an atom.

During this transition a photon maybe emitted from the atom. This fluorescent light is called the characteristic X-ray of the element as shown in figure 3.5. The energy of the emitted photon will be equal to the difference in energies between the two orbitals occupied by the electron making the transition. Because the energy difference between two specific orbital shells, in a given element, is always the same (i.e. characteristic of a particular element), the photon emitted when an electron moves between these two levels, will always have the same energy. Therefore, by determining the energy (wavelength) of the x-ray light (photon) emitted by a particular element, it is possible to determine the identity of that element.

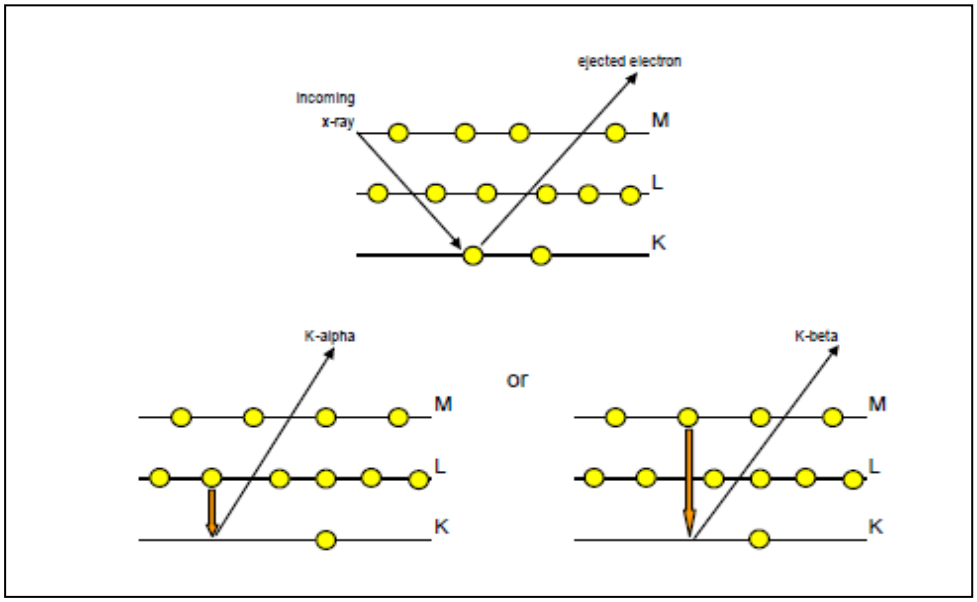

Figure 3.5: A schematic diagram of x-ray fluorescence process

For the characteristic energy (wavelength) of fluorescent light emitted by an element, the peak intensity or count rate is related to the amount of that element analyzed in the sample. The count rates for all detectable elements within a sample, are calculated by counting the number of photons that are detected for the various analyses characteristic x-ray energy lines for a set amount of time. It is important to note that peaks with a semi- Gaussian distribution are observed for these fluorescent lines due to the imperfect resolution of modern detector technology.

Therefore, it is possible to qualitatively establish the elemental composition of the samples and to quantitatively measure the concentration of these elements by determining the energy of the x-ray peaks in a sample's spectrum, and calculating the count rate of the various elemental peaks.

3.4: Spectrophotometry

Spectrophotometry is a method to measure how much a chemical substance absorbs light by measuring the intensity of light as a beam of light passes through sample solution. Every chemical compound absorbs, transmits, or reflects light (electromagnetic radiation) over a certain range of wavelength. Transmittance T, is the fraction of light that passes through the sample and can be calculated using the equation: (Sanda *et al*. 2012)

$$\mathrm{T} = \frac{\boldsymbol{I}_t}{\boldsymbol{I}_0} \tag{3.4}$$

Where I_t is the light intensity after the beam of light passes through the sample and I_o is the light intensity before the beam of light passes through the sample. Transmittance is related to absorption by the expression: (Sanda *et al*. 2012)

$$Absorbance = -\log(T) = -\log\left(\frac{\boldsymbol{I}_t}{\boldsymbol{I}_o}\right) \tag{3.5}$$

Where absorbance stands for the amount of photons that is absorbed.

The total intensity of light falling on a sample is represented by the following equation

$$\text{Total Intensity} = \text{transmittance} + \text{absorbance} + \text{reflectance} \tag{3.6}$$

The total intensity represents 100% of the light from the light intensity thus the above equation can apply.

3.5: Optical and Electrical Characterization

a) Optical band gap

This is the energy difference between the top of valence band and the bottom of the conduction band. The fundamental absorption that corresponds to electron excitation from the valence band to conduction band can be used to determine the value of optical band gap. The relationship between the absorption coefficient, α, and the incident photon energy, hν, can be written as (Bag *et al*., 2012);

$$\alpha h\nu = A\left(h\nu - E_g\right)^n \qquad (3.7)$$

Where A is a constant n is a number related to the electron transition process, E_g is the band gap, $h\nu$ is the photon energy and α is the absorption coefficient. The value of n can be 2 and 2/3 for direct allowed and forbidden transitions respectively. Also, the value of n can be taken as 1/2 and 1/3 for indirect allowed and forbidden transitions. A graph of $(\alpha h\nu)^2$ versus hν or$(\alpha h\nu)^{\frac{1}{2}}$ versus hν for direct or indirect band gap respectively, is always used so as to determine the band gap.

b) Optical reflectance

Reflectance is the percentage measure of the ratio of the intensity of incident light to that of the reflected light. While using a spectrophotometer for its measurement, incident light of known wavelength is directed on the surface of a thin film and the intensity of the reflected light measured. The two intensities, that is, the incident light intensity and reflected light intensity are compared in a reference called the reflectance, (R), as given by the equation below;

$$R = \frac{I_R}{I_0} \times 100\% \qquad (3.8)$$

Where, I_0 and I_R are intensities of incident and reflected beams respectively.

c) Optical transmittance

Transmittance is the percentage measure of the ratio of the transmitted photon to that of the incident photon. Photons of selected wavelengths and beam intensity, I_0 (photons/cm^2), are directed at the thin film of thickness, *d*, and relative transmission is observed. For accurate

measurement of the band gap, $E_{g,}$ photons with energies less than the band gap do not excite electrons in the valence band to the higher states, hence are transmitted while those photons with energies greater than the band gap, excite the electrons in valence band to higher energy states and therefore are absorbed. The relationship is shown in the equation below:

$$T = \frac{I_t}{I_0} \times 100\% \qquad (3.9)$$

Where, I_t is the intensity of the transmitted photons and I_0 is the intensity of the incident photons.

d) Optical Absorption

The nature of the band gap E_g is a vital element in photon absorption. There are two types of bang gaps namely direct and indirect band gaps. A direct band gap material involves elevation of electrons across the gap if the photon energy is greater than band gap energy ($E_{photon} \rangle E_g$) while for an indirect band gap material, lattice vibration is involved in the transition process in order to conserve the momentum k. When the two kinds of band gaps are compared, the absorption probability is much higher for direct band gap material than in indirect band gap materials (Fahrenbruch and Bube , 2012). A thickness $1-3\mu m$is required for a direct band gap to absorb most of the available solar spectrum while $20-50\mu m$is required in the case of an indirect band gap material for the same to happen. (Fahrenbruch and Bube , 2012). Figure 3.5 below shows diagrams of direct and indirect band gap transition.

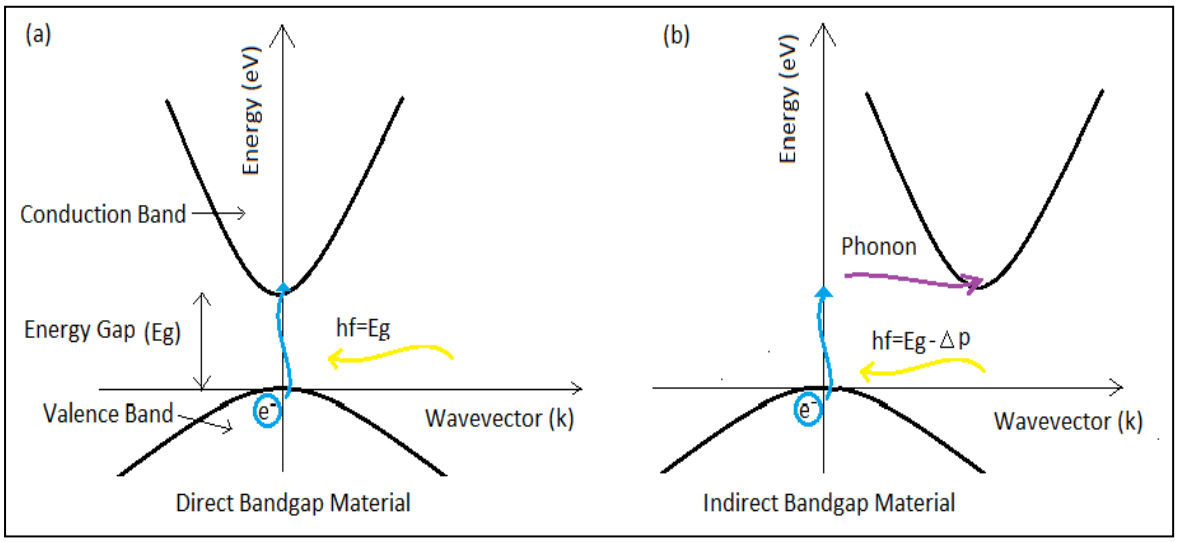

Figure 3.6: The direct (a) and indirect (b) band gap transitions in semiconductors (Kittel,1986)

e) Sheet Resistance

The sheet resistance and bulk (volume) resistivity of materials used in the semiconductor industry and in materials science is measured using four-point probe instrument. This instrument uses a long-established technique to measure the average resistance of a thin layer or sheet by passing current through the outside two points of the probe and measuring the voltage across the inside two points. If the spacing between the probe points is constant, and the conducting film thickness is less than 40% of the spacing, and the edges of the film are more than 4 times the spacing distance from the measurement point, then the average resistance of the film or the sheet resistance is given by the formulae below (Bishop, 2011)

$$R_S = 4.53 \times \frac{V}{I} \tag{3.10}$$

The relationship between thickness of substrate in cm, sheet resistance and its resistivity in ohms is given below (Bishop, 2011):

$$R_S = \frac{Re\,sistivity}{Thickness} \tag{3.11}$$

From the above relation, one can calculate the resistivity of the film when the thickness is known or may calculate the thickness when the resistivity is known. Figure 3.8 shows a schematic diagram of a 4-point probe configuration. As shown in the figure, the separate current and voltage electrodes are used to eliminate the contact resistance between the electrodes and the material. Furthermore, in the case of thin films, the distance between the two probe(s) is very high compared to the film thickness (d) hence equation 3.11 above can be used to determine sheet resistance.

Consider a regular 3-d conductor shown in the figure 3.7;

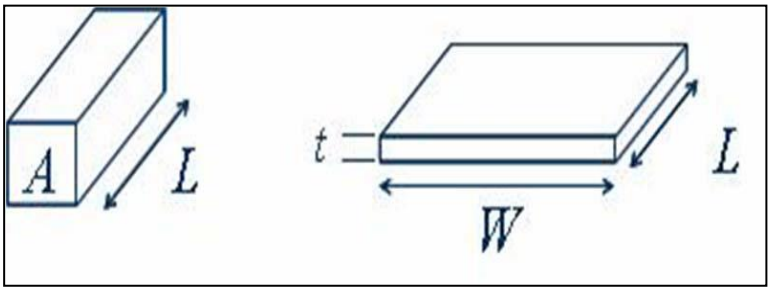

Figure 3.7: Regular 3-D conductor

Resistance *R* is given by;

$$R = \rho \frac{L}{A} = \rho \frac{L}{Wt} \tag{3.12}$$

Where ρ is the resistivity (Ω·m), *A* is the cross-section area, and *L* is the length. For *A* in terms of *W* and *t*, thus resistance can be re-written as;

$$R = \frac{\rho}{t} \frac{L}{W} = R_s \frac{L}{W} \tag{3.13}$$

Where R_s is the Sheet Resistance. Units are ohms, but can also express this as ohms per square, or Ω/□ or Ω/sq.

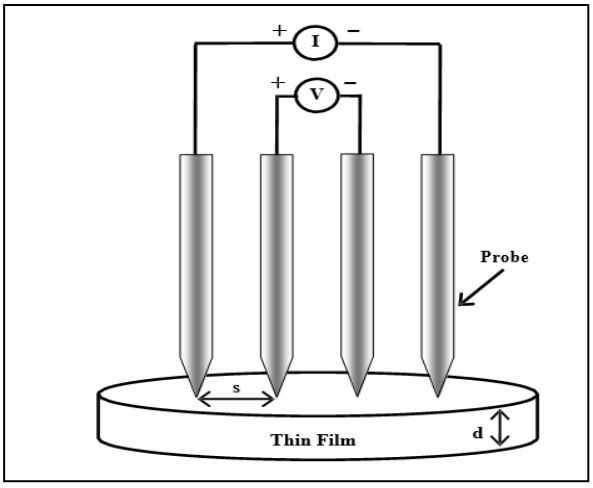

Figure 3.8: Schematic of 4- point probe configuration

When dealing with a bulk sample whose thickness d >> s, where *s* is the probe spacing, a spherical current from the outer probe tips can be assumed and the resistance can be obtained using the differential equation below:

$$\Delta R = \rho \left(\frac{dx}{A}\right) \tag{3.14}$$

where *ρ* is the resistivity, *dx* is the differential length and *A* is the surface area penetrated by the current from one probe.

To determine the resistance between the voltage measurement tips, one integrates between two defined points like x_1 and x_2:

$$R = \int_{x_1}^{x_2} \rho \frac{dx}{2\pi x^2}\Big| = \frac{\rho}{2\pi}\left(-\frac{1}{x}\right)\Big|_{x_1}^{x_2} = \frac{1}{2s}\frac{\rho}{2\pi} \tag{3.15}$$

Superposition of current at outer two tips leads to R = $\frac{V}{2I}$, so that

$$\rho = 2\pi s\left(\frac{V}{I}\right) \tag{3.16}$$

For a thin film sample (thickness d << s), we have the case of current rings, so that A = 2πxt
Thus the resistance is:

$$R = \int_{x_1}^{x_2} \rho \frac{dx}{2\pi xt} = \int_{s}^{2s} \rho \frac{dx}{2\pi xt} = \frac{\rho}{2\pi t}(\text{In } x)|_{s}^{2s} = \frac{\rho}{2\pi t}\text{In } 2 \tag{3.17}$$

Superposition of current at outer two tips leads to $R = \frac{V}{2I}$, so that the sheet resistivity for a thin film sample is:

$$\rho = \frac{\pi t}{\text{In } 2}\left(\frac{V}{I}\right) \tag{3.18}$$

When the expression is not dependent on s, ***Sheet Resistivity*** is defined as:

$$R_s = \frac{\rho}{t} = k\left(\frac{V}{I}\right) \tag{3.19}$$

Where *k* is a geometric factor, which for a semi-infinite thin film is $\frac{\pi}{ln\,2} = 4.532$. This equation is in agreement with the first equation.

CHAPTER FOUR: MATERIALS AND METHODS

4.0 Overview

This chapter presents the methodology used in preparation and characterization of copper zinc tin sulphide (Cu_2ZnSnS_4) thin films. The chapter begins by describing the equipment used in sample preparation. It also outlines the substrate preparation before it was used in the deposition process. This chapter goes ahead to describe the sample characterization, electrical and optical measurements and finally it describes the methods used for data analysis.

4.1 Sample Preparation and Thin Film Deposition Process

4.1.1 Cleaning of glass substrate

Preparation of the substrates is extremely important for obtaining reproducible results**.** The substrate used in this study consisted of Fluorine doped Tin oxide (FTO) glass substrate measuring 20.0 mm × 35.0 mm. Prior to deposition, the substrates were thoroughly cleaned in order to remove dust, organic substances and any contaminants that could have been present on the surface. At first, a mixture of de-ionized water, liquid detergent and sodium hydroxide was made in the ratio of 3:2:1 respectively. The mixture was poured inside a wash bottle and the bottle was shaken thoroughly until foam was formed. The foam was applied to a cotton swab which was then used to scrub both sides of the glass substrate. The foam was thereafter removed by drag wiping the substrate using a lens cleaning tissue which was folded severally and held at an angle of 45.0 degrees. The glass substrate was again cleaned by drag wiping it using a wet lens cleaning tissue that at one edge with isopropyl alcohol. This was followed by another process of drag wiping the substrate using a new set of lens cleaning tissue that was wetted at one edge with acetone. The substrates were then ultrasonically cleaned with double distilled water for 30.0 minutes. Thereafter, the glass substrates were then blown dry using pressurized argon gas.

4.1.2 Preparation of precursor

The precursors that were prepared were the cationic and anionic precursor solutions. The cationic precursors were prepared from the chloride salts of copper, zinc and tin while the anionic precursor was prepared from sodium sulphide. These precursor chemicals were locally sourced and had purity of 99.9% weight. A mass of 1.363g of zinc chloride was weighed to make a solution of 0.1M. Similarly, a mass of 3.506g $SnCl_4$ was weighed to make a solution

of 0.1M and finally a mass of 1.705g of $CuCl_2$ was weighed to obtain a solution of 0.1M. The three solutions were then mixed in a beaker of 250ml. The anionic precursor solution was then prepared by weighing a mass of 0.780g of Na_2S to obtain a solution of 0.1M.

4.2 Fabrication of CZTS using *SILAR* technique

CZTS was fabricated from the precursor composed of $CuCl_2$, $ZnCl_2$, $SnCl_2$ and Na_2S using concentrations of the above precursors placed in beakers. The cleaned substrates are then successfully dipped into the beakers with the solutions beginning with cationic precursor containing a mixture of $CuCl_2$, $ZnCl_2$ and $SnCl_4$ then followed by dipping in distilled water to remove the loosely attached ions. After this, dipping is done in the anionic precursor of Na_2S then distilled water again and the cycle is repeated for the required number of cycles as shown in Fig 4.1 below.. The dipping duration was set to 10 seconds in every beaker containing the precursor to allow for adhesion of ions to the substrate.

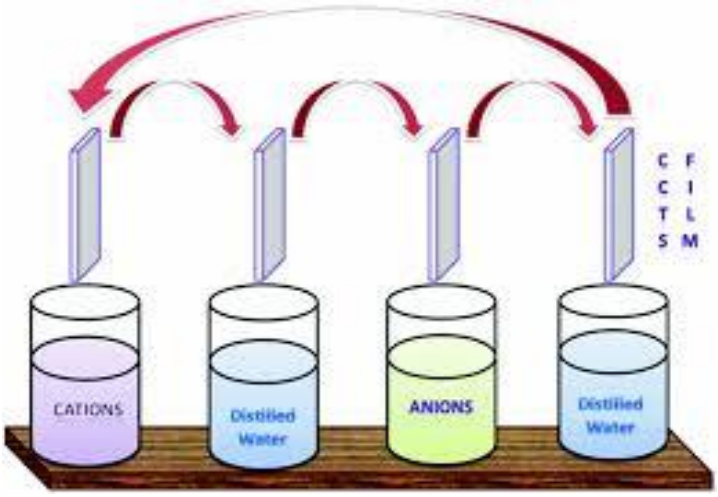

Figure 4.1. Schematic representation of successive ionic layer adsorption and reaction (SILAR) method.

The deposition of CZTS thin film was carried out using *SILAR* coating system HO-TH-03 (Holmarc Opto- Mechatronics Pvt Ltd, India) shown in Figure 4.2. SILAR coating system with stirrer is equipped with several components including substrate holder, heater plate, temperature controller, key pad, LCD display, stirrer and control box. The control box and the SILAR unit are the main functional unit of the SILAR coating system with stirrer. Prior to deposition, different parameters were set depending on the required specification and this was done on the LCD display in the control box. The beakers containing solutions solvents were

placed on the heater plates and the clean substrates were mounted firmly on to the system using substrate holder by inserting the substrates between the plates. The temperature of 27 ± 1^{o}C was set in the temperature controller for all the beaker. The number of cycles was varied between 20 and 70 in an interval of 20, 40, 60 and 70. After the number of cycles, the deposited film was left to dry for 40 minutes under normal room temperature and pressure conditions (25.0^{o}C, 100kpa).

Figure 4.2: SILAR coating equipment

The deposition parameters were set as follows;

Table 4.1: SILAR coating parameters used

Parameter	Values
Start position	3 mm
Dipping length	50 mm
Dip speed	9 mm/s
Retrieval speed	9 mm/s
Dip duration	10 seconds
Dry duration	5 second
Rotation speed	30 deg/s
Stir speed	200 rpm
Stir duration	5 seconds
Number of cycles	20,40,60,70.

The reaction mechanism in the *SILAR* process is as follows:

$$CuCl_2 + H_2O \longrightarrow Cu^{2+} + 2Cl^- + H_2O \quad (4.1)$$

$$ZnCl_2 + H_2O \longrightarrow Zn^{2+} + 2Cl^- + H_2O \quad (4.2)$$

$$SnCl_2 + H_2O \longrightarrow Sn^{2+} + 2Cl^- + H_2O \quad (4.3)$$

$$Na_2S + H_2O \longrightarrow 2Na^+ SH^- + OH^- \quad (4.4)$$

$$SH^{--} + OH^- \longrightarrow S^{2-} + H_2O \quad (4.5)$$

$$2Cu^{2+} + Zn^{2+} + Sn^{2+} \longrightarrow Cu_2{}^{2+}Zn^{2+}Sn^{2+}(aq) \quad (4.6)$$

$$Cu_2{}^{2+}Zn^{2+}Sn^{2+} + 4S^{2-} \longrightarrow Cu_2ZnSnS_4(S) \quad (4.7)$$

4.2.1 Annealing of CZTS thin film.

The sulphurization set up consisted of a horizontal Pyrex glass tube placed in the Labtech tube furnace. The chamber was purged with nitrogen gas flowing for 10.0 minutes as shown in Figure 4.3. This was done to eliminate oxygen in the system. 200.0g of high purity Sulphur powder (99.9% weight) was loaded in a crucible and the crucible was placed in a tube furnace. This was done to provide the Sulphur source environment. Dry nitrogen flown at 10 SCCM was used as the carrier gas for the Sulphur vapour. The samples were loaded into the tube furnace before the nitrogen gas was purged. The temperature of the tube furnace was raised to 150.0 ^oC in 5 minutes and then raised in interval of 50.0 ^oC with a temperature gradient of 10.0 ^oC per minute until the desired annealing temperature was reached, that is, 450^oC and 550^oC respectively When the annealing temperature was attained, the temperatures were left to stabilize at the desired value for 30.0 minutes. The thin films were then left to cool with the purging gas being supplied at a constant flow rate of 10 SCCM.

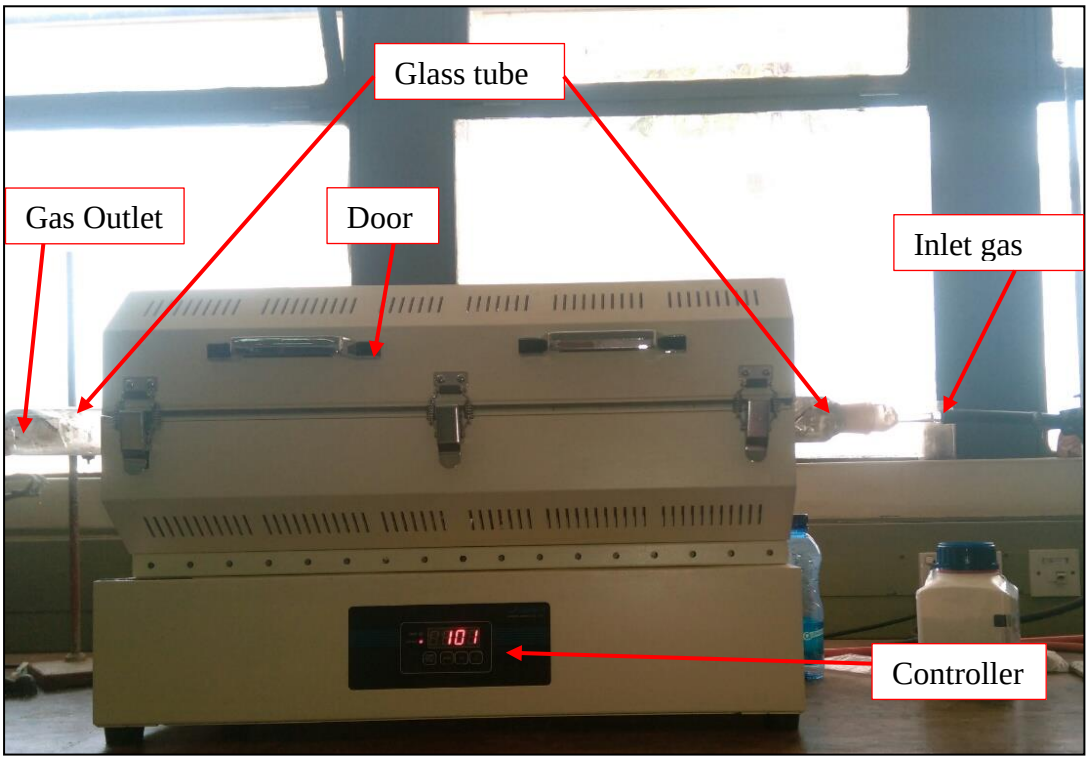

Figure 4.3: Labtech tube furnace

4.3 Sample Characterization

4.3.1 Film Thickness Measurement

The film thickness of CZTS samples were determined using KLA -Tensor Alpha step IQ surface profiler shown in the figure 4.4 below.

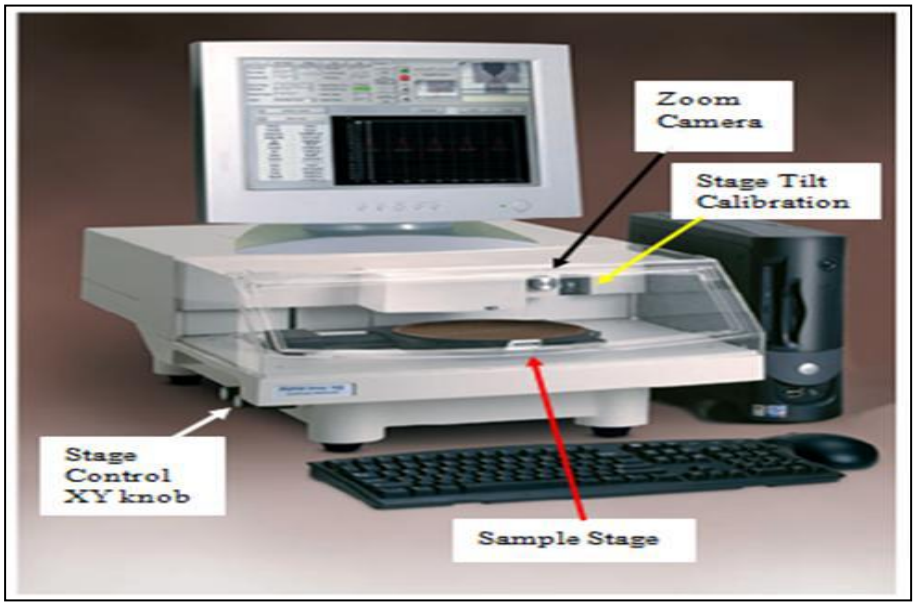

Figure 4.4: KLA tencor alphastep surface profilometer

This equipment is a stylus -based surface profile that is used to measure step heights between 100 angstroms to 2mm. A Teflon label tape was removed from the surface of the substrate to reveal the step and the glue leftovers were thoroughly cleaned using Ethanol. Before scanning the sample surface, the scanning parameters were specified first. The scan length, scan speed, sampling rate and sensor range were 500.0 µm, 50 µm/sec, 50.0 Hz and 400.0 µm/23.8 pm respectively. The film thickness was directly read out as the height of the step-contour trace. For accuracy, five scans in different positions along the sample surface near the step were performed and averaged to give average thickness values.

4.3.2 Electrical Characterization

Electrical resistivity measurement was carried out using Jandel RM3-AR four point probe shown in the figure 4.5. The instrument calibrates itself when it is switched on. To confirm the results, a 100 Ω test resistor sample was used to further calibrate it. This was done by setting current at 1.0 mA and then applying the set current in the forward bias. The expected voltage value was 100.0 mV. Instead readings of 99.9 and 100.1 mV were obtained, giving us an accuracy of 0.1% of the expected value. When the reverse bias was applied, the same value was obtained with a negative sign. This meant that the equipment was in good condition and was ready to measure the actual samples. The four point probe was then connected by removing the 100 Ω resistor test sample. Then the actual CZTS thin film samples were measured by feeding in a current of 1.0 mA and using the forward bias position. The values of sheet resistance and measured voltage were taken after a stabilization time of 10 mins.

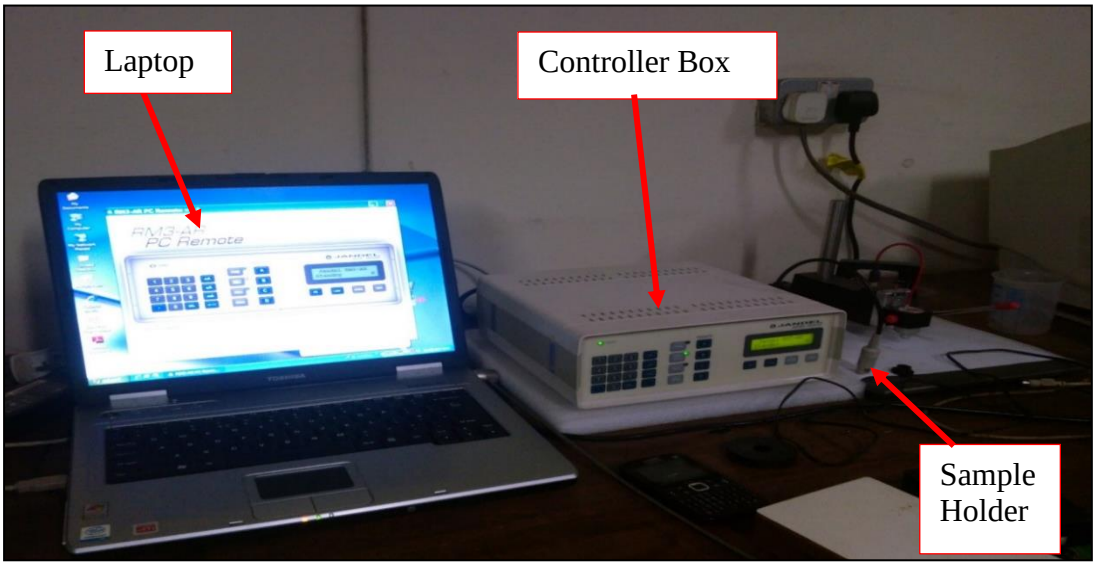

Figure 4.5: Jandel sheet resistance equipment

4.3.3 Optical Characterization

4.3.3.1 Transmittance and Reflectance Measurement

The transmittance and reflectance spectral measurements were done using a Shimadzu UV-VIS-NIR SolidSpec-3700 DUV spectrophotometer (figure 4.6). The spectrophotometer consists of a light source, a sample holder and three detectors; a photomultiplier tube (PMT) detector for ultraviolet and visible region and InGaAs and PbS detectors for near infrared region. The spectrophotometer was connected to a data acquisition computer. The equipment has three sample holders in different positions, one for transmittance, another for absorbance and the other for reflectance. The sample holder is located between the light source and the detectors. The light source, detectors and sample holder are designed to fit within a dark box that has a cover to prevent unwanted light interfering with the light source (50 W halogen lamp, 2,000 hours life and deuterium lamp, 300 hours life) during experimentation. The equipment employs the integrating sphere method. In transmittance measurements, samples were irradiated at or near normal incidence. The reflectance measurements were carried out under an incidence angle of 90^{o}. Two hours warm up of the equipment was the first procedure before actual measurements could be done to improve the accuracy of the measurements. The spectrophotometer was allowed to create a baseline prior to sample scanning. The spectral transmittance/reflectance measurements were in the $200 < \lambda < 2500$ nm wavelength range. The optical measurements of transmittance and reflectance were recorded by the computer using Shimadzu UV Probe software and these data were later used for analysis.

Figure 4.6: Shimadzu UV-VIS-NIR double beam 3700 DUV spectrophotometer

4.3.4 Raman Characterization of CZTS thin films

Raman spectroscopy measurement was performed using confocal laser Raman spectrometer (STR Raman Spectrum System, Seki Technotron Corp) equipped with a 785nm laser excitation with a diameter ≈ 7.0 µm spot size. Prior to the measurements, the set up was first calibrated to known Si peak at 520.7 cm^{-1}. In order to obtain all the CZTS peaks, the Raman spectra recorded was centred at 1,100.0 cm^{-1} and 5 spectra were taken from different parts of both the as deposited and annealed samples deposited with 70 cycles each. The average of the 5 spectra was obtained so as to get a single spectrum. Fifteen seconds of exposure time was used on each sample for measurement for 5 scans in order to reduce fluorescence and noise in the spectra. The number of accumulations was set to 15 and then this was followed with the collection of data. The Raman spectroscopy was performed on the samples so as to investigate the phase purity of the samples. The obtained data were then transferred to OriginPro 2016 64 Bits software for graphing.

4.3.5: Compositional Analysis using XRF

Compositional analysis of the CZTS sample was done using S1 Titan Bruker handheld X-ray fluorescence (XRF) instrument. The instrument generates x-rays which are focused on to the sample and has a SDD detector to detect the characteristic fluorescence emission from the sample to determine the chemical composition.

CHAPTER FIVE: RESULTS AND DISCUSSION

5.1 Optical Properties of CZTS films

The optical properties of CZTS thin films were studied on the basis of transmittance and reflectance measured using Shimadzu UV-VIS-NIR SolidSpec-3700 DUV spectrophotometer. The data were recorded in the wavelength range of $300 \leq \lambda \leq 900$ at room temperature. From this measurement the energy band gap was calculated.

5.1.1 Effect of Dipping cycles on film Thickness

Figure 5.1 shows the variation of film thickness with dipping cycles for the four samples of the as deposited CZTS thin films with different number of dipping cycles from 20 cycles to 70 cycles. It is observed from the figure that the film thickness increased nearly linearly with increase in dipping cycles.

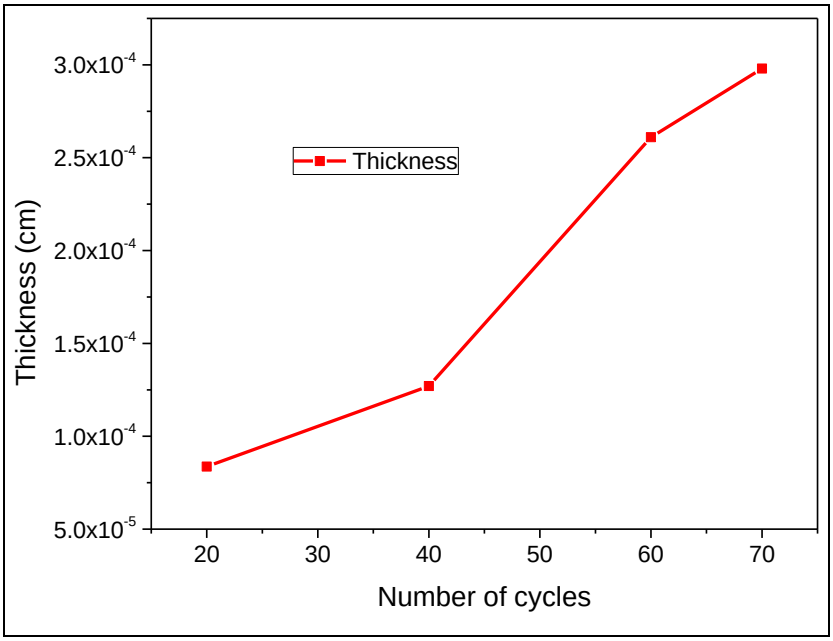

Figure 5.1: variation in film thickness with number of dipping cycles for as deposited CZTS thin film samples

A similar trend in variation was reported earlier by Shinde *et al.*, (2012). This could be attributed to an increase in the size of crystals in the film samples as the number of cycles increases. The slight variation from the linear behavior could be attributed to the growth by nucleation and coalescence process. This is because, more nucleation sites contribute to coagulation during the growth procedure (Lokhande *et al.*, 2011).

For a CZTS thin film to be used as an absorber layer in a solar cell, the thickness should be more than 1.0 µm for sufficient absorption of light (Yu *et al*., 2014). From the data, the film thickness was in the range of 0.837 - 2.98 µm. The film samples that were formed with 20, 40, 60 and 70 cycles attained a thickness of 0.837, 1.27, 2.61 and 2.98 µm respectively. Beyond 70 dipping cycles, the samples peeled off indicating that 70 cycles was the optimum dipping cycle. The peeling off phenomena could be attributed to the formation of outer porous film which may result in the development of stress causing delamination leading to peeling off of the film after the film reaches its maximum thickness (Lokhande *et al.,* 2011). A report by Shinde *et al*., (2012) and Lokhande *et al.*, (2011) indicated that they were able to obtain a maximum thickness of 1.94 µm and 2.4 µm at 100 and 130 cycles respectively.

5.1.2 Effect of Dipping Cycles on Transmittance and Reflectance

5.1.2.1 As-Deposited

Figure 5.2 (a) shows the spectral transmittance curves with wavelength of the four samples of the as deposited CZTS. It is evident that spectral transmittance of the CZTS thin film samples decreases with increase in the number of cycles. The 0.837 µm thick samples obtained with 20 cycles had the highest transmittance value with a peak of about 75% while the 2.98 µm thick samples obtained with 70 cycles has the lowest transmittance value with a peak of about 50%. The samples with 40 and 60 cycles has transmittance peaks of about 65% and 60% respectively. It can also be observed from the graphs that the spectral transmittance increases from 300 nm to 800 nm (UV and visible regions) then there is a slight decrease between 800 nm and 900 nm (NIR region). Consequently, the oscillations at wavelengths between 400 and 700 nm is observed which could be arising due to interference and reflectance.

Figure 5.2 (b) shows the reflectance spectra graphs of samples with 20, 40, 60 and 70 number of cycles as-deposited CZTS thin film. It is observed from the graphs that an increase in the number of cycles leads to a decrease in the reflectance. The sample with 20 cycles show some ripples in the reflectance spectra which could be attributed to optical interference effects. This phenomenon is missing in thicker films which could be due to increased grain size with increase in film thickness hence resulting to higher scattering of light. The thin films with 70 cycles showed low values of reflectance coupled with decreased values of transmittance (figure 5.2) within the visible range which makes this sample best suited for an absorber layer in the solar cell application. This is because a low transmittance and reflectance would result to high absorption of photon energy as illustrated in figure 5.11.

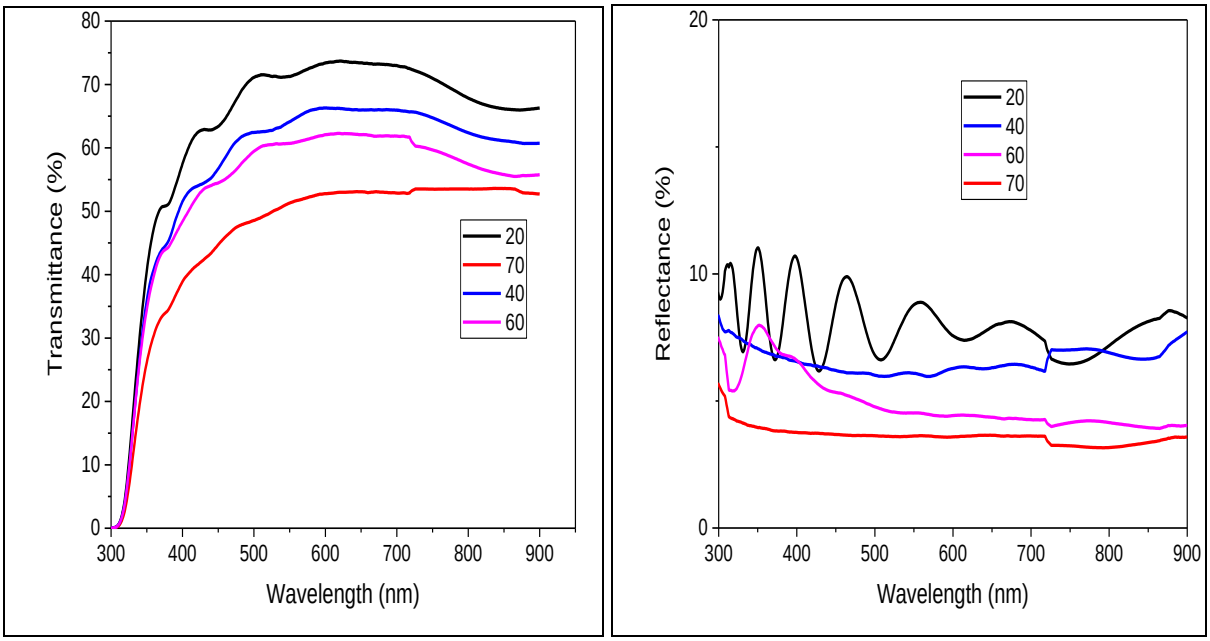

Figure 5.2: variation of Transmittance and reflectance spectra for as-deposited CZTS thin film samples with dipping cycles (a) Transmittance and (b) Reflectance

Figure 5.3 (a) shows variation of transmittance spectra with the film thickness for the as deposited samples in the visible region at 650nm and 826nm. From the graph, it is observed that the transmittance decreases with increase in the thickness of the film. It is also evident that the transmittance is higher at 650 nm compared to 850 nm. These observations can be attributed to an increase in the absorption of light energy in both cases. Maximum absorption of photon energy is evident in the thickest film sample which is at 2.98μm. This is because, the transmittance value is almost the same both at 650 nm and at 826 nm.

Figure 5.3 (b) shows variation of reflectance spectra with the film thickness for the as deposited samples in the visible region at 650.0 nm and at 826.0 nm. The same trend observed on the transmittance curve is noticeable. An increase in the film thickness results to a decrease in the reflectance value. The CZTS film sample which attained 2.98 μm has the lowest reflectance value of about 3% within the visible region. In general, the decrease in film transmittance and reflectance can be explained as being due to surface roughness which results to more scattering of light. This particular sample has a potential of being used as an absorber layer in the solar cell because of its low transmittance and reflectance value within the visible region since these aspects will ensure that most photon energy is absorbed.

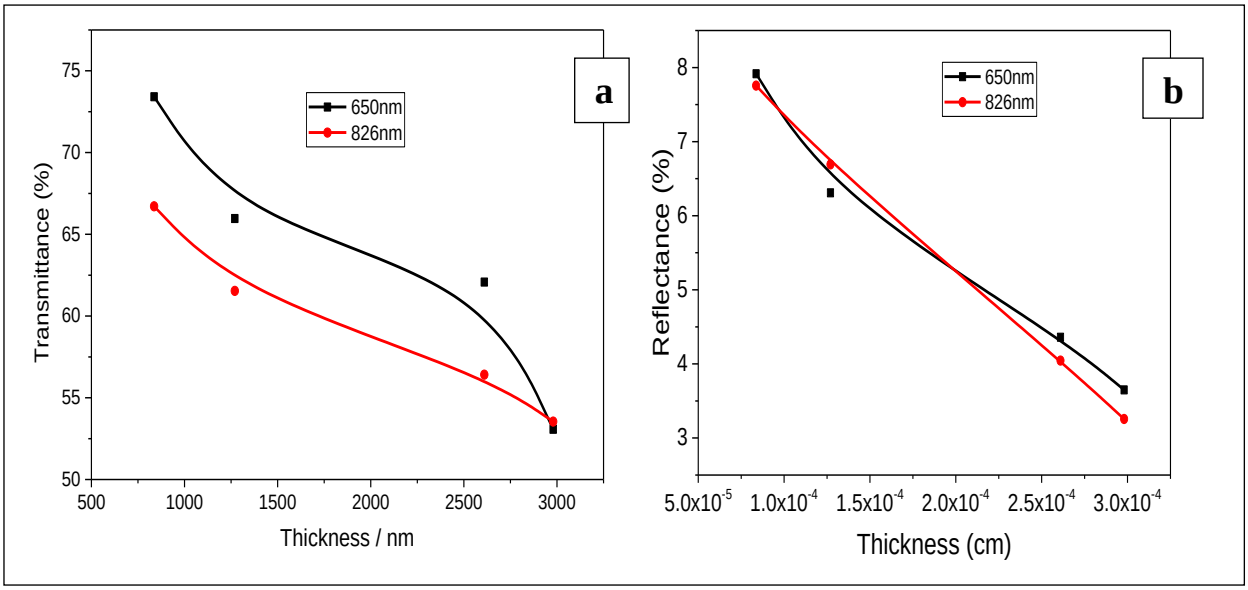

Figure 5.3: Variation of Transmittance and reflectance spectra with different film thickness at 650nm and 826nm for as deposited CZTS thin film samples (a) Transmittance and (b) Reflectance

5.1.2.2 Annealed at 450^{O}C

Figure 5.4 (a) shows the transmittance spectra of CZTS annealed at 450^{o}C in a Sulphur rich environment. It is noted that an increase in the number of cycles results to a decrease in the transmittance of the thin film. The same trend was noted with the as deposited thin film samples. Despite having the same trend as the as deposited samples it is seen that there is a decrease in the transmittance when annealing is done at 450^{o}C. The sample with 20 cycles still depicts high transmittance of about 55% and this is a decrease from 75% while the sample with 70 cycles has the lowest transmittance with a peak of about 30%, a reduced value from a peak of about 50%. Samples with 40 and 60 cycles has a transmittance value of about 45% and 40% respectively and when it is compared to the as deposited sample the value has decreased by 20%. This decrease in transmittance value could be due to improved film crystallinity. The spectral transmittance in the graphs increases both in the UV and visible region (300-800nm) then decreases slightly in the NIR (800-900nm).

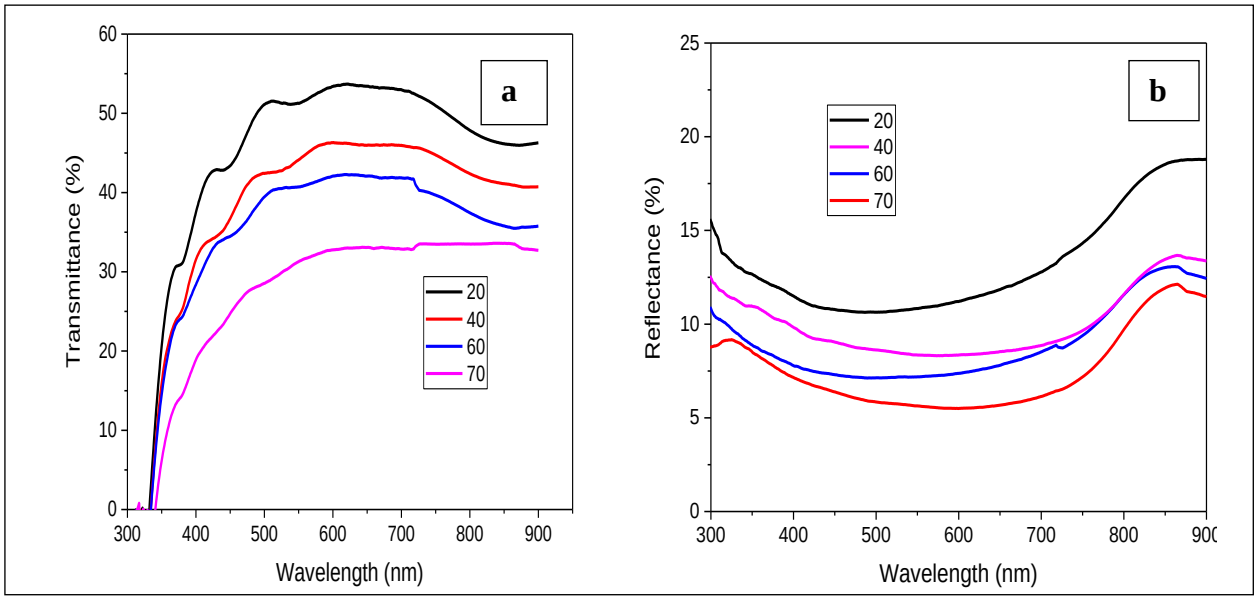

Figure 5.4: Transmittance and reflectance spectra showing the different number of cycles of CZTS thin film samples annealed in sulfur rich atmosphere at 450^{o}C (a) Transmittance and (b) Reflectance.

In Fig 5.4 (b) it's evident that the reflectance spectra of the CZTS samples annealed at 450^{0}C is in the same range as that of the as deposited samples, with the same trend followed as in the as deposited samples for the visible wave length region (380 -780) nm. Also noted is an increase in reflectance in the ultraviolet region (200-380) nm compared to the as deposited reflectance spectra which shows low values of transmittance in this region. The sample with 20, 40, 60 and 70 cycles have an increased reflectance value of about 18%, 25%, 35% and 50% respectively when it is compared to the as deposited reflectance values in the ultraviolet region. The reflectance value is expected to decrease with an increase in the annealing temperature as a result of improved crystallization and reduced surface roughness. On the contrary, it is observed that the reflectance of the film has increased instead with an increase in temperature. This can be attributed to high (increased) scattering of light on the samples compared to the as deposited samples. Another possible reason could be that the samples experience the presence of coherence between the primary light beam and the beam reflected between the film boundaries which is lost and in turn results in the disappearance of interference which results to a decrease in the transmittance (Abdullahi *et al*.,2017).

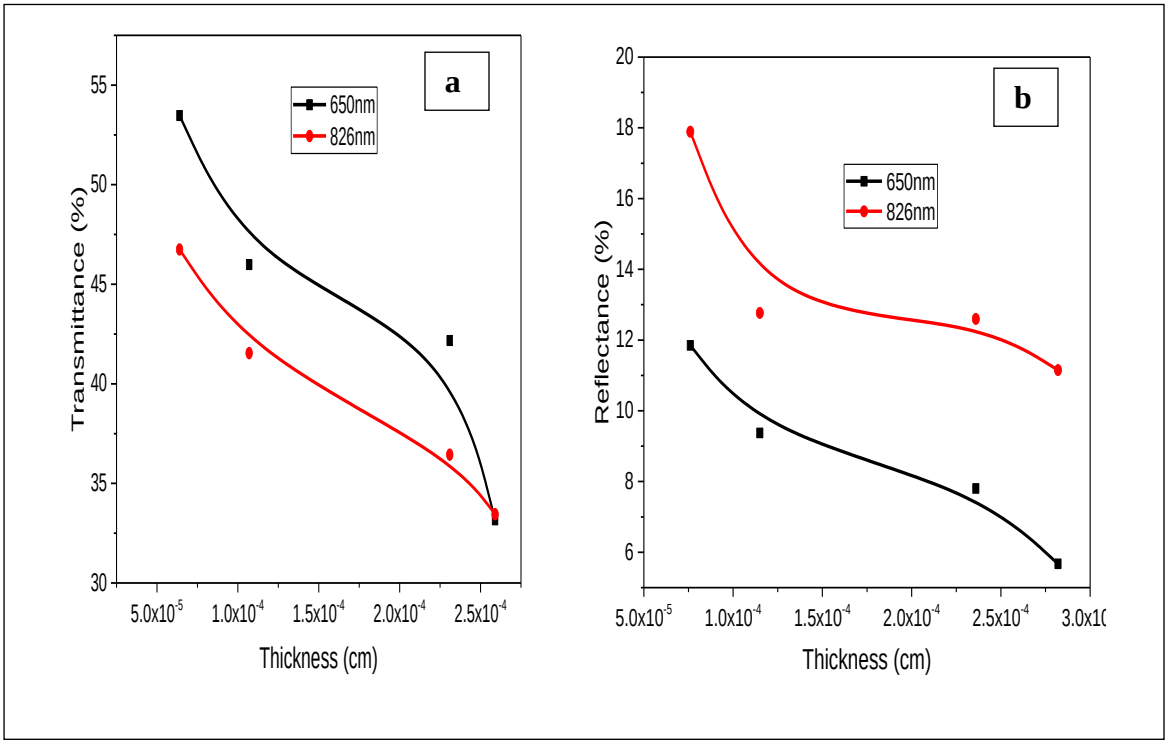

Figure 5.5: Variation of Transmittance and reflectance spectra with different film thickness at 650nm and 826nm for CZTS thin film samples annealed at 450^{o}C (a) Transmittance and (b) Reflectance

Figure 5.5 (a) shows the variation of transmittance spectra with the film thickness and an increase in the film thickness led to significant decrease in the transmittance value both at 650nm and 826nm. The same trend was observed in figure 5.5 (b) whereby an increase in the film thickness resulted in a decrease in the reflectance value of the CZTS thin film sample. The film sample with the highest thickness value of about 2.59µm had the lowest transmittance and reflectance value. This shows that the film with the highest film thickness had the best potential to be used as an absorber layer in solar cell application.

5.1.2.3 Annealed at 550^{O}C

From figure 5.6(a) it's evident that there was a further reduction in the transmittance values as the annealing temperature was increased from 450^{o}C to 550^{o}C and this implies that annealing at 550^{0}C improves the absorber properties of CZTS especially in the visible wavelength region (Chan *et al*. 2010). This improvement could be due to improved crystallinity, homogeneity and compact surface morphology (Tao *et al*., 2014).

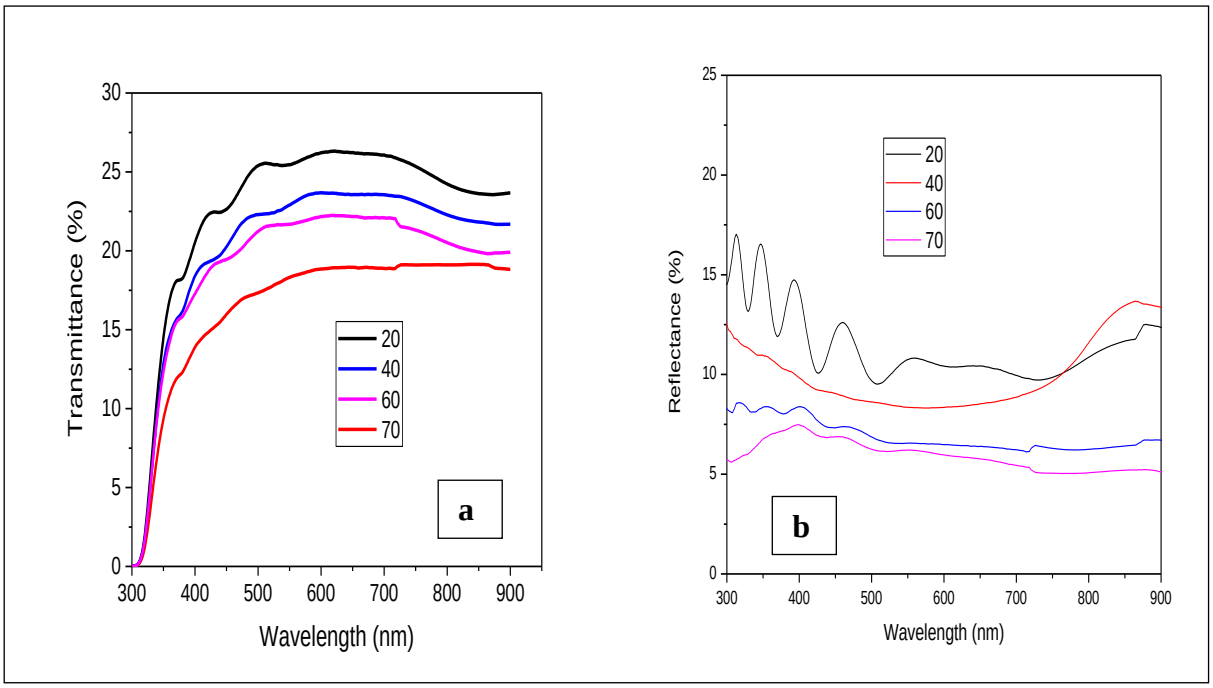

Figure 5.6: Spectral transmittance showing the different number of cycles of CZTS thin film samples annealed in sulfur rich atmosphere at 550^{o}C (a) Transmittance and (b) Reflectance.

The above improvement is also favored by the reflectance spectra (figure 5.6 (b)) since the same trend and almost same range values have been noted for as deposited, annealed at 450^{o}C and annealed at 550^{o}C samples. The 450^{o}C and 550^{o}C annealed samples shows a similar behavior of reflectance in the UV region of the spectra.

Generally, the sample with 70 SILAR cycles stand out as the best sample to be used as CZTS thin film absorber layer due to low transmittance (Islam *et al*., 2015) and low reflectance value. This is because from the relation A+T+R= 100% when is applied to the results above in figure 5.8, the absorbance of sample with 70 dipping cycles is observed to be more than 50% hence making it the best sample for solar cells application.

Figure 5.7 (a) shows variation of transmittance spectra with different film thickness at 650nm and 826nm for the CZTS thin film samples when they were annealed at 550^{o}C. The same trend is still observed whereby an increase in film thickness led to a decrease in the transmittance value both at 650nm and 826nm region.

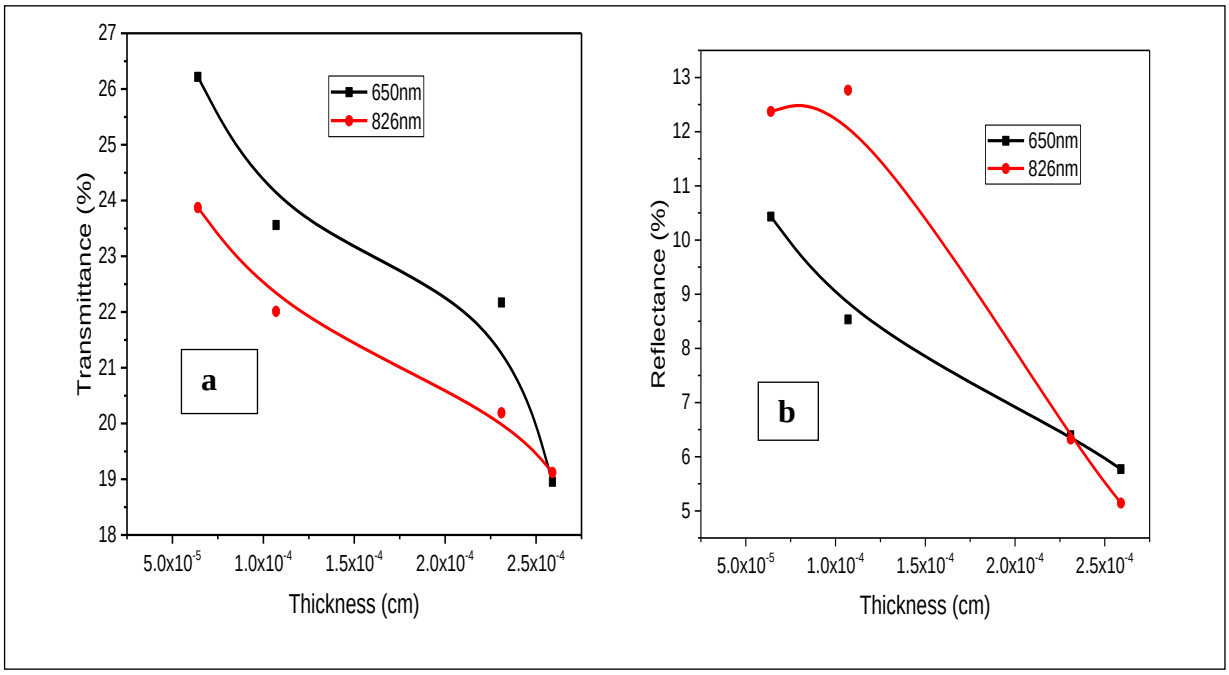

Figure 5.7: Variation of Transmittance and reflectance spectra with different film thickness at 650nm and 826nm for CZTS thin film samples annealed at 550^{o}C (a) Transmittance and (b) Reflectance

There is also a decrease in the transmittance value at 826nm region compared to 650nm region and this shows that there is more absorption of photon energy at 826nm than at 650nm. The lowest transmittance can be noticed at appoint where the film is much thicker which is 2.59µm indicating that the peak of photon absorption is enhanced at this particular thickness

Figure 5.7 (b) shows the variation of reflectance spectra with the film thickness of the samples. Generally, an increase in film thickness results to a decrease in reflectance value both at 650nm and 826nm region. However, a slight increase in the reflectance percentage can be observed as the light energy moves from 650nm to 826nm when the thickness increase from 0.64µm to 2.31µm and then a significant decrease is observed when the film gets to 2.59µm. The reflectance value is lowest when the film thickness is 2.59µm confirming that maximum absorption of photon happens at this point. Generally, the reflectance value is lower due to higher surface roughness which arises as a result of larger grain size. The larger grain size due to better nucleation process during annealing process (Nadi *et al.*, 2014). Consequently, from the relation A+T+R = 100%, it can be observed that from the results in figure 5.7, the Absorbance value for the film sample with 2.59µm thickness is higher due to low transmittance and reflectance hence the best sample for solar cell application.

5.1.3 Effect of Annealing on Film Thickness

Figure 5.8 shows the comparison of variation in film thickness with the number of cycles as-deposited and after annealing in a sulfur atmosphere at various temperatures. It is observed that there is a reduction in the film thickness with increasing annealing temperature. This decrease in film thickness can be attributed to densification/thermally initiated evaporation of the CZTS thin film during heating making them more compact. Thermal agitation during heating in the furnace results to the rearrangement of the CZTS lattice hence leading to a decrease in the film thickness (Nadi *et al*., 2014).

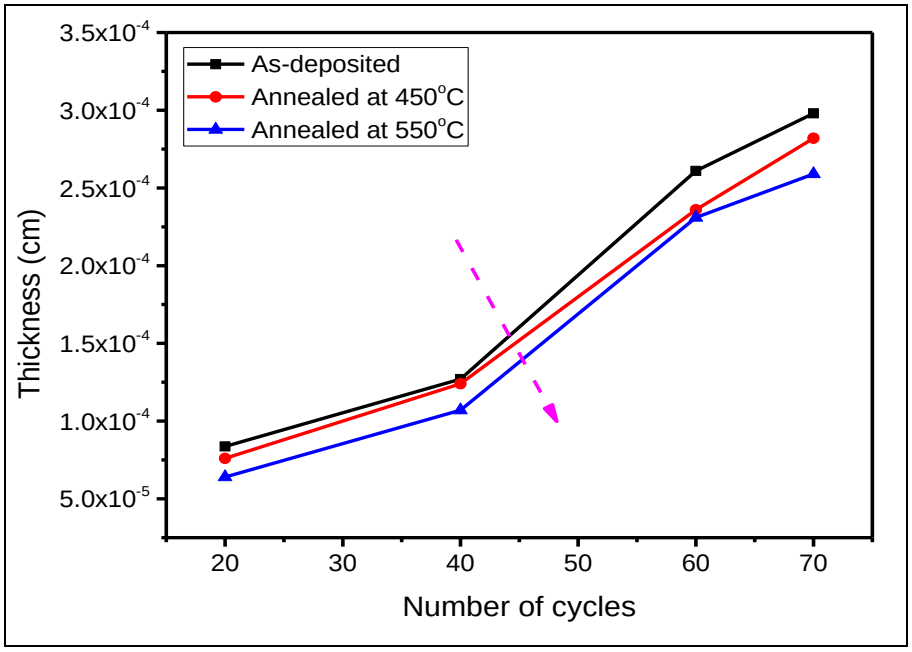

Figure 5.8: Thickness variation with the number of cycles for CZTS thin film samples As-deposited, annealed in sulfur atmosphere at 450°C and at 550°C

5.1.4 Effect of Dipping cycles on Transmittance and reflectance for annealed samples

Figure 5.9 (a) shows change in transmittance for the CZTS thin film samples as-deposited, annealed in sulfur atmosphere at 450°C and 550°C deposited with 20 cycles dipping. It is observed that there is a decrease in the spectra transmittance with an increase in annealing temperature. The as deposited sample has got the highest transmittance value of about 75%. When the sample was subjected to annealing at 450°C in a sulfur atmosphere, the transmittance value reduced to about 50% and further annealing at 550°C lead to a further reduction in spectra transmittance of about 25%. The same trend is observed in figure 5.9 (b) that shows a change in transmittance for the CZTS thin film samples as-deposited, annealed in sulfur atmosphere at 450°C and 550°C deposited with 70 cycles dipping. The as deposited film sample has the highest spectra transmittance value of about 55% followed by the sample annealed at 450°C

with a transmittance value of about 35% and finally the film sample that was annealed at 550°C has the lowest transmittance value of about 19%. The decrease in spectra transmittance can be attributed to an improve film crystallinity and homogeneity that leads to improved formation of CZTS film (Pawar *et al*., 2010).

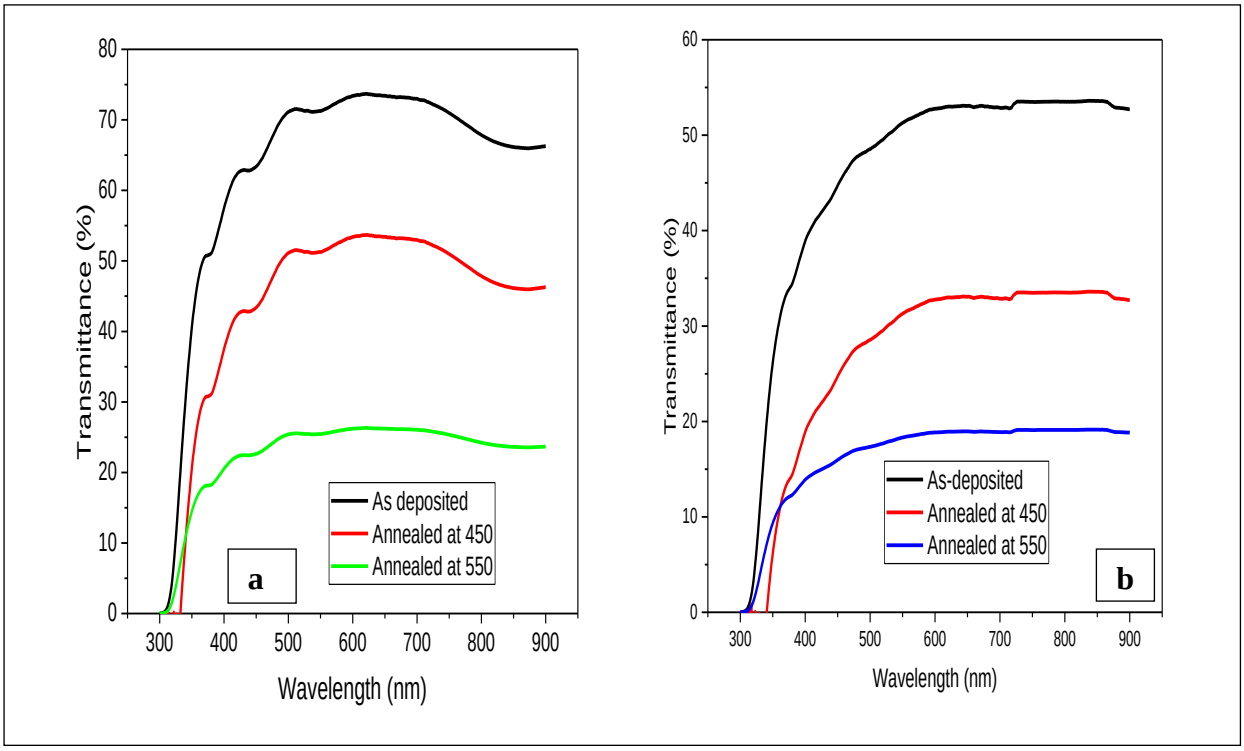

Figure 5.9: Change in transmittance for CZTS thin film samples As-deposited, annealed in sulfur atmosphere at 450°C and at 550°C (a) deposited with 20 cycles and (b) deposited with 70 cycles.

Figure 5.10 (a) shows change in reflectance for CZTS thin film samples deposited with 20 cycles dipping. It can be noted that the as deposited sample has the lowest reflectance value. Slight increment in the reflectance value of about 5% after annealing in the sulfur atmosphere at 450°C and 550°C is observed. A similar trend is observed in figure 5.10 (b) which shows a change in reflectance for CZTS thin film samples deposited with 70 cycles dipping. There is a slight increment of about 5% of the reflectance value after annealing in a sulfur atmosphere at 450°C and an increment of about 2.5% after annealing in 550°C. Generally, the reflectance value for both thin film samples after annealing in 450°C and 550°C is still low hence making CZTS thin film a potential material to be used as an absorber layer in a solar cell. This is

because from the relation A+T+R = 100%, the absorbance value is high when both the reflectance and transmittance is low resulting to maximum absorption of photon energy.

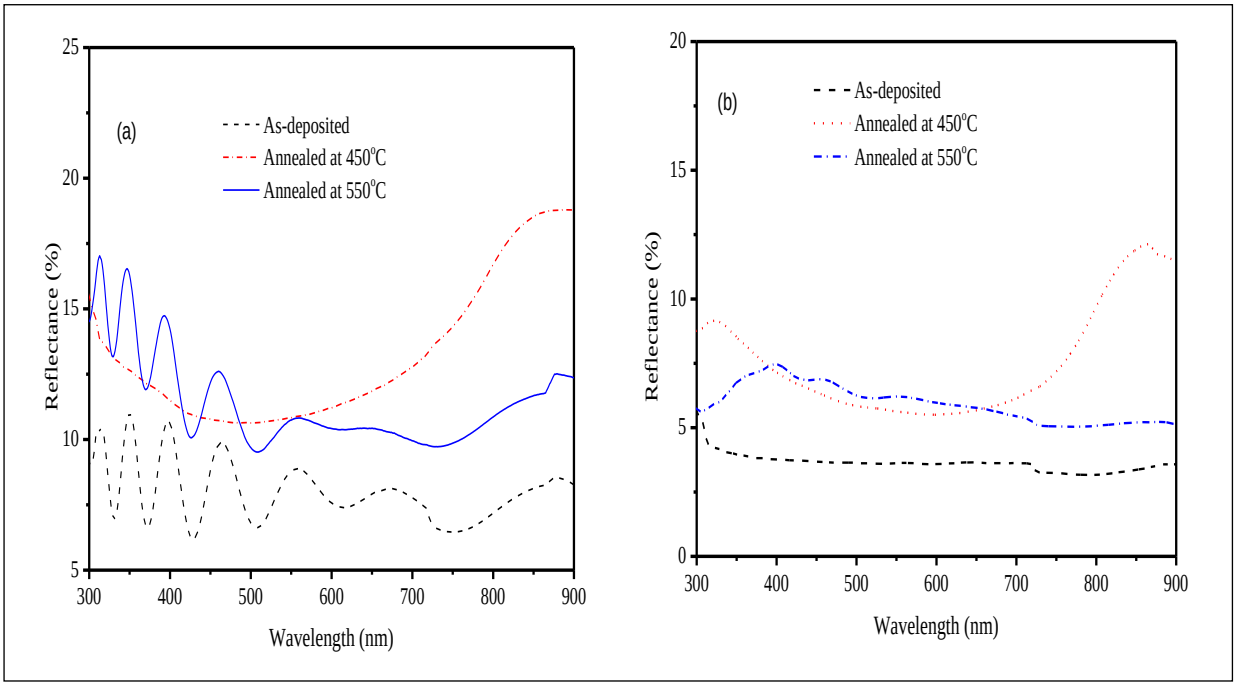

Figure 5.10: Change in reflectance for CZTS thin film samples as-deposited, annealed in sulfur atmosphere at 450°C and at 550°C (a) deposited with 20 cycles and (b) deposited with 70 cycles.

5.1.5 Optical Absorption Coefficient

The optical absorption coefficient (α) of CZTS thin film samples were calculated using the equation (Adelifard, 2015)

$$\alpha = \left(\frac{1}{t}\right) ln\left(\frac{(1-R)^2}{T}\right) \qquad 5.1$$

where t is the film thickness, R is the reflectance and T is the transmittance (Khalkar *et al.*, 2013). Figure 5.11 shows graphs of absorption coefficient for the as deposited CZTS thin film samples. It can be observed that the sample that was deposited with 20 cycles has lowest absorption coefficient followed with the sample with 40 cycles. The samples with 60 cycles had the highest absorption coefficient in this category with the order of up to 10^5 cm^{-1} after the sample with 70 cycles which has an absorption coefficient of up to the order 10^4 cm^{-1}. This is to the contrary to the expected observation in which the sample with 70 cycles is expected to have the highest absorption coefficient based on the reflectance and transmittance results as shown in figure 5.2. This can either be attributed to the presences of some water content in the

sample since it is not yet annealed which could be missing in the sample with 60 cycles hence a decrease in the absorption coefficient.

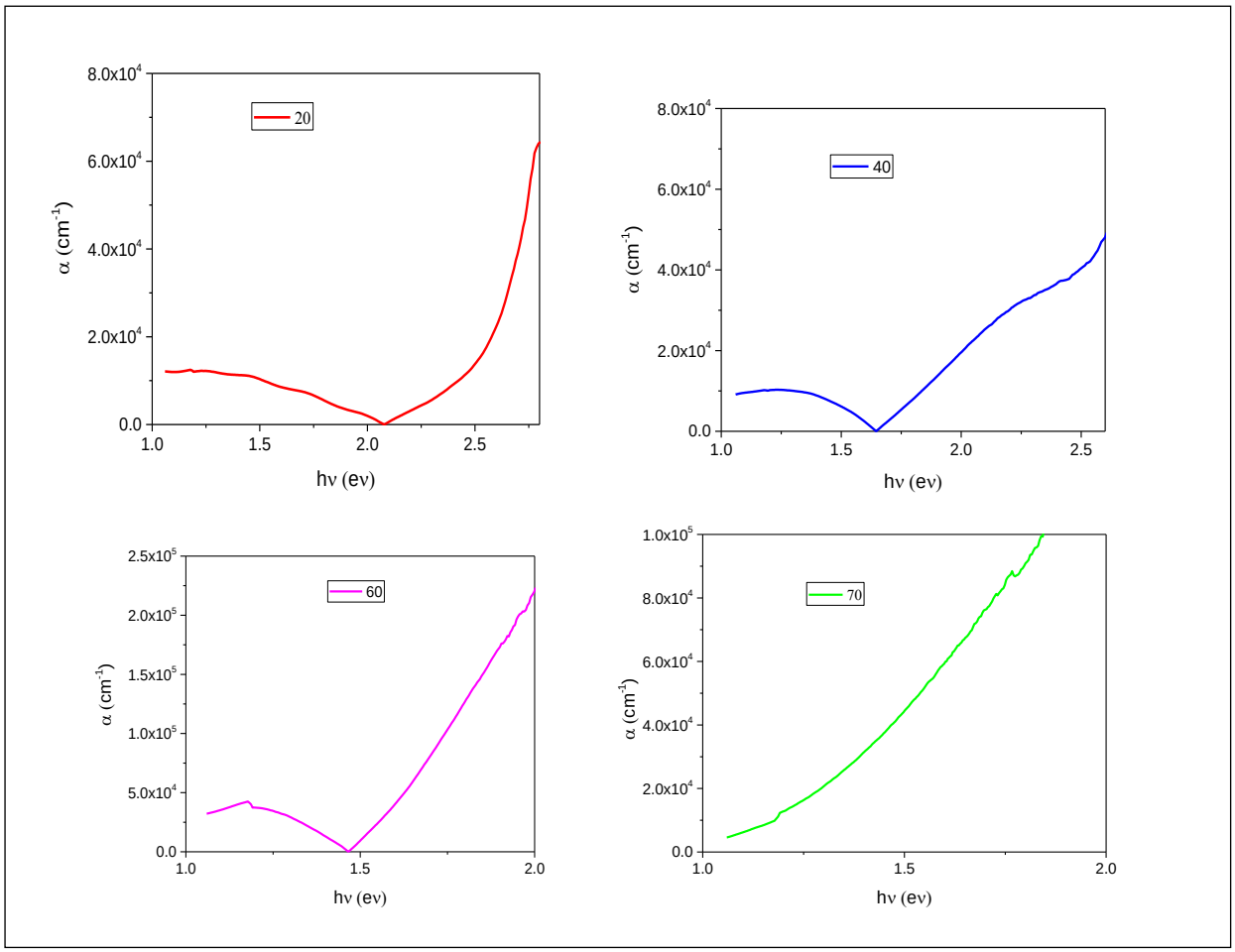

Figure 5.11: Absorption coefficient of the as-deposited CZTS thin film samples

Figure 5.12 (a) shows the variation of the absorption coefficient with photon energy for as prepared CZTS thin film samples annealed at 450^{o}C at various dipping cycles while Figure 5.12 (b) shows the same effect for the samples annealed at 550^{o}C. It is observed that the absorption coefficient increases with an increase in the number of dipping cycles with the sample with 70 cycles having the highest absorption coefficient values for given photon energy. This observation is clearly illustrated in Figure 5.13. The absorption values in figure 5.12(b) are of the order 10^4 cm^{-1} and it is on the increasing trend for all the samples. This observation is in good agreement with the literature reported earlier ([a]Mali *et al.*, 2012). From Figure 5.12(b), it is observed that the absorption coefficient increases with annealing temperature. The absorption coefficient value is in the range of 10^4-10^5 cm^{-1}. This can be attributed to improved

crystallinity that has led to decreased transmittance values hence improving the absorption properties of the film samples.

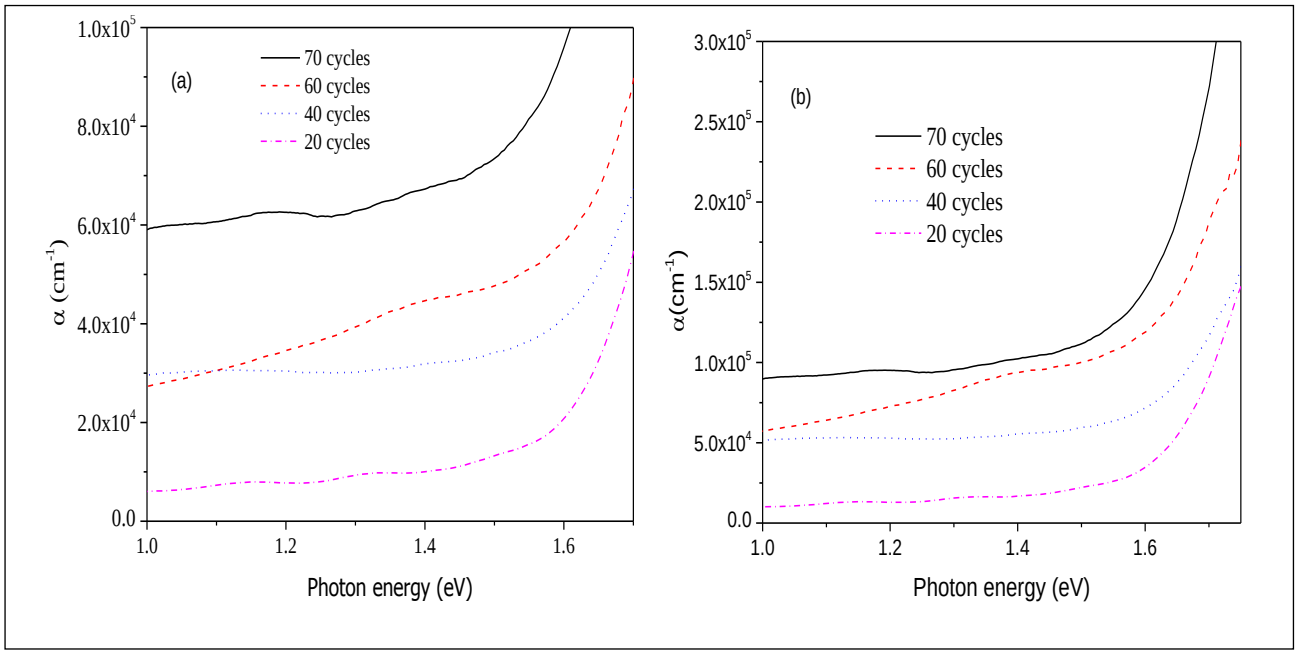

Figure 5.12: Absorption coefficient of the CZTS thin film samples annealed in sulfur atmosphere at (a) 450°C and (b) 550°C

It is also observed from Figure 5.13 that annealing at high temperatures increases the absorption coefficient. This could be because the water content was evaporated during the annealing process. It is noted that annealing the samples has great impact on the absorption property of the samples. The as deposited samples have the lowest absorption coefficient value followed with the samples annealed at 450°C while the samples that were annealed at 550°C has the best absorption values. This is because during annealing, the ternary phases disappear leading to formation of CZTS thin film and the crystallization of this material is enhanced. It can be noted very clearly that there is improvement in the absorption value after annealing for every sample. This observation is in agreement with a research results reported by Zhang *et al*. (2013)

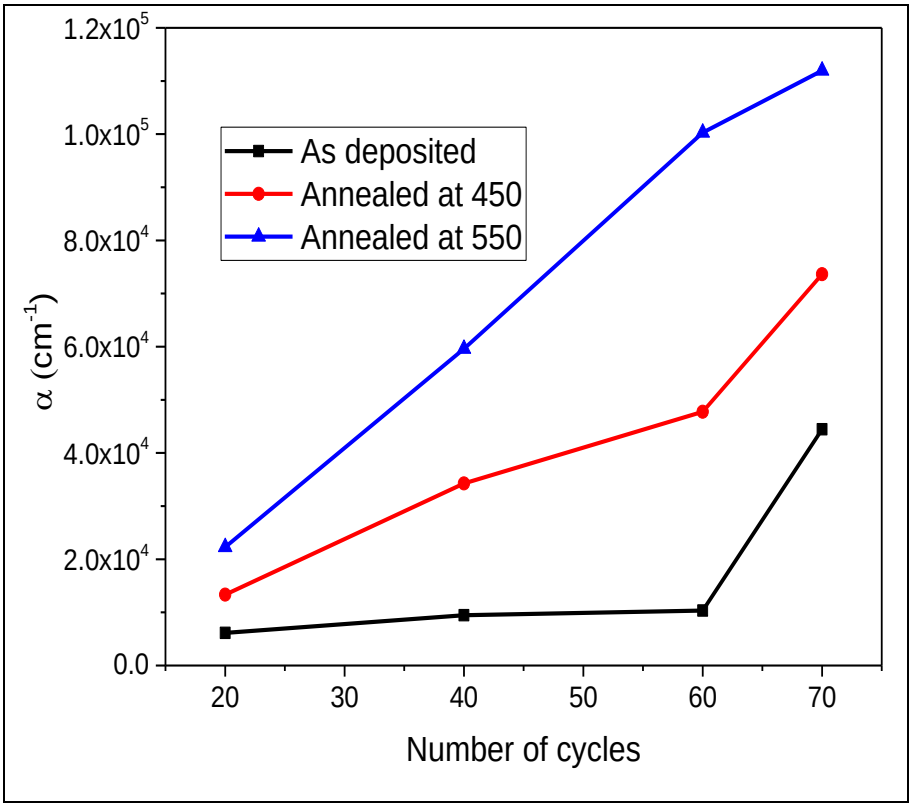

Figure 5.13: Variation of absorption coefficient with the number of cycles at 826nm for CZTS thin film samples of As-deposited, annealed in sulfur atmosphere at 450^{o}C and at 550^{o}C

5.1.6 Optical Band Gaps as a function of Post-Deposition Treatment

In order to confirm the nature of all the film samples, the optical data obtained from spectrometer were analyzed using the classical absorption equation below (Mali *et al*., 2012);

$$\alpha = \frac{A(h\nu - E_g)^n}{h\nu} \qquad 5.2$$

Where A is a proportional constant, $h\nu$is the incident photon energy, E_g is the optical band gap i.e. the separation between the bottom of conduction and the top of the valence band and$n$ is the constant. For the allowed direct transition, $n = \frac{1}{2}$ and for allowed indirect transition $n = 2$ (Pawar *et al*, 2010). The graphs of $(\alpha h\nu)^2$ against hν for all the CZTS samples for 20, 40, 60 and 70 cycles of as-deposited, annealed at 450^{O}C and 550^{O}C plotted are shown in the figures below. The optical band gap (*Eg*) of the film samples were determined by extrapolating linear region of $(\alpha h\nu)^2$versus $h\nu$ (photon energy) curve to intercept $h\nu$axis as shown in the figure 5.14, 5.15 and 5.16. It is clear from the curves that as the annealing temperature increases, the band gap decrease

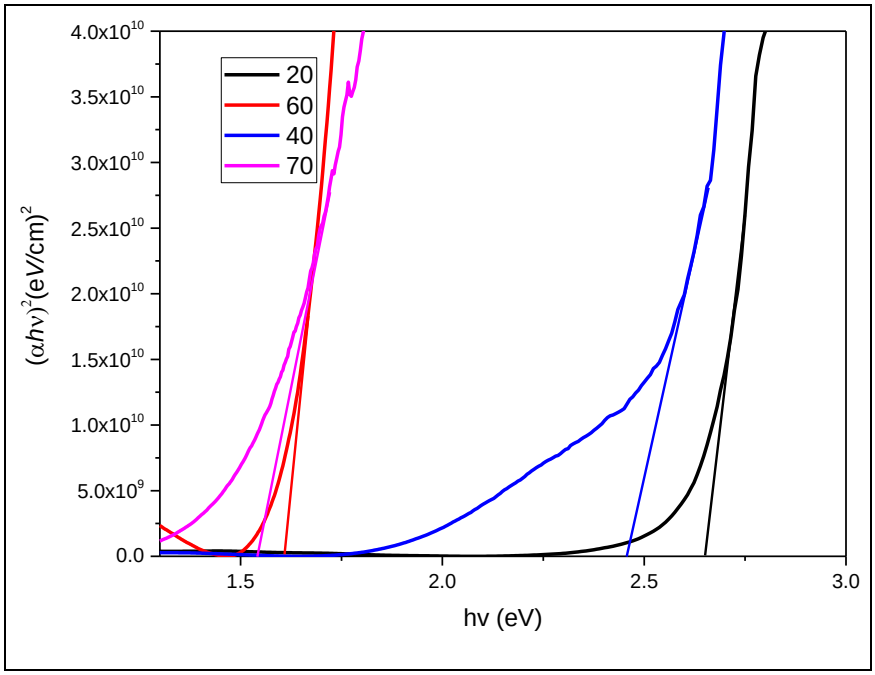

Figure 5.14: Optical band gap for as deposited CZTS thin film samples with different number of dipping cycles

Figure 5.14 above shows a graph of $(\alpha hv)^2$ versus hv for the as deposited CZTS thin film samples. It was observed that an increase in the number of cycles resulted to a decrease in the energy band gap of the film samples. The sample with the highest number of cycles that is 70 cycles had an energy band gap of 1.52 *eV* while the sample with 20 cycles had an energy band gap of 2.60 *eV* and this is very far from the optimum value of 1.50 *eV* (Shinde *et al*., 2012). The film samples with 40 and 60 number of cycles were found to have an energy band gap of 2.42 and 1.60 *eV* which was slightly high compared to the optimum value of the CZTS thin film energy band gap. This could be attributed to the presence of the binary phases like CuS, SnS, ZnS and Cu_3SnS_4 components hence the film material is still amorphous. This is in good agreement with the earlier report by Shinde *et al*., (2012).

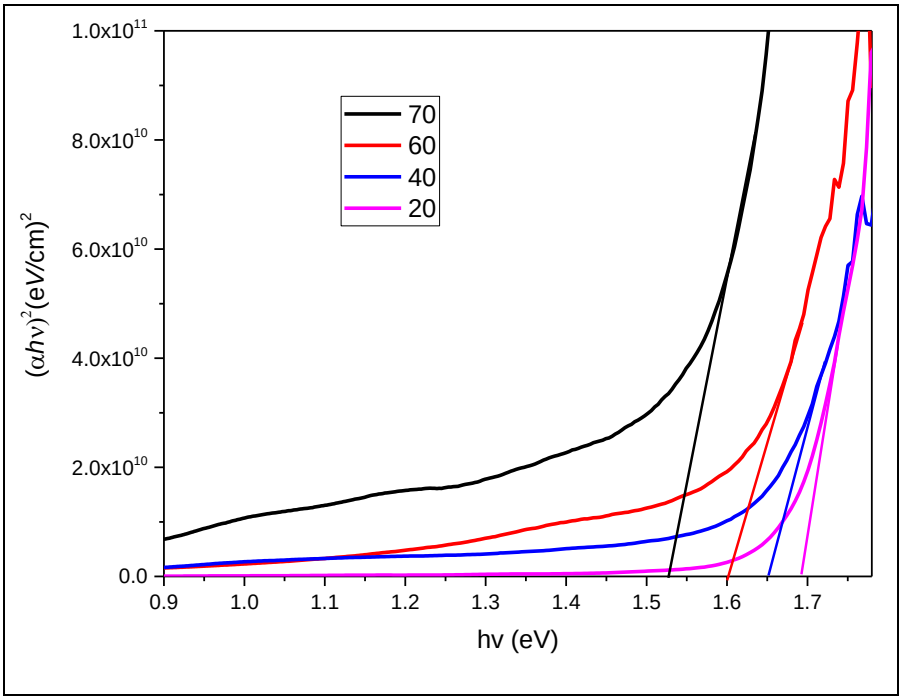

Figure 5.15: Optical band gap for CZTS thin film samples annealed in sulfur rich atmosphere at 450^{o}C

Figure 5.15 represents graphs of $(\alpha hv)^2$ versus hv for the CZTS thin film samples annealed at 450^{o}C. The energy band gaps of the samples have decreased compared to the as deposited samples. It is still evident that thinner films had larger energy band gap. The samples with 20, 40, 60 and 70 number of cycles had band gaps of 1.66, 1.65, 1.60 and1.53*eV* respectively. It is well known that the band gap energy is indirectly proportional to the grain size (Jain and Arun, 2013) hence the band gap energy is expected to reduce with an increase in the film thickness as shown in the graph. The grain size is expected to continue growing with an increase in dipping cycles therefor the sample with 70 cycles will exhibit large grain compared to the other samples hence having a higher thickness as it was reported earlier. The decrease in band gap energy with an increase in the film thickness can also be due to change in the barrier height of crystalline film. The band gap values are now much closer to the optimum value and the sample with 70 number of cycles has managed to attain that particular value. This is because annealing the samples in the sulphur atmosphere helps in the elimination of binary phases having higher band gaps, the film undergoes crystallization and the formation of CZTS is improved (Pawar *et al*., 2010).

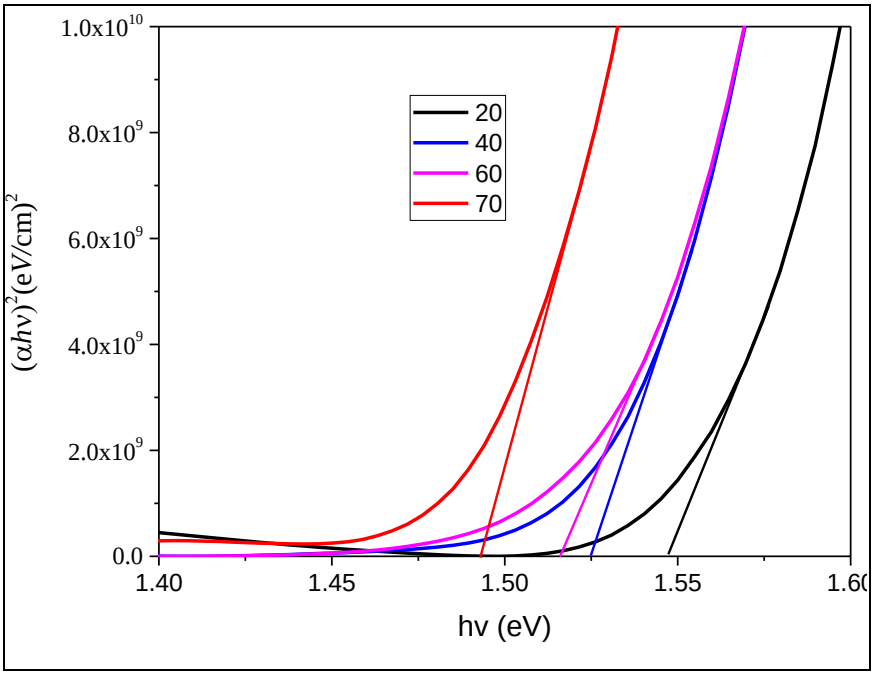

Figure 5.16: Optical band gap for CZTS thin film samples annealed in sulfur rich atmosphere at 550^{o}C

The figure 5.16 above shows graphs of energy band gap of the CZTS thin films annealed at 550^{o}C. The same trend as the other graphs is very evident but the band gaps of the samples are within the optimum range of 1.44-1.6 *eV*. The samples with 20, 40, 60 and 70 have energy band gaps of 1.54, 1.52, 1.51, and 1.49 respectively. This is because the thin films have fully crystallized and the secondary phases have been eliminated when it was annealed at 550^{o}C in the sulphur rich atmosphere as reported under Raman spectra (Fig 5.21). This range of values is in good agreement with the reported direct band gaps of CZTS of 1.45-1.6 *eV* (Katagiri *et al.*, 2001). Absorption coefficient of the samples was found to be greater than 10^4 cm^{-1} and thus it was concluded that the films had good absorbance in the visible region of the electromagnetic spectrum and it is also in agreement with the previous reports (Ennaoui *et al.*, 2009). Any other information regarding secondary phases was not available from absorption spectra. It can be observed from the three figures above (Figure 5.14, 5.15 and 5.16) that any increase in the temperature leads to a decrease in the band gap energy of the film sample and this is good agreement with the previous report (Pawar *et al.*, 2010).

Table 5.1 below gives a summary of the variation of temperature with the band gap for every sample. It can be observed that the band gap is between 1.49 *eV* and 2.64 *eV*for the film samples depending with the number of cycles. The sample with 70 cycles attains a near

optimum band gap of 1.53eV and 1.49 eV when it was annealed at 450°C and 550°C respectively. A similar phenomenon has been reported previously (Amin *et al*., 2013).

Table 5.1: Band gaps of CZTS thin film samples at different temperatures

Number of cycles	Band gaps (eV) at different temperatures		
	As-deposited	Annealed at 450°C	Annealed at 550°C
20	2.64	1.69	1.54
40	2.45	1.65	1.52
60	1.61	1.60	1.51
70	1.54	1.53	1.49

5.2 Elemental and Structural Characterisation

5.2.1 X-Ray Flouresence Analysis (XRF)

The compositional atomic ratios of $\frac{Cu}{(Zn+Sn)}$, $\frac{Zn}{Sn}$ and $\frac{S}{metals}$ were investigated using XRF on the CZTS thin film sample deposited with 70 cycles is tabulated as shown in table 5.2 below. It can be observed that the CZTS sample was nearly stoichiometric with $\frac{Cu}{(Zn+Sn)}$ratio in the range of 0.74-0.84, $\frac{Zn}{Sn}$ ratio in the range of 1.07-1.14 and $\frac{S}{metals}$ ratio in the range of 0.84-0.89. For stoichiometric sample, all the above ratios should be equal to 1 and this shows that our film sample is copper-poor and zinc-rich (Kahraman *et al*., 2013). Reports by (Todorov *et al*., 2010 and Katagiri *et al*., 2009) reveals that higher efficiencies have been obtained with zinc-rich and copper-poor compositions. The Cu deficit enhances the formation of Cu vacancies which give rise to shallow acceptors (Kahraman *et al.*, 2013). It is also observed from the results on table 5.2 that there is loss of 1.3% Sn when the thin film sample's temperature was elevated from 450 to 550°C. Weber *et al*, (2010) also observed a similar phenomenon and they suggested that CZTS thin film should be deposited at a temperature lower than 550°C so as to suppress the evaporation of tin sulfide. A slight loss in Zn during annealing is also evident leading to a drop in the$\frac{Zn}{Sn}$ratio and this has also been reported earlier (Tang *et al*., 2013).

Table 5.2: Elemental composition of Cu_2ZnSnS_4 film sample with 70 cycles as-deposited, annealed at 450^{O}C and annealed at 550^{O}C

Elements	Atomic percentages (%)		
	As-deposited	Annealed at 450°C	Annealed at 550°C
Cu	23.1	23.2	24.1
Sn	14.3	14.7	13.4
Zn	16.4	15.8	15.3
S	45.7	46.3	47.2
$\frac{Zn}{Sn}$	1.11	1.07	1.14
$\frac{Cu}{(Zn+Sn)}$	0.74	0.76	0.84
$\frac{S}{Metals}$	0.84	0.86	0.89

When the optical band gaps is compared with compositions of the CZTS thin films samples , it is observed that there is a decrease in optical band gap with an increase in Cu/(Zn+Sn) ratio. This is in accordance with previous report (Lin et al., 2013) where the optical band gap shifted toward higher energies as the Cu/(Zn+Sn) ratio of the CZTS thin film decreased. The optical band gap of semiconductor materials is determined by the valence band maximum and the conduction band minimum. Therefore, the shift of the band gap may be due to the increase of valence band maximum with increasing Cu/(Zn+Sn) ratio.

5.2.2: Raman Spectra Analysis

Raman spectral measurement was performed on the CZTS thin film to determine the presence of secondary phases in the film. Raman spectroscopy is a technique that can be used to detect both organic and inorganic species as well as measure crystallinity of solids (Schroder, 2006). When the incident photon imparts part of its energy to the lattice in the form of phonon, it emerges as a lower energy photon. This is a 'down converted frequency shift' which is known as Stokes shifted scattering. When the photon absorbs a phonon and emerges with higher energy, it is known as Anti-Stokes shifted scattering. Stokes mode scattering is usually monitored because Anti-Stokes mode is much weaker than the Stokes mode scattering. In Raman spectroscopy, a laser beam known as the pump, is incident on the sample. The weak scattered light on the Raman signal is passed through double monochromator so as to reject the Rayleigh scattered light and the Raman shifted wavelengths are detected by a photo detector.

Various properties of the semiconductors, mainly composition and crystal structure, can be determined using this technique. Information about structure, phase, grain size and phonon confinement can be obtained from Raman spectroscopy. For amorphous semiconductors, the lines become very broad, allowing distinction to be made between single crystal, polycrystalline, and amorphous materials.

In this work, Raman analyses of the samples over the range of 200-500 cm^{-1} were made. Figure 5.17 below shows Raman spectra of as-deposited film sample. Peaks corresponding to SnS, ZnS, CuS, Cu_3SnS_4 and CZTS phases were observed at 219 cm^{-1}, 275 cm^{-1}, 473 cm^{-1}, 348 cm^{-1} and 373 cm^{-1}respectively. These observations are in agreement with published Raman data reported by (Sinsermsuksakul *et al.*, 2011; Kim *et al.*, 2012; Abdullaeva *et al.*, 2013 and Fontane *et al.*, 2011). It is evident that before annealing, the film sample contains CZTS and the ternary secondary phases. The formation of CZTS is more evident when the film sample is subjected to the annealing process as shown in figure 5.18 below. The main peaks of CZTS thin film can be noticed at about 337 cm^{-1}, 289 cm^{-1} and 285 cm^{-1}. There are other weaker peaks of CZTS that can be noticed at 373 cm^{-1}, 356 cm^{-1} which corresponds to 350 cm^{-1} and 257 cm^{-1} which corresponds to 252 cm^{-1}. These values are in agreement with the previous reports on Raman data (Fontane *et al.*, 2011 and Miskin *et al.*, 2015). It is clear that even after annealing in Sulphur atmosphere at 450 ^oC, there is still presence of ternary secondary phase like SnS and ZnS that can be noticed at 218 cm^{-1}, 229 cm^{-1} and 312 cm^{-1} respectively. These peaks have been reported earlier in case of formation of these compounds (Sinsermsuksakul *et al.*, 2011 and Kim *et al.*, 2012). Figure 5.19 shows Raman spectroscopy contains strong peaks at phonon frequency of 337 cm^{-1} and 285 cm^{-1} corresponding to A1 symmetric mode in kesterite CZTS. This result is in agreement with the published Raman reports (Kahraman *et al.*, 2013). Other weaker modes of CZTS film can be observed at 356 cm^{-1} and 379 cm^{-1} while 265 cm^{-1} corresponds to cubic CTS peak at 267 cm^{-1} and 214cm^{-1} corresponds to SnS. The strong major peaks in figure 5.19 is an indication of the good crystalline quality of the compound (Tang *et al*. 2017). Secondary phase of SnS and a ternary phase of Cu_2SnS_4 can still be identified even after annealing the samples at 550^oC, in addition to the main CZTS peak. It's likely that the CZTS thin film sample also contains ZnS, a secondary phase but it cannot be detected by the Raman spectroscopy at this point. This observation is in agreement with the previous report (Ahmed *et al.*,2012). Generally, annealing the thin films at 450^oC and at 550^oC helps to

eliminate ternary phases by reacting with Sulphur at these high annealing temperatures in order to directly generate CZTS which in turn results to the formation of CZTS thin films. The annealed thin films are highly pure coupled with better crystallinity compared to the as deposited samples (Aldalbahi *et al*. 2016).

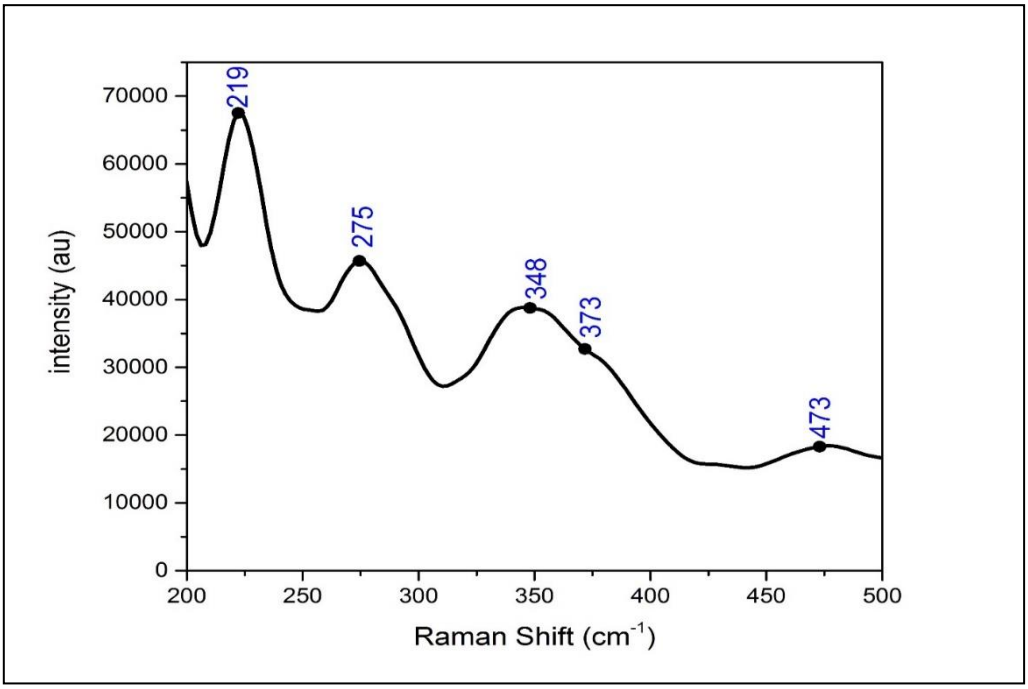

Figure 5.17: Raman spectra of CZTS thin film sample As-deposited

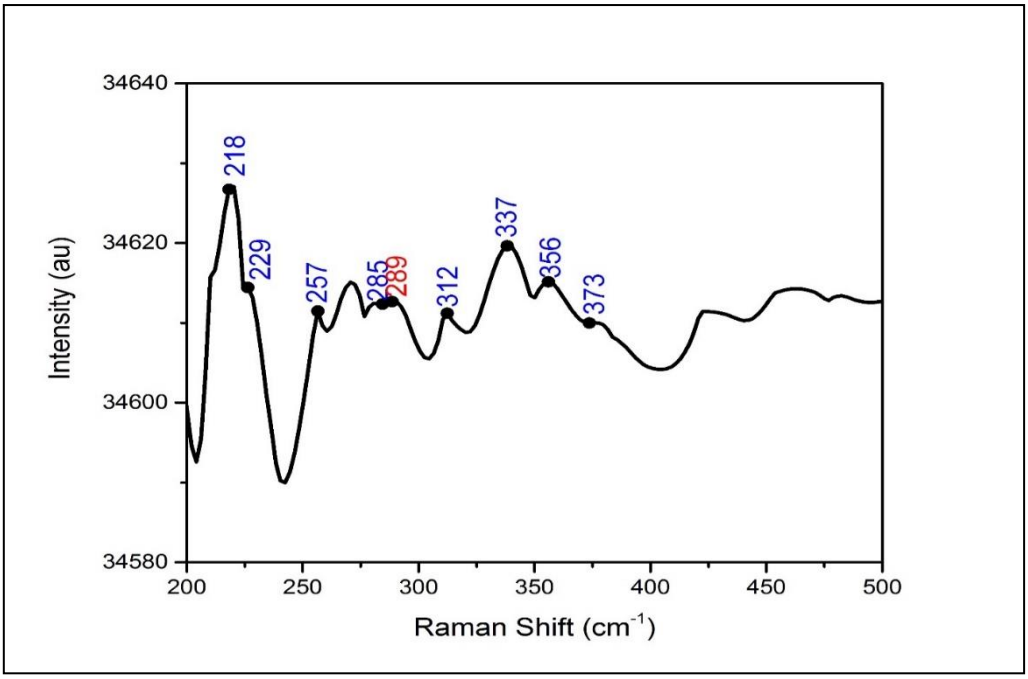

Figure 5.18: Raman spectra of CZTS thin film sample annealed in a sulfur rich atmosphere at 450°C

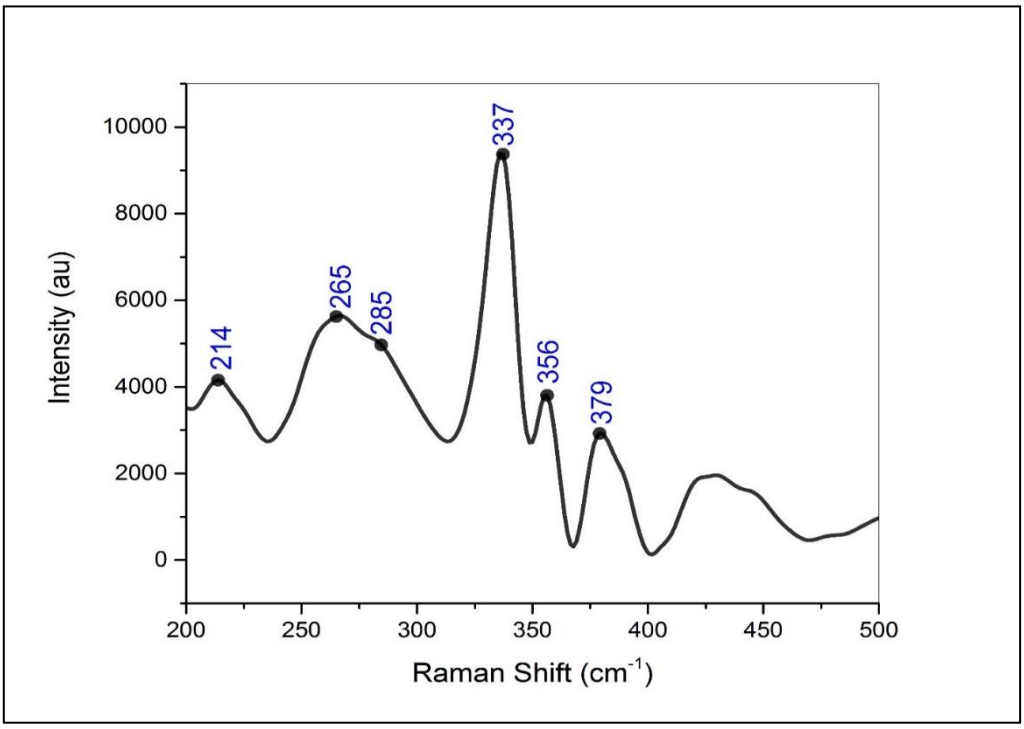

Figure 5.19: Raman spectra of CZTS thin film sample annealed in a sulphur rich atmosphere at 550°C

5.3 Electrical Properties of CZTS

The electrical property is vital in the determination of whether a material can be an absorber layer in a solar panel. Sheet resistance of the film samples with different number of cycles was measured using Jandel RM3-AR four-point probe and it is observed that an increase in the number of cycles leads to a decrease in the value of sheet resistance. The resistivity of the film samples was calculated using Equation 5.1 (Henry *et al.*, 2015)

$$\rho = R_{sheet}t \tag{5.3}$$

Where $\rho$is the resistivity, R_{sheet} is the sheet resistance and $t$is the thickness of the film sample. It is equally important that an electrical conductivity (σ) of the CZTS thin films samples to be determined too and this was done using Equation 5.2

$$\sigma = \frac{1}{\rho} \tag{5.4}$$

Where $\sigma$is the electrical conductivity and $\rho$is the electrical resistivity.

Table 5.3 shows the resistivity and conductivity data for the thin films. It can be observed from the Table that the resistivity of the film samples decreases with increase in film thickness (or

with increase in the number of dipping cycles) while the behavior of conductivity of the same film samples is the opposite of resistivity. The electrical conductivity also increases with an increase in the annealing temperature which can be related to the diminished grain boundary scattering as a result of improved crystallinity hence leading to reduction of the number of grain boundaries.

In general, this indicates the semiconducting behavior of CZTS. From tables 5.3 and 5.4 below, it is also evident that with an increase in the annealing temperature, the resistivity of the samples reduces. This can be attributed to the fully crystallization of the sample to form a compact CZTS thin film with no binary elements as the temperature is elevated from 450.0 ^{o}C to 550.0 ^{o}C. The sheet resistivity increases with an increase both in the film thickness and annealing temperatures. This is because an increase in film thickness and annealing temperature results in increased grain sizes of CZTS and this is in agreement with some observations reported earlier (Sheng *et al*., 2012; Henry *et al*., 2015).

The electrical resistivity for the samples annealed at 450 ^{o}C is observed to be in the order of 10^{-3} and $10^{-4}\Omega$.cm while the samples annealed at 550.0 ^{o}C is in the range of 10^{-3} and $10^{-5}\Omega$.cm. The samples in the orders of 10^{-4} and $10^{-5}\Omega$.cm is observed to be lower than the expected values which have been previously reported to be in the order of $10^{-3}\Omega$.cm (Shinde *et al*., 2012). This difference could be attributed to different microstructural compositions of the samples (Sheng *et al*., 2012).

Table 5.3: Sheet resistance and resistivity of film samples annealed at 450^{o}C

Number of cycles	Thickness (cm)	Sheet resistance (Ω)	Resistivity(Ω.cm)	Conductivity ($\Omega^{-1}cm^{-1}$
20	7.6×10^{-5}	88.57197	6.731×10^{-3}	148.5663
40	1.15×10^{-4}	10.19337	1.172×10^{-3}	853.2423
60	2.36×10^{-4}	0.98957	2.335×10^{-4}	4282.6552
70	2.82×10^{-4}	0.463816	1.308×10^{-4}	7645.2599

Table 5.4: Sheet resistance and resistivity of film samples annealed at 550°C

Number of cycles	Thickness (cm)	Sheet resistance (Ω/□)	Resistivity(Ω.cm)	Conductivity ($\Omega^{-1}cm^{-1}$)
20	6.4×10^{-5}	76.5763	4.901×10^{-3}	204.0400
40	107×10^{-4}	5.7016	6.100×10^{-4}	1639.3443
60	2.31×10^{-4}	0.476576	1.101×10^{-4}	9082.6521
70	2.59×10^{-4}	0.081583	2.113×10^{-5}	47326.0767

The refractive index (n) and dielectric constant (ε_∞) of an absorber material in a solar cell are very vital elements in the determination of the optical and electrical properties of the thin film which is essential in the solar cell application. The refractive index of all the sample films were determined using two different relations namely Moss relation and Herve and Vandamme relation equations. By Moss relation, refractive index is found to be directly related to the fundamental band gap energy (E_g) and it is given by equation 5.5 (Henry *et al.*, 2015)

$$E_g n^4 = K \tag{5.5}$$

Where E_g is the band gap energy, n is the refractive index and K is a constant with a value of 108 eV. Herve and Vandamme relation equation is another relation between the refractive index and the band gap energy and it was also used in the determination of the refractive index of all the samples before annealing and after annealing. The relation is given by the equation below

$$n = \sqrt{1 + \left(\frac{A}{E_g + B}\right)^2} \tag{5.6}$$

Where n is the refractive index, E_g is the band gap energy, A and B are the numerical constants with values of 13.6eV and 3.4 eV respectively. Evaluation of both the static and high frequency optical dielectric constants was carried out for all the film samples. The high frequency dielectric constant (ε_∞) for the CZTS thin film samples was determined using the relation below

$$\varepsilon_\infty = n^2 \tag{5.7}$$

Where n is the refractive index of the samples. On the other hand, the static dielectric constant was calculated using a relation expressing the dependence of band gap energy to the static dielectric constant (ε_0) for semiconductor materials following the equation below

$$\varepsilon_0 = 18.52 - 3.08E_g. \tag{5.8}$$

Tables 5.4, 5.5 and 5.6 below shows the calculated values of refractive index (n), static dielectric constant (ε_0) and high frequency optical dielectric constant (ε_∞) of the as deposited CZTS thin films, annealed at 450.0^{o}C and at 550.0^{o}C respectively. It is observed that the refractive index increases as well as the dielectric constant when the samples are annealed compared to the as deposited thin films.

Table 5.5: Refractive index (n) and dielectric constant (ε_∞) values of the as deposited CZTS thin films

Number of cycles	E_g (eV)	Static dielectric constant (ε_0)	Herve & Vandamme relation		Moss relation	
			n	ε_∞	n	ε_∞
20	2.64	10.6044	2.4879	6.1896	2.5461	6.4826
40	2.45	11.0664	2.5418	6.4607	2.5847	6.6807
60	1.61	13.6228	2.9031	8.4280	2.8708	8.2415
70	1.54	13.9924	2.9663	8.7989	2.9277	8.5714

Table 5.6: Refractive index (n) and dielectric constant (ε_∞) values of the CZTS thin films annealed at 450^{o}C

Number of cycles	E_g (eV)	Static dielectric constant (ε_0)	Herve & Vandamme relation		Moss relation	
			n	ε_∞	n	ε_∞
20	1.69	13.4072	2.8678	8.2243	2.8401	8.066
40	1.65	13.5612	2.8929	8.3689	2.8619	8.1905
60	1.60	13.9000	2.9502	8.7037	2.9130	8.4856
70	1.53	14.1464	2.9935	8.9610	2.9531	8.7208

Table 5.7: Refractive index (n) and dielectric constant (ε_∞) values of the CZTS thin films annealed at 550°C

Number of cycles	E_g (eV)	Static dielectric constant (ε_0)	Herve & Vandamme relation		Moss relation	
			n	ε_∞	n	ε_∞
20	1.54	13.8076	2.9343	8.6101	2.8986	8.4019
40	1.52	13.9000	2.9502	8.7037	2.9130	8.4856
60	1.51	14.0540	2.9771	8.8631	2.9377	8.6301
70	1.49	14.0848	2.9826	8.8959	2.9428	8.6601

The refractive index of the CZTS thin film was found to be in the range of 2.4-2.9 depending with the number of cycles. The increase in the refractive index with an increase in the number of cycles as well as the annealing temperature could be attributed to the fact that refractive index is dependent on the atomic mass of components and the density of material (Tawari *et al*., 2014). Therefore, an increase in the annealing temperature results to an increase in grain growth leading to increased density thus the refractive index of films increases. The high optical frequency dielectric constant was in the range of 8.3-8.9. This is in agreement with the previous report (Henry *et al.,* 2015). An increase in dielectric constant indicates an improvement in electronic transition which is a fundamental phenomenon in semiconductor thin films hence the sample with 70 cycles is the best in solar cell application.

CHAPTER SIX: CONCLUSIONS AND RECOMMENDATIONS

6.1: **Conclusion**

In this work, the effect of number of cycles and annealing temperature on the electrical and optical properties of Cu_2ZnSnS_4 (CZTS) based thin films for solar cell applications were studied. The study focused on the determination of the effect of annealing temperature of 450^{o}C and 550^{o}C on the spectral transmittance and energy band gap of the film samples. *SILAR* technique was used in the deposition of CZTS thin films onto FTO glass substrate and it was carried out at room temperature. The study revealed that CZTS had a sheet resistance of the order magnitude in the range 10^{-1}-10^{1} Ω/sq when it was annealed in at 450^{o}C and 10^{-2} -10^{1}Ω/sq when the samples were annealed at 550^{o}C depending on the number of cycles. The electrical resistivity of the films was in the order magnitude of 10^{-3} – 10^{-4}Ω.cm and an electrical conductivity in the range of 10^{2}-10^{3} $(\Omega.cm)^{-1}$ when they were annealed at 450^{O}C. When the samples were annealed at 550^{O}C, the resistivity and conductivity of the thin films was in the order magnitude of 10^{-3}-10^{-5} (Ω.cm) and 10^{2}-10^{4} $(\Omega.cm)^{-1}$ respectively. The same trend was observed when the effect of number of cycles on the electrical properties was investigated.

The optical transmittance of CZTS thin films showed a significant decrease in the percentage values when the annealing temperature and the number of cycles was increased. The films that were annealed at 550^{o}C showed very interesting results since it combined both low spectral transmittance, low electrical resistivity, high electrical conductivity, high absorption coefficient $\geq 10^{4}$ $cm^{-1}$and an energy band gap within the range of an optimum band gap of 1.50 eV. The refractive index of the CZTS thin films was found to be in the range of 2.4-2.9 while the dielectric constant of the same samples was in the range of 6.0-8.9.

The trend for the transmittance of CZTS thin film within the visible region showed a decrease in the percentage values with an increase in the number of cycles for the as deposited and post annealing in the temperatures of 450^{o}C and 550^{o}C. Nevertheless, the CZTS thin film with 70 cycles showed a significant potential as an absorber layer for a solar cell application before and even after annealing. The sample with 70 cycles was found to be the best film displaying optimum value of energy band gap in both cases before and after annealing. It had the lowest transmittance value and the best band gap.

The CZTS sample was found to be nearly stoichiometric with $\frac{Cu}{(Zn+Sn)}$ratio in the range of 0.74-0.84, $\frac{Zn}{Sn}$ ratio in the range of 1.07-1.14 and $\frac{S}{metals}$ ratio in the range of 0.84-0.89. It was also noticed that when the sample annealing temperature was raised from 450^{O}C to 550^{O}C, there was a loss of 1.3% Sn. The thin film structure improved significantly when the sample was annealed at 550^{O}C compared to 450^{O}C as indicated in the Raman results. The CZTS peak was more pronounced in the sample that was annealed at 550^{O}C. This was due to increase in the sample size, increased crystallization as well as elimination of secondary phases.

6.2: Recommendations

In this study, the effect of number of cycles and annealing temperature on the optical and electrical properties of CZTS based thin films have shown sufficient optical absorption coefficient in the visible region and good conductivity. More work on the optimization of deposition parameters and film thickness is recommended. This could be of more importance in the improvement of optical and electrical properties in order to determine their suitability for solar cell application.

It is suggested that the study on investigation of deposition duration and solvent temperature may further improve the optical, electrical and structural properties of CZTS thin films. These parameters have a potential of influencing spectral transmittance values, spectral reflectance values, optical absorption values, energy band gap and electrical conductivity. Nevertheless, the study on the optimization of solvent concentration and sulfurization temperature is advised in order to minimize the transmittance and energy band gap values of CZTS thin film.

REFERENCES

Abdullaeva, Z., Omurzak, E., & Mashimo, T. (2013, January). Synthesis of Copper Sulfide Nanoparticles by Pulsed Plasma in Liquid Method. In *Proceedings of World Academy of Science, Engineering and Technology* (No. **78**, p. 1035). World Academy of Science, Engineering and Technology (WASET).

Abdullahi S., Momoh M., Moreh A.U., Bayawa A. M., Hamza B., Argungu G.M., Popoola O. T. (2017) Influence of Annealing Temperature on Optical and Electrical Properties of Cu_2ZnSnS_4 (CZTS) thin Films Deposited by Sputtering Method from a Single Quaternary Target. International Journal of Scientific Research in Science and Technology, 3(1),77-82

Adelifard, M. (2015). Nanostructured Cu2ZnSnS4 thin films: influence of substrate temperature on structural, morphological, optical and electrical properties. *Applied Physics A*, ***121***(1), 95–101. doi:10.1007/s00339-015-9389-4

Ahmed, S., Reuter, K. B., Gunawan, O., Guo, L., Romankiw, L. T., and Deligianni, H. (2012). A high efficiency electrodeposited Cu_2ZnSnS_4 solar cell. *Advanced Energy Materials **2*** (2), 253-259.

Aldalbahi, A., Mkawi, E. M., Ibrahim, K., & Farrukh, M. A. (2016). Effect of sulfurization time on the properties of copper zinc tin sulfide thin films grown by electrochemical deposition. Scientific Reports, **6**(1), 1-9. doi:10.1038/srep32431

Ali M. (1999). Growth and study of magnetostrictive FeSiBC thin films for device applications,

Altomonte, H. (2012). Japan's nuclear disaster: Its impact on electric power generation worldwide [In My View]. Power and Energy Magazine, *IEE*, **10**(3):96 –94

Amin Emrani, Parag Vasekar, Charles R. Westgate (2009). Effects of Sulfurization temperature on CZTS thin film solar cell performances. *Solar Energy*, **98**, 335-340.

Ananthan, M. R., & Mahalaksmi, B. (2014). Review on CZTS based solar cells. *Advances in Natural and Applied Sciences*, **8**(21), 72-76.

Araki, H., Kubo, Y., Jimbo, K., Maw, W. S., Katagiri, H., Yamazaki, M.,Oishi K. and Takeuchi A. (2009). Preparation of Cu_2ZnSnS_4 thin films by sulfurization of co-electroplated Cu-Zn-Sn precursors. *physica status solidi (c)*, ***6*** (5), 1266-1268.

Asif, M., & Muneer, T. (2007). Energy supply, its demand and security issues for developed and emerging economies. *Renewable and Sustainable Energy Reviews*, ***11***(**7**), 1388-1413.

Bag S., Gunawan O., Gokmen T., Zhu Y., Todorov T.K., Mitzi D. B. (2012). Low band gap liquid processed CZTSe solar with 10.1% efficiency, *Energy Environ. Sci.* **5**, 7060

[a]Bär, M., Schubert B. A., Marsen B., Krause S., Pookpanratana S., Unold T.,Weinhardt L.,Heske C and Schock H. W. (2011). Impact of KCN etching on the chemical and electronic surface structure of Cu_2ZnSnS_4 thin-film solar cell absorbers. *Applied Physics Letters*, ***99***(15), 152111.

[b]Bär M., Schubert B. A., Marsen B., Krause S., Pookpanratana S., Unold T.,Weinhardt L., Heske C and Schock, H. W. (2011). Native oxidation and Cu-poor surface structure of thin film Cu_2ZnSnS_4 solar cell absorbers. *Applied Physics Letters*, ***99*(**11), 112103.

Bishop A.C (2011). 5 - Process Diagnostics and Coating Characteristics. Vacuum Deposition onto Webs, Films and Foils (Second Edition). William Andrew Publishing, pp 81-114

Brémaud, D. J. L. (2009). Investigation and development of CIGS solar cells on flexible substrates and with alternative electrical back contacts (Doctoral dissertation, Diss., Eidgenössische Technische Hochschule ETH Zürich, Nr. 18194,2009)

Chalapathy, R. B. V., Jung, G. S., &Ahn, B. T. (2011). Fabrication of Cu_2ZnSnS_4 films by sulfurization of Cu/ZnSn/Cu precursor layers in sulfur atmosphere for solar cells. *Solar Energy Materials and Solar Cells*, ***95***(12), 3216-3221.

Chan C.P., Lam H. & Surya C., (2010). Preparation of Cu_2ZnSnS_4 films by electrodeposition using ionic liquids. *Solar Energy Materials and Solar Cells*, **94**(2),207-211.

Chaudhari T. K. and Tiwari D. (2012). Earth-abundant non-toxic Cu_2ZnSnS_4 thin films by direct liquid coating from metal–thiourea precursor solution**.** *Solar Energy Material and Solar Cells*, **101**, 46-50.

Liu F., Li Y., Zhang K., Wang B., Yan C., Lai Y., Zhang Z., Li J.and Liu Y., (2010). *In situ* growth of Cu_2ZnSnS_4 thin films by reactive magnetron co-sputtering. *Solar Energy Materials and Solar Cells*, **94**(12), 2431-2434.

Chen S., Yang J., Gong X. G., Walsh A. and Wei S. (2010). Intrinsic point defects and complexes in the quaternary kesterite semiconductor Cu_2ZnSnS_4. *Physical Review B, **81***, 245204 (1)

Conti J., Holtberg P., Diefenderfer J., LaRose A., Turnure J. T., & Westfall L. (2016). International Energy Outlook 2016 With Projections to 2040. United States. doi:10.2172/1296780.

Dai, P., Shen, X., Lin, Z., Feng, Z., Xu, H., and Zhan, J. (2010). Band-gap tunable $(Cu_2Sn)_{x/3}Zn_{1-X}S$ nanoparticles for solar cells. *Chemical Communications*, ***46*(**31), 5749-5751.

Das, S., Mandal, K. C., & Bhattacharya, R. N. (2016). Earth-Abundant Cu_2ZnSn (S, Se)$_4$ (CZTSSe) Solar Cells. In *Semiconductor Materials for Solar Photovoltaic Cells* (pp. 25-74). Springer International Publishing.

Delbos S. (2012). Kesterite thin films for Photovoltaics: a review, *EPJ Photovoltaics* **3**, 35004

Deligianni, H., Ahmed, S., & Romankiw, L. T. (2011). The next frontier: electrodeposition for solar cell fabrication. *Interface-Electrochemical Society*, ***20***(2), 47.

Edoff M., Scragg J., Flammersberger H., Kubart T. and Platzer-Björkman C. (2012) Influence of precursor sulfur content on film formation and compositional changes in Cu_2ZnSnS_4 films and solar cells. *Solar Energy Materials and Solar Cells* **98**, 110-117.

Eisenberg R. and Nocera D. G. (2005). Preface: Overview of the Forum on Solar and Renewable Energy. *Journal of Inorganic chemistry* **45**,6799.

Ennaoui, A., Lux-Steiner, M., Weber, A., Abou-Ras, D., Kötschau, I., Schock H. W.,Schurr R.,Hölzing A.,Jost S., Hock R, Voß T., Schulze J. and Kirbs, A. (2009). Cu_2ZnSnS_4 thin film solar cells from electroplated precursors: Novel low-cost perspective. *Thin Solid Films, 517*(**7**), 2511-2514.

Fahrenbruch, A., and Bube, R. (2012). *Fundamentals of solar cells: photovoltaic solar energy conversion*. Elsevier.

Farahbod, F., Zamanpour, A., & Fard, M. H. Z. S. (2014). Copyright© 2014 by Academic Publishing House Researcher Published in the Russian Federation European Journal of Technology and Design. *European Journal of Technology and Design*, ***6***(4).

Fernandes P. A., Salome P. M. P., Da Cunha A. F. and Schubert B. (2010). Cu_2ZnSnS_4 solar cells prepared with sulphurized dc-sputtered stacked metallic precursors. *Thin Solid Films*, **519 (**21), 7382-7385. doi.org/10.1016/j.tsf.2010.12.035

Friedlmeier TM, Wieser N, Walter T, Dittrich H &H.W.Schock. (1997). Heterojunctions based on Cu_2ZnSnS_4 and $Cu_2ZnSnSe_4$ thin films. Proceedings of the 14th European Conference of Photovoltaics Science and Engineering and Exihibition , Bedford, 1997, p.1242-1245.

Fontané X., Calvo-Barrio L., Izquierdo-Roca V., Saucedo E., Pérez-Rodriguez A., Morante J. R., Berg D. M, Dale P.J & Siebentritt, S. (2011). In-depth resolved Raman scattering analysis for the identification of secondary phases: characterization of Cu_2ZnSnS_4 layers for solar cell applications. *Applied Physics Letters*, ***98***(18), 181905.

Goetzberger, A., Hebling, C., & Schock, H. W. (2003). Photovoltaic materials, history, status and outlook. *Materials Science and Engineering: R: Reports*, **40**(1), 1-46.

Guo Q., Hillhouse H. W. andAgrawal, R. (2009). Synthesis of Cu_2ZnSnS_4 nanocrystal ink and its use for solar cells. *Journal of the American Chemical Society*, **131**(33), 11672-11673.

Guo Q., Ford G. M., Yang W. C., Walker B. C., Stach E. A., Hillhouse, H. W. and Agrawal, R. (2010). Fabrication of 7.2% efficient CZTSSe solar cells using CZTS nanocrystals. *Journal of the American Chemical Society*, **132**(49), 17384-17386.

Hall S.R., Szymanski J.T. and Stewart J.M. (1978). Kesterite $Cu_2(ZnFe)SnS_4$ and stannite $Cu_2(FeZn)SnS_4$ structurally similar but distinct minerals. *Canadian Mineralogist* **16**, 131-137

Henry J., Mohanraj K. and Sivakumar G. (2015). Electrical and optical properties of CZTS thin films prepared by SILAR method. *Journal of Asian Ceramic Societies*, **199**, 1-4

International Atomic Energy Agency (IAEA), 2007. Energy, Electricity and Nuclear Power: Developments and Projections- 25 years Past and Future.

Islam, S., Hossain, M. A., Kabir, H., Rahaman, M., Bashar, M. S., Gafur, M. A., Kabir.A., Bhuiyan M. M. R., Ahmed F & Khatun, N. (2015). Optical, Structural and Morphological Properties of Spin Coated Copper Zinc Tin Sulfide Thin Films. *International Journal of Thin Films Science and Technology*, ***4***(3), 155-161.

Iqbal, M. (2012). *An introduction to solar radiation*. Elsevier. Chapter 3, 43-57.

Ito K and Nakazawa T. (1988) Electrical and Optical Properties of Stannite-Type Quaternary Semiconductor Thin Films, *Japanese Journal of Applied Physics*, **27**, 2094-2097.

Jain P. and Arun P. (2013). Influence of grain size on the band-gap of annealed SnS thin films. *Thin Solid Films*, **548**, 241-246.

Jiang, M., & Yan, X. (2013). Cu_2ZnSnS_4 Thin Film Solar Cells: Present Status and Future Prospects, chapter 5, 107-143.

Kamoun N, Bouzouita H and Rezig B. (2007) Fabrication and characterization of Cu_2ZnSnS_4 Thin films deposited by spray pyrolysis technique. *Thin Solid Films*, **515**, 5949-5952.

Kahraman, S., Çetinkaya, S., Podlogar, M., Bernik, S., Çetinkara, H. A., & Güder, H. S. (2013). Effects of the sulfurization temperature on sol gel-processed Cu_2ZnSnS_4 thin films. *Ceramics International*, ***39***(8), 9285-9292.

Kahraman, S., Podlogar, M., Bernik, S., & Güder, H. S. (2014). Facile synthesis of Cu2ZnSnS4 photovoltaic absorber thin films via sulfurization of Cu_2SnS_3/ZnS layers. *Metallurgical and Materials Transactions A*, ***45***(4), 2326-2334.

Katagiri H, Sasaguchi N, Hando S, Hoshino S, Ohashi J and Yokota T., (1996). Preparation and evaluation of Cu_2ZnSnS_4 thin films by sulfurization of E–B evaporated precursors . *Technical Digest of the 9th International Conference of Photovoltaic Science and Engineering* , Miyazaki, p745-746

Katagiri H., Sasaguchi N., Hando S., Hoshino S., Ohashi J. and Yokota T. (1997). Preparation and evaluation of Cu_2ZnSnS_4 thin films by sulfurization of E□B evaporated precursors**.** *Solar Energy Materials and Solar Cells*, **49 (**1-4**)**, 407-414.

[a]Katagiri H, Ishigaki N, Ishida T, and Saito K.(2001) Characterization of Cu_2ZnSnS_4 thin films prepared by vapor phase sulfurization, *Japanese Journal of Applied Physics I*, ***40***(2), 500–504.

[b]Katagiri H, Saitoh K, Washio T, Shinohara H, Kurumadani T, and Miyajima S.(2001).Development of thin film solar cell based on Cu_2ZnSnS_4 thin films. *Solar Energy Materials and Solar Cells*, ***65***(1), 141–148.

Katagiri H, Jimbo K, Moriya K &Tsuchida K. (2003) Solar cell without environment pollution using CZTS thin film. *Proceeding of 3rd world Conference on Photovoltaics Solar Energy Conversion* , Osaka, .2874.

Katagiri Hironori. (2005) Cu_2ZnSnS_4 thin film solar cells. *Thin Solid Films* 480–481, 426–432

Katagiri H., Jimbo K, Kimura R, Kamimura T, Yamada S, Maw W.S, Araki H. and Oishi K. (2007) Cu_2ZnSnS_4-type thin film solar cells using abundant materials, *Thin Solid Films*, ***515***(15), 5997–5999

Katagiri H, Jimbo K, Yamade S, Kamimura T, Maw WS, Fukano T, Ito T and Motohiro T. (2008) Enhanced conversion efficiencies of Cu_2ZnSnS_4-based thin film solar cells by using preferential etching technique. *Applied Physics Express*, 1, 041201-(1-2)

Katagiri H, Jimbo K, Tahara M, Araki H, and Oishi K.(2009). The Influence of the Composition Ratio on CZTS-Based Thin Film Solar Cells,*CambridgeUniv Press*, pp. M04-01.

Khalkar, A., Lim, K. S., Yu, S. M., Patole, S. P., & Yoo, J. B. (2013). Effect of growth parameters and annealing atmosphere on the properties of Cu_2ZnSnS_4 thin films deposited by cosputtering. *International Journal of Photoenergy*, ***2013***, 1-7.

Kim, J. H., Rho, H., Kim, J., Choi, Y. J., & Park, J. G. (2012). Raman spectroscopy of ZnS nanostructures. *Journal of Raman Spectroscopy*, ***43***(**7**), 906-910.

Kittel, C. (1986). Introduction to Solid State Physics. Sixth edition. Chapter 8, p186-208.

[a]Kumar Y.B., Babu G. S., Bhaskar P.U. and Raja V.S. (2009) Preparation and characterization of spray-deposited Cu_2ZnSnS_4 thin films. *Solar Energy Material and Solar Cells* , **93**, 1230-1237.

[b]Kumar Y.B., Babu G.S., Bhaskar P.U. and Raja V.S. (2009) Effect of Starting-solution pH on the growth of Cu_2ZnSnS_4 thin films deposited by spray pyrolysis. *Physica Status Solidi A*, **206**, 1525-1530.

[c]Kumar Y.B., Babu G.S., Bhaskar P.U. and Raja V.S. (2009) Effect of copper salt and thiourea concentrations on the formation of Cu_2ZnSnS_4 thin films by spray pyrolysis. *Physica Status Solidi A*, **207**,149-156.

Lin X., Kavalakkat J., Kornhuber K., Levcenko S., Lux-Steiner M. C., Ennaoui A. (2013). Structural and optical properties of Cu_2ZnSnS_4 thin film absorbers from ZnS and Cu_3SnS_4 nanoparticle precursors. *Thin Solid Films*, **535**, 10-13

Lokhande, C. D., Shinde, N. M., Kim, J. H., & Moon, J. H. (2011). Photosensitive Cu2ZnSnS4 (CZTS) Thin Film Grown at Room Temperature by Novel Chemical Method. *Invertis Journal of Renewable Energy*, ***1***(3), 142-149.

Lu X., Zhuang Z., Peng Q., and Li, Y. (2011). Wurtzite Cu_2ZnSnS_4nanocrystals: a novel quaternary semiconductor. *Chem. Commun.*, ***47***(11), 3141-3143.

Madarász J., Bombicz P., Okuya M., and Kaneko S. (2001). Thermal decomposition of thiourea complexes of Cu (I), Zn (II), and Sn (II) chlorides as precursors for the spray pyrolysis deposition of sulfide thin films. *Solid State Ionics*, **141**, 439-446.

[a]Mali, S. S., Shinde, P. S., Betty, C. A., Bhosale, P. N., Oh, Y. W., & Patil, P. S. (2012). Synthesis and characterization of Cu_2ZnSnS_4 thin films by SILAR method. *Journal of Physics and Chemistry of Solids*, ***73***(6), 735-740.

[b]Mali, S. S., Patil, B. M., Betty, C. A., Bhosale, P. N., Oh, Y. W., Jadkar, S. R., Devan R.S., Ma Y.R. & Patil, P. S. (2012). Novel synthesis of kesterite Cu_2ZnSnS_4 nanoflakes by successive ionic layer adsorption and reaction technique: characterization and application. *Electrochimica Acta*, ***66***, 216-221.

Miao, C., Zheng, C., Liang, O., & Xie, Y.-H. (2011). Chemical Vapor Deposition of Graphene. Physics and Applications of Graphene - Experiments. doi:10.5772/15543

Miles, R. W., Hynes, K. M., & Forbes, I. (2005). Photovoltaic solar cells: An overview of state-of-the-art cell development and environmental issues. *Progress in Crystal Growth and Characterization of Materials*, ***51***(1), 1-42.

Miskin, C. K., Yang, W. C., Hages, C. J., Carter, N. J., Joglekar, C. S., Stach, E. A., & Agrawal, R. (2015). 9.0% efficient $Cu_2ZnSn(S, Se)_4$ solar cells from selenized nanoparticle inks. *Progress in Photovoltaics: Research and Applications*, ***23***(5), 654-659.

Moriya, K., Tanaka, K., &Uchiki, H. (2007). Fabrication of Cu_2 $ZnSnS_4$ thin-film solar cell prepared by pulsed laser deposition. *Japanese Journal of Applied Physics*, **46**(9R), 5780.

Moholkar, A. V., Shinde, S. S., Babar, A. R., Sim, K. U., Lee, H. K., Rajpure, K. Y.,Patil P.S., Bhosale C.H. and Kim, J. H. (2011). Synthesis and characterization of Cu_2ZnSnS_4 thin films grown by PLD: Solar cells. *Journal of Alloys and Compounds*, **509**(27), 7439-7446.

Mostako, A. T. T., & Khare, A. (2012). Effect of target–substrate distance onto the nanostructured rhodium thin films via PLD technique. *Applied Nanoscience*, **2**(3), 189–193.

Nakayama T and Ito K. (1996). Sprayed films of stannites Cu_2ZnSnS_4. *Applied Surface science*, **92**, 171-175.

Nandi, S. A., Chelvanathan, P., Zakaria, Z., Alam, M. M., Alothman, Z. A., Sopian, K., & Amin, N. (2014). Postdeposition Annealing Effect on Cu_2ZnSnS_4 Thin Films Grown at Different Substrate Temperature. *International Journal of Photoenergy*, 1-8.

Nelson, J. (2003). *The physics of solar cells* (Vol**. 1**, pp. 1-15). London: Imperial college press

Nozaki H., Fukano T., Ohta S., Seno Y., Katagiri H., and Jimbo K.(2012)Crystal structure determination of solar cell materials: Cu_2ZnSnS_4 thin films using X-ray anomalous dispersion, *Journal of Alloys and Compounds*,***524***(25), 22–25

Patel, K., Shah, D. V., & Kheraj, V. (2014). Influence of deposition parameters and annealing on Cu_2ZnSnS_4 thin films grown by SILAR. *Journal of Alloys and Compounds*, ***622***, 942-947.

Pawar S. M., Pawar B. S., Moholkar A. V., Choi D. S., Yun J. H., Moon J. H., Kolekar S.S and Kim J. H. (2010). Single step electrosynthesis of Cu_2ZnSnS_4(CZTS) thin films for solar cell application. *ElectrochimicaActa*, ***55***(12), 4057-4061

Pawar S.M., Inamdar A.I. , Pawar B.S. , Gurav K.V. , Shin S.W. , Yanjun Xiao , Kolekar S.S. , Jung-Ho Lee d, Jin H. K. and Hyunsik Im. (2014) Synthesis of Cu_2ZnSnS_4 (CZTS) absorber by rapid thermal processing (RTP) sulfurization of stacked metallic precursor films for solar cell applications. *Material Letters*, **118**, 76-79

Rajeshmon V.G., Kartha C.S., Vijayakumar K.P., Sanjeeviraja C., Abe T., and Kashiwaba, Y. (2011). Role of precursor solution in controlling the opto-electronic properties of spray pyrolysed Cu_2ZnSnS_4 thin films. *Solar Energy*, ***85***(2), 249-255.

Ramasamy K., Malik M. A. and O'Brien, P. (2011). The chemical vapor deposition of Cu_2ZnSnS_4 thin films. *Chemical Science*, ***2***(6), 1170-1172.

Riha, S. C., Parkinson, B. A., and Prieto, A. L. (2009). Solution-based synthesis and characterization of Cu_2ZnSnS_4 nanocrystals. *Journal of the American Chemical Society*, ***131***(34), 12054-12055.

Sagadevan, S. (2013). Recent trends on nanostructures based solar energy applications: a review. *Rev. Adv. Mater. Sci*, ***34,*** 44-61.

Sakthivel, S., & Baskaran, V. (2013). Applications of Successive Ionic Layer Adsorption and Reaction (SILAR) Technique for CZTS Thin Film Solar Cells. *Nano vision* Vol **3**(3), 235-239

Sakthivel, S., & Baskaran, V. (2015). Preparation, Characterization and Fabrication of Cu_2ZnSnS_4 (CZTS) Thin Film Solar Cells Using Spray Pyrolysis and Silar Techniques. *Nano vision* **5**(7-9), 276-282

Sanda F. M,Victor M. E., Monica T.A &Alina C. (2012). Spectrophotometric Measurements Techniques for Fermentation Process: Base Theory For UV-VIS Spectrophotometric Measurements. University of Oradea, Romania.

Saxena, A., Agarwal, N., & Tirth, V. (2011). Performance studies of an improved solar dryer in the climate of Uttar Pradesh. In *International Conference on National Solar Mission*.

Schroder, D. K. (2006). *Semiconductor material and device characterization*. John Wiley & Sons.

Scragg J. J., Dale P. J., Peter L. M., Zoppi G. and Forbes I.(2008) .New routes to sustainable photovoltaics: evaluation of Cu_2ZnSnS_4 as an alternative , *Phys. Status Solidi B* **245**,1772–1778

Scragg, J. J., Dale, P. J., & Peter, L. M. (2009). Synthesis and characterization of Cu_2ZnSnS_4 absorber layers by an electrodeposition-annealing route. *Thin Solid Films*, ***517***(**7**), 2481-2484.

Scragg, J. J., Berg, D. M., & Dale, P. J. (2010). A 3.2% efficient Kesterite device from electrodeposited stacked elemental layers. *Journal of Electroanalytical Chemistry*, **646**(1-2), 52–59. doi:10.1016/j.jelechem.2010.01.008

Schubert B. A., Marsen B., Cinque S., Unold T., Klenk R., Schorr S., and Schock H. W. (2011). Cu_2ZnSnS_4 thin film solar cells by fast coevaporation. *Progress in Photovoltaics: Research and Applications*, ***19***(1), 93-96.

Shelke P. N., Khollam Y. B., Patil K. R., Gunjal S. D., Jadkar S. R., Takwale M .G. & Mohite K. C. (2011). Studies on electrochemical deposition and characterization of Co_3O_4 films. *Journal of Nano- and Electronic Physics* **3**, 486–498.

Sheng C. Y., Jun Y. W., Rui L., Hua G. J., Xiao L. J., and Shi E. Y., (2014), Preparing Cu_2ZnSnS_4 films using the co-electrodeposition method with ionic liquids, *China Physics B*, ***21***(5) 058801 1-4

Shi, L., Pei C., Xu Y., and Li Q. (2011). Template-directed synthesis of ordered single-crystalline nanowires arrays of $Cu_2ZnSnS4$ and $Cu_2ZnSnSe_4$. *Journal of the American Chemical Society*, ***133***(27), 10328-10331.

Shinde, N. M., Dubal, D. P., Dhawale, D. S., Lokhande, C. D., Kim, J. H., & Moon, J. H. (2012). Room temperature novel chemical synthesis of Cu_2ZnSnS_4 (CZTS) absorbing layer for photovoltaic application. *Materials Research Bulletin*, ***47***(2), 302-307.

Singh O.P., Muhunthan N., Singh V. N., Singh B.P. (2015). Effect of annealing time on the composition, microstructure and band gap of Copper zinc tin sulfide thin films. *Journal of Advanced Materials Letters* ***6***(1), 2-7.

Sinsermsuksakul P., Heo J., Noh W., Hock A. S., and Gordon R. G. (2011). Atomic layer deposition of tin monosulfide thin films. *Advanced Energy Materials*, ***1***(6), 1116-1125.

Solangi, K. H., Islam, M. R., Saidur, R., Rahim, N. A., & Fayaz, H. (2011). A review on global solar energy policy. *Renewable and sustainable energy reviews*, ***15***(4), 2149-2163.

Steinhagen C., Panthani M. G., Akhavan V., Goodfellow B., Koo B., and Korgel B. A. (2009). Synthesis of Cu_2ZnSnS_4nanocrystals for use in low-cost photovoltaics. *Journal of the American Chemical Society*, ***131***(35), 12554-12555.

Su, Z., Yan, C., Sun, K., Han, Z., Liu, F., Liu, J., ... & Liu, Y. (2012). Preparation of Cu_2ZnSnS_4 thin films by sulfurizing stacked precursor thin films via successive ionic layer adsorption and reaction method. *Applied Surface Science*, ***258***(19), 7678-7682.

Suryawanshi M. P., Agawane G. L., Bhosale S. M., Shin S. W., Patil P. S., Kim J. H. and Moholkar A. V., (2013). CZTS based thin film solar cells: a status review. *Material Technology*, **28**(1-2), 98-109.

[a]Suryawanshi, M. P., Patil, P. S., Shin, S. W., Gurav, K. V., Agawane, G. L., Gang, M. G., ... & Moholkar, A. V. (2014). The synergistic influence of anionic bath immersion time on the photoelectrochemical performance of CZTS thin films prepared by a modified SILAR sequence. *RSC Advances*, ***4***(36), 18537-18540.

[b]Suryawanshi, M. P., Shin, S. W., Ghorpade, U. V., Gurav, K. V., Agawane, G. L., Hong, C. W., ... & Moholkar, A. V. (2014). A chemical approach for synthesis of photoelectrochemically active Cu_2ZnSnS_4 (CZTS) thin films. *Solar Energy*, ***110***, 221-230.

Tanaka T., Nagatomo T., Kawasaki D., Nishio M., Guo Q., Wakahara A., Yoshida A., and Ogawa H. (2005). Preparation of Cu_2ZnSnS_4 thin films by hybrid sputtering. *Journal of Physics and Chemistry of Solids*. ***66***(11), 1978–1981

Tanaka T, Kawasaki D, Nishio M, Guo Q, and Ogawa H. (2006). Fabrication of Cu2ZnSnS4 thin films by co-evaporation. *Physica Status Solidi C*, ***3***(8), 2844–2847.

Tang, A., Li, Z., Wang, F., Dou, M., Pan, Y., & Guan, J. (2017). One step electrodeposition of Cu_2ZnSnS_4 thin films in a novel bath with sulfurization free annealing. *Applied Surface Science*, **402**, 70–77. doi:10.1016/j.apsusc.2017.01.079

Tang D., Wang Q., Liu F., Zhao L., Han Z., Sun K., Lai Y., Li J., & Liu, Y. (2013). An alternative route towards low-cost Cu_2ZnSnS_4 thin film solar cells. *Surface and Coatings Technology*, ***232***, 53-59.

Tao J., Liu J., He J., Zhang K., Jiang,J., Sun L., Pingxiong Y. & Chu J. (2014). Synthesis and characterization of Cu_2ZnSnS_4 thin films by the sulfurization of co-electrodeposited Cu–Zn–Sn–S precursor layers for solar cell applications. *RSC Advances*, ***4***(46), 23977-23984.

Tiwari, D., Chaudhuri, T. K., Shripathi, T., Deshpande, U., & Sathe, V. G. (2014). Structural and optical properties of layer-by-layer solution deposited Cu_2SnS_3 films. *Journal of Materials Science: Materials in Electronics*, ***25***(9), 3687-3694.

Tickner, J. A., Raffensperger, C., & Myers, N. (1999). *The precautionary principle in action: a handbook*. Windsor, North Dakota: Science and Environmental Health Network.

Todorov, T. K., Reuter, K. B., & Mitzi, D. B. (2010). High-Efficiency Solar Cell with Earth-Abundant Liquid-Processed Absorber. *Advanced Materials*,***22***(20),E156–E159. doi:10.1002/adma.200904155

Tsukasa Washio, Hiroshi Nozaki, Tatsuo Fukano, Tomoyoshi Motohiro, Kazuo Jimbo and Hironori Katagiri. (2011).Analysis of lattice site occupancy in kesterite structure of Cu_2ZnSnS_4 films using synchrotron radiation x-ray diffraction, *Journal of Applied Physics* ***110***(**7**), 074511.

Vanalakar, S.A., Mali, S.S., Jo, E.A., Kim, J.Y., Kim, J.H., Patil, P.S. (2014). Triton-X mediated interconnected nanowalls network of cadmium sulfide thin films via chemical bath deposition and their photoelectrochemical performance. *Solid-State Sciences*. **36**, 41–46

Wang, H. (2011). Progress in thin film solar cells based on. *International journal of Photoenergy*. Volume **2011**, Article ID 801292, pp 1-10

Wang H. and Bell J., (2011). Thin Film Solar Cells based on Cu_2ZnSnS_4 absorber . In The 5th World Congress on Engineering Asset Management (WCEAM 2011), Brisbane Convention and Exhibition Centre, Brisbane, Qld.

Wang K., Gunawan O., Todorov T., Shin B., Chey S. J., Bojarczuk, N. A., Mitzi D. & Guha, S. (2010). Thermally evaporated Cu_2ZnSnS_4 solar cells. *Applied Physics Letters*, ***97***(14), 143508-143508.

Washio, T., Shinji, T., Tajima, S., Fukano, T., Motohiro, T., Jimbo, K. andKatagiri, H. (2012). 6% Efficiency Cu_2ZnSnS_4-based thin film solar cells using oxide precursors by open atmosphere type CVD. *Journal of Materials Chemistry*, ***22***(9), 4021-4024.

Weber A., Mainz R., and Schock H. W. (2010). On the Sn loss from thin films of the material system Cu–Zn–Sn–S in high vacuum. *Journal of Applied Physics*, ***107***(1), 013516

Wang W., Winkler M. T., Gunawan O., Gokmen T., Todorov T. K., Zhu Y. and Mitzi D. B. (2013). Device Characterization of CZTSe Thin- Film Solar Cells with 12.6% Efficiency, *Advanced Energy Mat*erials,**44** (7). DOI: 10.1002/aenm.201301465

Wu, J., Lan, Z., Lin, J., Huang, M., Huang, Y., Fan, L., & Luo, G. (2015). Electrolytes in dye-sensitized solar cells. *Chemical reviews*, ***115***(5), 2136-2173.

Yu, X., Ren, A., Wang, F., Wang, C., Zhang, J., Wang, W., Wu, L., Li, W., Zeng, G. & Feng, L. (2014). Synthesis and Characterization of CZTS Thin Films by Sol-Gel Method without Sulfurization. *International Journal of Photoenergy*, ***2014***,1-6

Zhang, J., Long, B., Cheng, S., & Zhang, W. (2013). Effects of Sulfurization Temperature on Properties of CZTS Films by Vacuum Evaporation and Sulfurization Method. International Journal of Photoenergy, **2013**, 1–6. doi:10.1155/2013/986076

EMPA 2013, www.empa.ch/bilder. Media release ID=118774, Duebendorf, St. Gall, Thun, 17 January 2013.

Firstsolar. http://investor.firstsolar.com/releasedetail.cfm?ReleaseID=828273. Retrieved on 26 August, 2014.

Solar Frontier, 2015. https://en.wikipedia.org/wiki/Thin-film_solar_cell. Retrieved on 19 March, 2015.

SunPower,2016. https://www.forbes.com/sites/michaelkanellos/2016/06/27/sunpowers-24-1-efficiency-mark-are-we-near-the-ceiling/#585530365075. Retrieved on 27 June,2016

ZSW 2016 https://www.zsw-bw.de/en/newsroom/news/news-detail/news/detail/News/zsw-sets-new-world-record-for-thin-film-solar-cells.html. Retrieved on 15 June, 2016.